UFL/COEL-89/013

RESPONSE OF FINE SEDIMENT-WATER INTERFACE TO SHEAR FLOW

By

Rajesh Srinivas

1989

Thesis

RESPONSE OF FINE SEDIMENT-WATER INTERFACE TO SHEAR FLOW

By

RAJESH SRINIVAS

A THESIS PRESENTED TO THE GRADUATE SCHOOL
OF THE UNIVERSITY OF FLORIDA IN
PARTIAL FULFILLMENT OF THE REQUIREMENTS
FOR THE DEGREE OF MASTER OF SCIENCE

UNIVERSITY OF FLORIDA

1989

ACKNOWLEDGEMENTS

I would like to express my sincere gratitude to my advisor and chairman of my graduate committee, Dr. Ashish J. Mehta, for his valuable and imaginative guidance and ideas which have made this thesis possible. I am indebted to him for going out of his way in acting like a mentor and guardian. My thanks also go to Dr. R.G. Dean and Dr. D.M. Sheppard for serving on my committee. I am also grateful to the personnel at the Coastal Engineering Laboratory, Roy Johnson, Danny Brown and, especially, Vernon Sparkman for their help and suggestions in building the flume and pump. Special thanks are also due to Shannon Smythe and Barry Underwood for their excellent drafting work.

Finally, I would like to thank my parents for their unqualified support and faith in me.

This study was supported by the U.S. Army Engineer Waterways Experiment Station, Vicksburg, MS (contract DACW39-89-K-0012) with project manager, Allen M. Teeter.

TABLE OF CONTENTS

ACKNOWLEDGEMENTS ii

LIST OF FIGURES vi

LIST OF TABLES viii

LIST OF SYMBOLS ix

ABSTRACT xiii

CHAPTERS

1 INTRODUCTION 1

1.1 Need for Study of Fluid Muds 1

1.2 Some Observations of Fluid Mud Entrainment 2

1.3 Approach to the Problem 8

1.4 Objectives 11

1.5 Plan of Study 12

2 INSTABILITY MECHANISM 14

2.1 Discussion 14

2.2 Kelvin-Helmholtz Instability 15

2.2.1 Case of a Vortex Sheet 15

2.2.2 Generalized Form of Kelvin-Helmholtz Instability 20

3 INSTABILITY OF STRATIFIED SHEAR FLOWS 27

3.1 Background 27

3.2 Literature Review 30

3.2.1 Browand and Wang (1971) 30

3.2.2 Smyth, Klaassen and Peltier (1987) 31

3.2.3 Lawrence, Lasheras and Browand (1987) 33
3.2.4 Narimousa and Fernando (1987) 34
3.3 Conclusions 38
4 ENTRAINMENT IN STRATIFIED SHEAR FLOWS 40
4.1 General Aspects 40
4.2 Moore and Long (1971) 40
4.2.1 Results of Two Layer Steady State Experiments 41
4.2.2 Results of Entrainment Experiments 44
4.2.3 Summary 44
4.3 Long (1974) 45
4.4 Narimousa, Long and Kitaigorodskii (1986) 47
4.4.1 Deduction of u_* 48
4.4.2 Entrainment Rates Based on u_* 49
4.5 Wolanski, Asaeda and Imberger (1989) 50
4.6 Conclusions 51
5 METHODOLOGY 53
5.1 Apparatus 53
5.2 Procedure 61
6 RESULTS AND ANALYSIS 67
6.1 Definition of Richardson Number 67
6.2 Initial Conditions 68
6.3 Evolution of Characteristic Profiles 70
6.4 Shear Layer 74
6.5 Observations on the Interface 80
6.6 Entrainment Rate 84
6.7 Discussion in Terms of Equilibrium Peclet Number 95
6.8 Comparison with Soft Bed Erosion 98

7 SUMMARY AND CONCLUSIONS 101
7.1 Summary 101
7.2 Conclusions 101
7.3 Recommendation for Further Work 104
APPENDICES
A TEST MATERIALS 105
A.1 Kaolinite 105
A.2 Bentonite 105
B A NOTE ON RICHARDSON NUMBER 107
B.1 Introductory Note 107
B.2 Small Disturbances 107
B.3 Energy Considerations 108
BIBLIOGRAPHY 110
BIOGRAPHICAL SKETCH 114

LIST OF FIGURES

1.1 Definition sketch for fluid mud (source: Ross et al. 1988). 3

1.2 Evolution of Suspended Sediment Concentration (source: Kirby 1986) 5

1.3 Internal waves produced by the passage of sailing vessels in the Rotterdam Waterway (source: van Leussen and van Velzen 1989). 6

1.4 Field evidence of gravity driven underflows (source: Wright et al. 1988). 7

2.1 Definition sketch of the flow for the case of a vortex sheet 16

3.1 Offset Velocity and Density Profiles 28

3.2 Physical description of the complete flow configuration, with density and velocity profiles (adapted from Narimousa and Fernando 1987. 35

5.1 Recirculating flume of plexiglass used in the present investigation (dimensions in centimeters). 55

5.2 Section A-A of the flume, from Figure 5.1 (dimensions in centimeters). 56

5.3 Section B-B of the flume, from Figure 5.1 (dimensions in centimeters). 57

5.4 Details of the disk pump system used in the present investigation (dimensions in centimeters). 59

6.1 Sequence of concentration profiles of Run 9 with kaolinite depicting the evolution of concentration with time. IF denotes interface. 71

6.2 Evolution of the velocity profile in the mixed-layer for Run 6 with kaolinite. IF denotes interface. 73

6.3 Change in the mixed-layer depth with time for Run 10 with bentonite. 75

6.4 Rate of change of mixed-layer depth in Run 10 with bentonite. . 76

6.5 Non-dimensional shear layer thickness vs. Richardson number . 78

6.6 Non-dimensional shear layer thickness vs. Richardson number on a log-log scale 79

6.7 Turbulent entrainment at t $\sim$ 0.5 minute. Sediment- kaolinite. . 81

6.8 Interface at $Ri_u < 10$. Sediment-kaolinite. 81

6.9 Interface at $Ri_u < 10$. Sediment-kaolinite. 82

6.10 Highly irregular interface at $Ri_u > 10$. Sediment- kaolinite. . . . 82

6.11 Scour of growing crest at $Ri_u > 10$. Sediment- kaolinite. 83

6.12 Scour of grown crest at $Ri_u > 10$. Sediment- kaolinite. 83

6.13 Subsiding crest at $Ri_u > 10$. Sediment-kaolinite. 85

6.14 Smoke-like wisp being ejected from the tip of disturbances. Sediment-kaolinite. 85

6.15 Appearance of the interface at high Richardson numbers, $Ri_u >$ 25. Sediment-kaolinite. 86

6.16 Non-dimensional buoyancy flux vs. Richardson number for all the experiments. 93

6.17 Comparison of erosion rates of soft beds with the rates predicted by equation (6.9). 100

LIST OF TABLES

6.1	Initial conditions of all Runs	69
6.2	Relevant measured parameters for runs with kaolinite	87
6.3	Relevant measured parameters for runs with bentonite	88
6.4	Richardson numbers and entrainment rates for runs with kaolinite	89
6.5	Richardson numbers and entrainment rates for runs with bentonite	90
6.6	Peclet numbers for equilibrium conditions	98
A.1	Chemical composition of kaolinite	106
A.2	Chemical composition of bentonite	106

LIST OF SYMBOLS

b = buoyancy.

b_∞ = buoyancy of unperturbed layer.

b_1 = rms buoyancy fluctuation.

C = concentration of the suspension.

C_1 = mean concentration of the mixed-layer.

C_2 = concentration of fluid mud at the level of the interface.

$\bar{C}_2$ = mean concentration of fluid mud.

c = disturbance wave speed.

c' = turbulent speed.

d = distance between the centers of the shear layer and the density interface.

dm = change in mass with time.

dt = time of the interval.

E = entrainment coefficient.

$\bar{E}$ = erosion rate.

$\bar{E}_f$ = floc erosion rate.

F = Froude number.

F_z = vertical flux.

H = depth of the fluid mud layer.

$\hat{H}$ = total depth of the two-layered system.

i = $\sqrt{-1}$.

h = depth of the mixed-layer.

J = local Richardson number.

k = horizontal (x-direction) wave number of the perturbation.

K_z = eddy diffusion coefficient.

$\hat{k}$ = resultant horizontal wave number of the perturbation.

L_e = mixing length.

l = horizontal (y-direction) wave number of the perturbation.

l_1 = length scale.

M_2 = mass per unit area of the fluid mud.

N = buoyancy frequency.

n = Manning's resistance coefficient.

P = probability that a particle reaching the bed will deposit.

Pe = Peclet number.

p = pressure in the fluid.

p' = perturbation in the pressure due to the disturbance.

Q = non-dimensional bouyancy flux.

q = bouyancy flux.

Ri = Richardson number.

Ri_{cr} = critical Richardson number.

Ri_{min} = minimum Richardson number.

Ri_o = overall Richardson number.

Ri_u = Richardson number based on the mean velocity of the mixed layer.

Ri_* = Richardson number based on the friction velocity.

s = complex angular frequency of the disturbance.

T = surface tension.

T_a = advective time scale.

T_d = diffusion time scale.

U = velocity of fluid.

u = representative velocity.

u' = perturbation in the horizontal (x-direction) velocity due to the disturbance, or horizontal (x-direction) turbulent velocity.

$\bar{u}$ = mean velocity of the mixed-layer.

$\tilde{u}$ = rms turbulent horizontal velocity.

u_e = entrainment velocity.

u_* = friction velocity.

V = potential energy.

V_1 = potential energy per unit mass.

v' = perturbation in the horizontal (x-direction) velocity due to the disturbance.

W = width of the side-walls.

w' = perturbation in the vertical (z-direction) velocity due to the disturbance, or vertical turbulent velocity.

w_s = particle settling velocity.

w_1 = turbulent fluctuation of the vertical velocity.

w_* = friction velocity of the side-walls.

x = horizontal co-ordinate.

y = horizontal co-ordinate.

z = vertical co-ordinate.

α = horizontal (x-direction) of the perturbation.

α' = a rate coefficient.

β = horizontal (y-direction) of the perturbation.

Δb = interfacial buoyancy jump.

$\Delta\rho$ = interfacial density jump.

δ = thickness of the density interface.

δT = kinetic energy per unit volume of the flow.

δW = work done to overcome gravity.

δ_s = thickness of the shear layer.

δ_w = amplitude of the interfacial wave.

ϵ = dissipation function.

η = displacement of the interface.

λ = wavelength of the disturbance.

ν = kinematic viscosity.

ρ = density of the fluid.

ρ' = perturbation in the fluid density due to the disturbance.

$\bar{\rho}_1$ = mean density of the mixed-layer.

τ = shear stress.

ϕ = velocity potential.

ϕ' = perturbation in the velocity potential due to the disturbance.

Abstract of Thesis Presented to the Graduate School
of the University of Florida in Partial Fulfillment of the
Requirements for the Degree of Master of Science

RESPONSE OF FINE SEDIMENT-WATER INTERFACE TO SHEAR FLOW

By

RAJESH SRINIVAS

August 1989

Chairman: Ashish J. Mehta
Major Department: Coastal and Oceanographic Engineering

An experiment was conceived and executed to simulate the effects of turbulent shear flow on fine sediment, specifically fluid mud. The tests were conducted in a "race-track" shaped recirculating flume with a disk pump. Experiments were run with two types of fluid mud, consisting of kaolinite and bentonite in water. Shear layer thickness and the nature of the interfacial instabilities were qualitatively examined. Entrainment rates of fluid muds were examined as a function of increasing Richardson number and an empirical relation was obtained between the non-dimensional buoyancy flux and the Richardson number. This relationship was then compared with that obtained by previous experimenters for salt- stratified systems. This comparison made apparent the effect of sediment particles in causing additional dissipation of turbulent kinetic energy at higher Richardson numbers as the entrainment rate decreased substantially. Peclet number consideration showed that the mixed-layer at these higher Richardson numbers appears to behave like a suspension in equilibrium. The effect of varying the clay constituent of fluid mud on the entrainment rate could not be fully investigated, although within the limits of data no discernible trend differences could be clearly identified. A brief comparison of the fluid mud entrainment rate, which is proportional to the cube of the flow

velocity, with soft bed erosion rate, which is proportional to the square of the flow velocity, showed that fluid mud entrainment can dominate over bed erosion at low current velocities.

CHAPTER 1
INTRODUCTION

1.1 Need for Study of Fluid Muds

A challenging aspect of many coastal and estuarine problems is the elucidation of fine sediment transport behavior. The compelling factors for such investigations are both economical and environmental. The last couple of decades have seen extensive effort being applied to experimental and theoretical studies with a variety of mathematical models developed for simulation of fine and cohesive sediment transport. The common aspect in the modeling approach is a soil bed subject to layer by layer or massive erosion. However, experimental observations verify the existence of the sediment population in three distinct states: mobile, upper column suspensions, high concentration near-bed suspensions, and settled muds (e.g., see Kirby and Parker 1983). In mobile suspensions, the particles are dispersed and stay in suspension by turbulent momentum exchange. Near-bed high concentration suspensions or fluid muds, are partially supported by the fluid and partially by their particle network while in settled muds the particles rest at the bottom supported by their infrastructure (soil matrix).

The relatively high concentrations of fluid muds play a substantial role in horizontal transport to sedimentation-prone areas. Indeed, in spite of low near bed velocities, the horizontal sediment mass flux can be considerable and can lead to "fluff" accumulation in navigational channels. The movement of fluid muds has been cited as the most likely cause of rapid sedimentation in ports located in muddy estuaries. Obviously, ignoring fluid muds can lead to gross underestimation of sedimentation rates. Almost totally neglected has been the issue of their upward turbulent en-

trainment and mixing due to vorticity generation by shear flows (of current) above them. Their loose structure permits fluid muds to entrain into the water column easily and contribute substantially to degradation of water quality. This facet of transport is evidently not simulated in solely considering erosion of cohesive beds (which have a measurable shear strength).

Thus, one can assert that the consideration of the entrainment behavior of this state of fluid muds is necessary to comprehensively simulate the mechanics of fine sediment transport effectively. This implies that the prediction of fluid mud behavior to hydrodynamic forcing by shear flows is necessary. Entrainment rates need to be established and possible physical mechanisms causing this kind of response need to be formulated, neither of which are presently widely available in detail. These aspects are briefly examined in this experimental study.

1.2 Some Observations of Fluid Mud Entrainment

Typical variations in concentration and velocity with depth for muds, and the related definition terminology are presented in Figure 1.1. Fluid muds are confined to the region between the lutocline, i.e., the zone with a steep concentration gradient, and the partially or fully consolidated bottom. The upper zone of fluid mud may have both horizontal and vertical motion, while the lower zone may have some vertical motion only. Using concentration as a measure, it is generally accepted that these fluid muds fall in the range 20 to 320 g/l (Ross et al. 1987). These concentrations correspond to the bulk density range of 1.01 to 1.20 g/cm^3, given a sediment granular density of 2.65 g/cm^3.

Fluid mud behavior is largely time dependent, varying with the physico-chemical properties of both sediment and water. The rheological properties of fluid muds are strongly affected by factors such as pH, salinity, mineralogical composition and particle size. Their mechanical behavior is generally pseudoplastic while at very high concentrations they resemble Bingham plastics (Bryant et al. 1980), as at

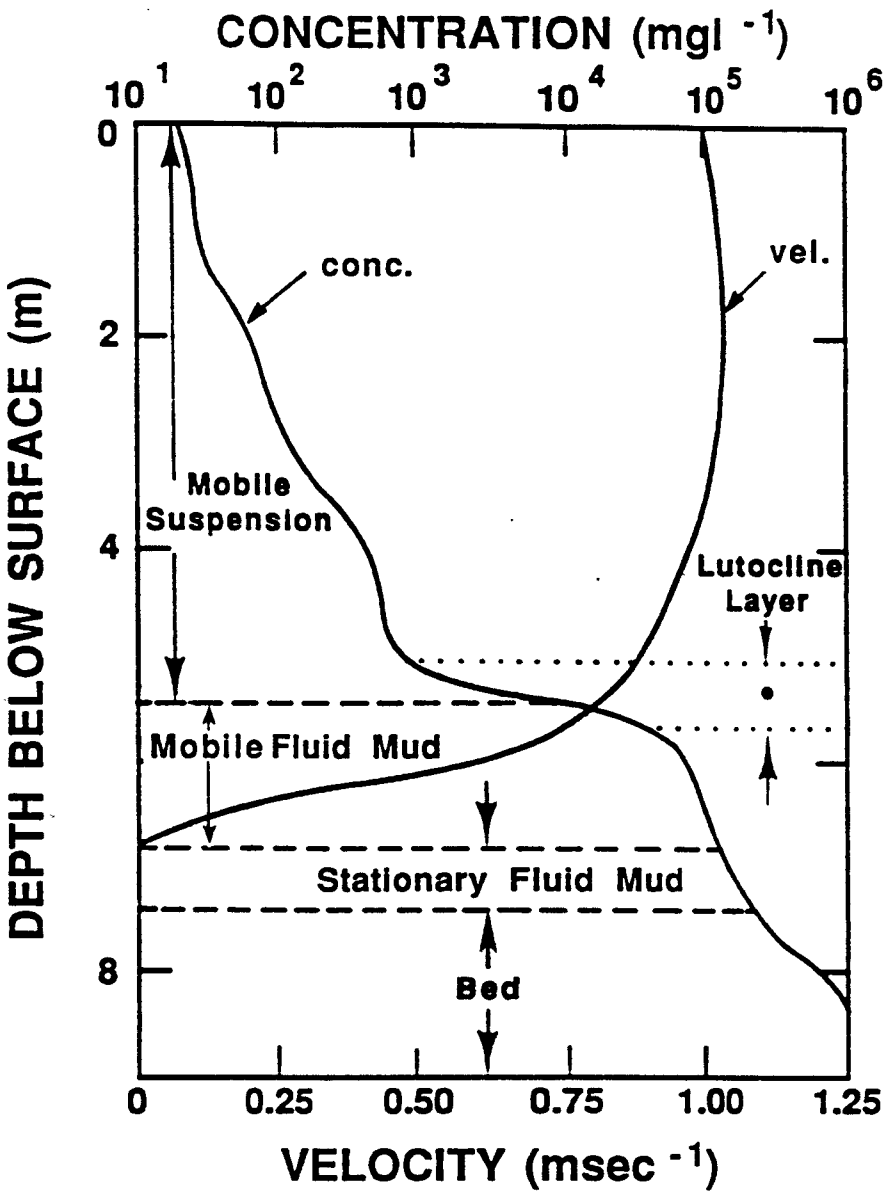

Figure 1.1: Definition sketch for fluid mud (source: Ross et al. 1988).

high concentrations strong inter-particle bonds provide an initial resistance to shear deformation (when the applied stress is less than the yield stress, elastic deformation is possible without any breakdown of structure leading to fluidization).

The dynamic behavior of fluid muds during a tidal cycle is well recognized by presenting the sequence of concentration profiles recorded by Kirby (1986) (see Figure 1.2). These are given for accelerating flow, while the reverse sequence prevails for decelerating flow. Zone 1 is a very low concentration suspension, Zone 2 is the lutocline layer, i.e., the zone with steep concentration gradients, while, Zone 3 is high concentraion susoension (similar to fluid mud). At slack water, the destabilizing shear forces are small compared to buoyancy stabilization and there is no entrainment. The physical situation corresponds to a two-phased system with fluid mud seperated from the overlying water by a distinct interface. As the velocity picks up, the resulting turbulent kinetic energy becomes sufficient to overcome the stable stratification of the fluid mud and there is subsequent entrainment.

High concentration ($\sim$ 300 g/l) fluid mud layers of thicknesses more than a meter have been observed in the Rotterdam Waterway (van Leussen and van Velzen 1989). The passage of sailing vessels over these layers produces internal waves (see Figure 1.3) at their surface, in spite of the fact that the bottom stresses are quite low.

Wright et al. (1988) made field measurements of dispersion of concentrated sediment suspensions over the active delta front of the Yellow River in China. They provided evidence of the existence of both hypopycnal (buoyant) plumes as well as gravity driven hyperpycnal (near bottom) dispersal modes. Downslope advection within the hyperpycnal plume of mixed, lower salinity water from the river mouth caused vertical instability as regards the excess bulk density (including sediment concentration, salinity and temperature). Once deposition began, tidal currents contributing to vertical momentum exchange resulted in instability induced en-

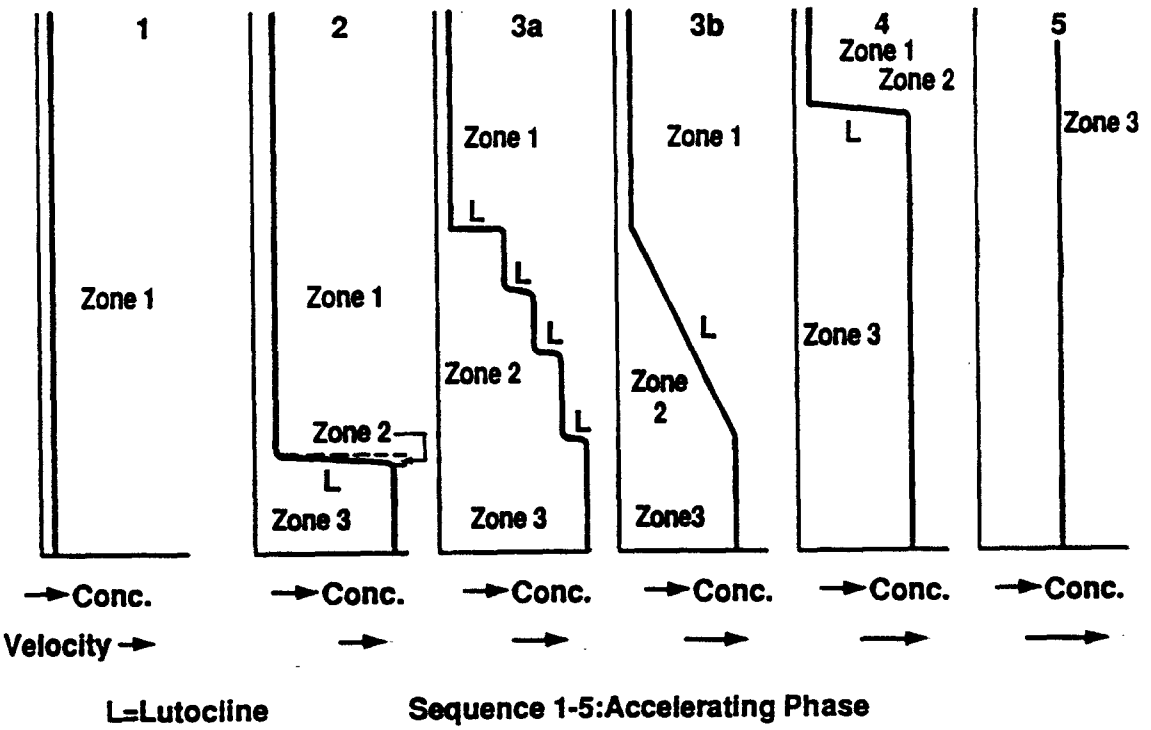

Figure 1.2: Evolution of Suspended Sediment Concentration (source: Kirby 1986)

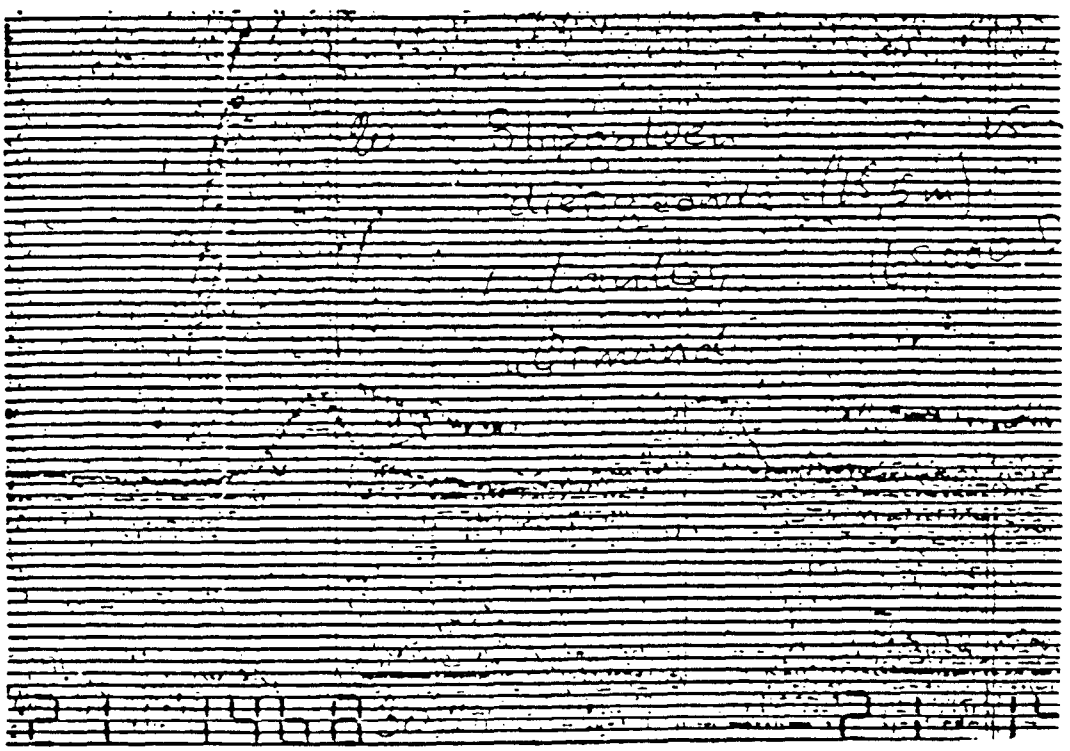

Figure 1.3: Internal waves produced by the passage of sailing vessels in the Rotterdam Waterway (source: van Leussen and van Velzen 1989).

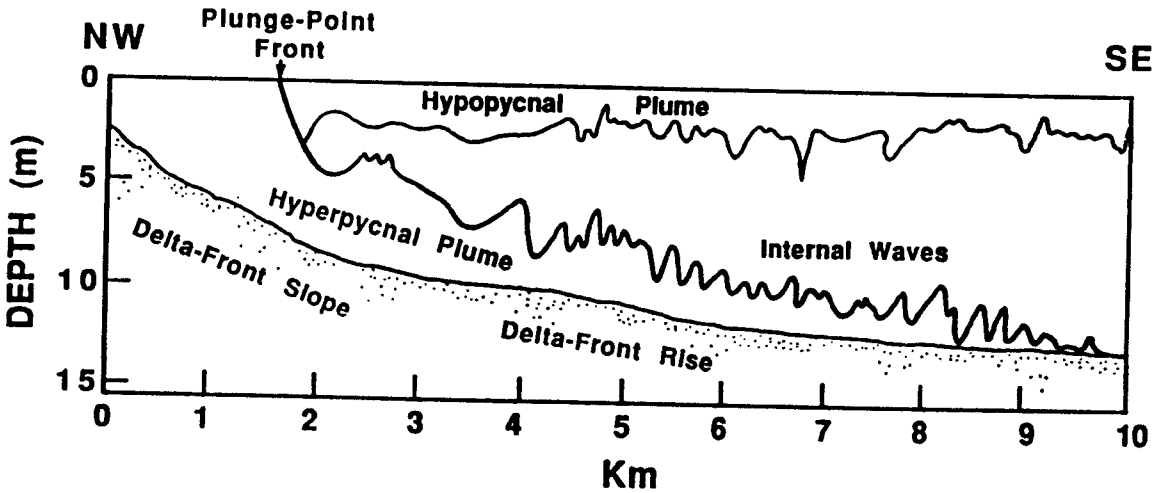

Figure 1.4: Field evidence of gravity driven underflows (source: Wright et al. 1988).

hanced mixing. They observed large amplitude high frequency internal waves at close to the Brunt-Väisälä frequency.

1.3 Approach to the Problem

In a most general sense, it can be asserted that shear flow in a stratified fluid is a natural occurence and a crucial mechanism for turbulence production in the atmosphere and oceans. A number of practical engineering problems, often associated with a desire to thoroughly mix effluents entering the surroundings, also requires a knowledge of the behavior of stratified shear flows.

There are numerous situations in nature where an understanding of the behavior of velocity-sheared density interfaces is important:

- Wind generated waves in the ocean can be a manifestation of Kelvin-Helmholtz type instabilities at the air-water interface.
- The tangential stress which occurs when the wind blows over the ocean generates a drift current in the upper layers of the ocean, which causes entrainment of the stratified layers below. This has been cited as the mechanism responsible for bringing deep- sea nutrients into more accesible regions (Phillips 1977).
- Substantial bearing on the world climate is attributed to drift currents in the upper atmosphere causing growth of this mixed layer against previously stable inversions.
- The rising and subsequent spreading of methane gas in coal mines has an important bearing on safety (Ellison and Turner 1959).
- Gravity currents under a stratified layer over sloping bottoms are very common in oceans.
- In estuaries, the oceanic salt-water wedge penetrates upstream and under lighter river water.

- Finally, as mentioned before, shear flows can cause entrainment of underlying fluid mud, which is the focal point of interest of this study.

Again, it can be stated in general terms that vorticty generation by shear flows causes instabilities to appear at the density interface and these seem to be the prime cause for mixing across this interface. A gamut of literature exists for the same general kind of problem, with density stratification caused by salinity, or thermal effects, or both. These are analogous because of comparable density ranges and statically stable arrangements. Salinity experiments have been conducted to simulate oceanic situations which have velocity shear values similar to estuarine environments, with resulting comparable values of the ratio of buoyancy to shear forces. Interfacial instabilities and entrainment rates have been examined, theoretically as well as experimentally. However, a peculiar feature of these studies is the fact that most investigators seem to arrive at quite different results, which they then generally proceed to explain satisfactorally. So, relative newcomers are saddled with numerous and quite different relationships and explanations for observed phenomena, without any explicit kind of unification. This is a potent indicator of the fact that this process of production and dissipation of turbulent kinetic energy which governs the buoyancy flux and generation, growth and collapse of instabilities is a very complex process and far from being well understood.

Experiments considered here have additional complications due to non-Newtonian rheology. Fluid muds are not autosuspensions. Settling is characteristic, and the downward buoyancy flux due to particle fall velocity causes additional dissipation of turbulence, which is obviously not the case for salinity and temperature stratified experiments.

Defining, h as the the depth of the turbulent mixed layer, u_e as a relevant entrainment velocity = dh/dt (rate of propagation of the mixed layer), u_1 as the turbulent velocity scale for the mixed layer, Δb as the buoyancy step across the

density interface = $(g\Delta\rho)/\rho_0$, $\Delta\rho$ as the interfacial density step, and ρ_0 as a reference density, the Buckingham-π theorem for dimensional analysis can be used for determining the relevant non-dimensional parameters governing the dynamics of this situation. Intuitively, one can see that density and acceleration due to gravity should be coupled as buoyancy. We can in fact identify the pertinent variables to be $\Delta b, u_1, u_e$ and h; the fundamental dimensions being that of length, L, and time, T (as mass becomes implicit in buoyancy). Choosing u_1 and Δb as our repeating variables we can form the combinations $\Delta b^{\alpha} u_1^{\beta} h$ and $\Delta b^{\gamma} u_1^{\delta} u_e$. Now, we demand the exponents of L and T to be zero in each combination. So, we obtain $\alpha = 1$, $\beta = -2$, $\gamma = 0$, and $\delta = -1$, giving us the non-dimensional parameters $\frac{\Delta b\, h}{u_1^2}$ and $\frac{u_e}{u_1}$, the first of which is the Richardson number (Ri), whereas the second is an entrainment coefficient (E). The dimensional analysis is completed by the statement f(Ri,E) = 0, or, further,

$$E = \mathcal{F}(Ri) \tag{1.1}$$

The fact that such a functional relationship exists is borne out by the experimental results of many previous investigators, albeit in different forms.

This relationship between E and Ri represents interaction between mechanical mixing energy and the potential energy stored in stratification that it is working against. As entrainment is considered a turbulent process, effects of molecular diffusion are largely ignored, although, some investigators have pointed out that at high Ri, when turbulence is relatively weak, molecular diffusion does become important for salinity and thermal types of experiments.

Experimenters have arrived at different power laws (of the form $E \propto Ri^{-n}$) for subranges of Ri (for example, see Christodoulou 1986 and Narimousa et al. 1986). More complicated relationships have also been derived by evaluation of the turbulent kinetic energy budget (Zemen and Tennekes 1977; Sherman et al. 1978; Deardorff 1983; Atkinson 1988).

1.4 Objectives

With the preceeding discussion in mind, and after an in-depth review of pertinent literature regarding the mechanism of instabilities and the consequent entrainment, it was decided to run experiments to simulate entrainment of fluid muds by turbulent velocity-shear flows in a specially-designed flume. A 'race-track' shaped recirculating flume was constructed for this purpose in which a two-layered system of fluid mud and water could be established. The flume was built of plexiglass, as one of the prime objectives of the present investigation was to observe the nature of interfacial instabilities. Shear flow was generated by using a specially designed disk pump which is basically a system of interlocking plates on two parallel externally-driven shafts rotating in opposite directions. The horizontal velocity of the driven fluid was constant over the depth of the disk-pump. This disk-pump was instrumental in imparting horizontal homogeneity to the flow . The velocity profile diverged from the vertical at a distance from the level of the bottom disk of this pump, thus producing flow with mean-shear.

The ultimate objective of this investigation was to run a series of experiments to simulate the effects of shear flow on the fluid mud-water interface and the resulting entrainment of relatively low to medium concentration fluid muds, and to make phenomenological observations to obtain qualitative descriptions of interfacial instabilities and quantitative expression(s) for rates of entrainment by measuring mass flux in relation to the destabilizing velocity-shear. Another objective was to determine the effect of varying the degree of cohesion of sediment on rates of entrainment. This was done by using kaolinite and bentonite (see Appendix A), which vary greatly in their degree of cohesion, since kaolinite is only weakly cohesive while bentonite is cohesive and thixotropic.

1.5 Plan of Study

The following chapters document the investigation of the issue of entrainment of fluid mud by shear flow to find a quantifiable relationship for this process, which, as mentioned before, has hitherto remained largely unaddressed. Starting with the justifiable surmise that fluid mud entrainment is a manifestation of interfacial instability due to current shear, theoretical background for the production and propagation of instabilities is first discussed, and thus the investigation begins in Chapter 2 with a theoretical background of Kelvin-Helmholtz type of hydrodynamic instability. The classic case of stability of a vortex sheet is discussed first in this chapter, and this is followed by the more generalized version of Kelvin-Helmholtz instability.

In Chapter 3, some of the more pertinent work of previous investigators on the subject of instability of shear flows is reviewed. Considerable work has been done in the area of numerical simulations of instabilities, but adequate support in the form of accurately documented experimental evidence seems to be lacking. It must be mentioned, however, that the recent work of Narimousa and Fernando (1987) is both comprehensive as well as enlightening.

The question of entrainment rates due to shear flows of stably stratified fluids is examined in Chapter 4. Again, the volume of work which has been done is considerable, and only directly pertinent literature is considered for review.

Chapter 5 is devoted to the experimental methodology of the present investigation. The details of the flume and the disk pump constructed for the present study, the procedure of experimentation and methods of measurement are documented.

In Chapter 6, the results of the investigation are presented and analysed, while Chapter 7 gives the main conclusions of the study.

In Appendix A a description of the constituent materials of fluid mud, namely kaolinite and bentonite, prepared in the laboratory is included, while Appendix B

traces the history of the definition of the critical Richardson number for stability of a stratified shear flow.

CHAPTER 2
INSTABILITY MECHANISM

2.1 Discussion

In general, instability occurs when there is an upset in the equilibrium of the external, inertia and viscous forces in a fluid. Examples of external forces are buoyancy in a fluid of variable density, surface tension, magneto-hydrodynamic, Coriolis and centrifugal forces. Surface tension and magnetic forces usually tend to stabilize, while an interesting point to be noted regarding viscosity is that it can both inhibit or amplify disturbances. An obvious effect is of dissipation of energy, whence any flow is stable if viscosity is large enough. However, it's effect of diffusing momentum may render flows unstable, as in parallel shear flows, which are stable for the inviscid case.

The analysis is restricted to primarily steady flows, although tidal action in estuaries is obviously unsteady. However, tidal flows may be considered to be steady for the purpose at hand, since one is dealing with widely different time scales. Analysis of unsteady flows is very complex in general. Boundaries of the flow are an important factor, as well; the closer the boundary, the more efficient is the constraining of disturbances, although boundary layer momentum diffusive effects may serve to enhance instability.

Any flow is likely to be disturbed, at least slightly, by irregularities or vibrations of the basic flow. This disturbance may die away, persist at the same magnitude, or grow so much as to alter the very flow. Such flows are termed stable, neutrally stable and unstable, respectively. Stability of parallel inviscid fluid flow has been investigated since the latter half of the nineteenth century, when the instability

of homogeneous and non-homogeneous flows were considered. Subsequent analyses have been with subtle modifications to this same basic problem, including for compressible fluids, considerations for rotational systems, magneto-hydrodynamic effects, etc. A wide range of literature has emerged, of interest to specialized sectors in engineering. The consideration in this section will be for the most general case, fluid dynamical, for studying this phenomenon of instability, rather than its occurence or application.

2.2 Kelvin-Helmholtz Instability

2.2.1 Case of a Vortex Sheet

Formulation of the Problem

It has been understood since the nineteenth century that the dynamic instability of a weakly stratified parallel shear flow leads to the formation of vortex-like structures called Kelvin- Helmholtz (KH) waves. Consider the basic flow of incompressible, inviscid fluids in two infinite horizontal streams of different velocities and densities, one above the other (see Figure 2.1), and given by

$$\phi = \phi_2 \quad U = U_2 \quad \rho = \rho_2 \quad P = p - \rho_2 g z \qquad (z > 0)$$

$$\phi = \phi_1 \quad U = U_1 \quad \rho = \rho_1 \quad P = p - \rho_1 g z \qquad (z < 0)$$

The interface has an elevation z = η (x,y,t), when the flow is disturbed.

The governing differential equation is

$$\nabla^2 \phi = 0 \qquad (2.1)$$

i.e.,

$$\nabla^2 \phi_2 = 0 \quad z > \eta$$

$$\nabla^2 \phi_1 = 0 \quad z < \eta$$

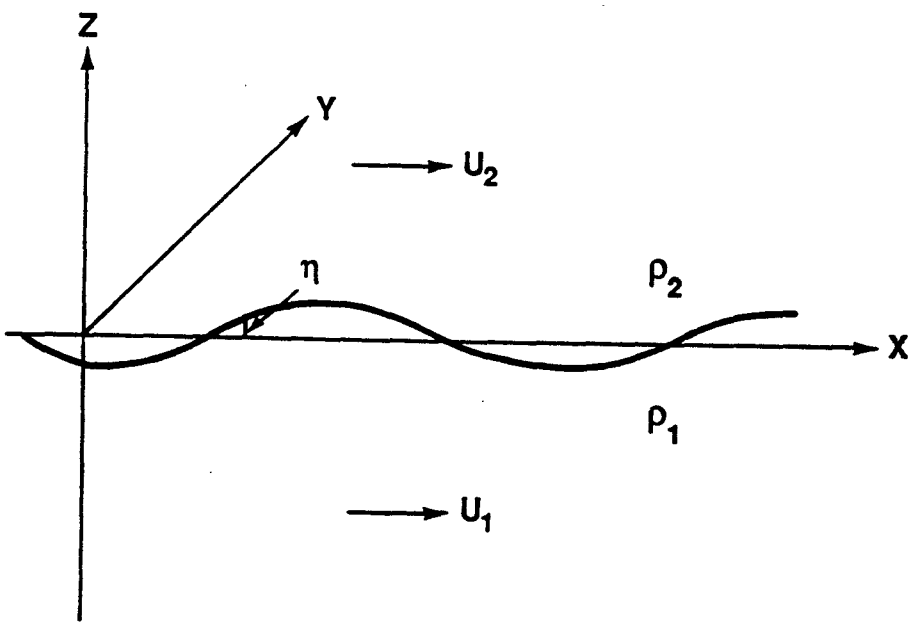

Figure 2.1: Definition sketch of the flow for the case of a vortex sheet

Boundary Conditions

(a) The initial disturbance is constrained to a finite region

$$\nabla \phi \to U \quad \text{as } z \to \pm\infty \tag{2.2}$$

(b) A particle at the interface moves with it, i.e.,

$$\frac{D[z - \eta(x,y,t)]}{Dt} = 0 \tag{2.3}$$

(c) Pressure is continuous across the interface

$$\begin{aligned} \rho_2(C_2 - \frac{\partial \phi_2}{\partial t} - \frac{1}{2}(\nabla \phi_2)^2 - gz) = \\ \rho_1(C_1 - \frac{\partial \phi_1}{\partial t} - \frac{1}{2}(\nabla \phi_1)^2 - gz) \qquad \text{at } z = \eta \end{aligned} \tag{2.4}$$

by Bernoulli's theorem.

Solution

The above equations pose the non-linear problem for instability of the basic flow. For linear stability, we consider

$$\phi_2 = U_2 x + \phi_2' \quad (z > \eta) \tag{2.5}$$

$$\phi_1 = U_1 x + \phi_1' \quad (z < \eta) \tag{2.6}$$

Products of small increments ϕ_1', ϕ_2' and η are neglected. There being no length scale in the basic flow, it is difficult to justify linearization as regards η. However, it appears plausible assuming that the surface displacement and it's slopes are small, and $g\eta \ll U_1^2, U_2^2$.

With these these assumptions, linearisation yields,

$$\nabla^2 \phi_2' = 0 \quad z > 0 \tag{2.7}$$

$$\nabla^2 \phi_1' = 0 \quad z < 0 \tag{2.8}$$

$$\nabla \phi_2' = 0 \quad z \to +\infty \tag{2.9}$$

$$\nabla\phi_1' = 0 \quad z \to -\infty \tag{2.10}$$

$$\frac{\partial\phi_i'}{\partial z} = \frac{\partial\eta}{\partial t} + U_i\frac{\partial\eta}{\partial x} \quad z = 0 \quad (i = 1,2) \tag{2.11}$$

$$\rho_1(U_1\frac{\partial\phi_1'}{\partial x} + \frac{\partial\phi_1'}{\partial t} + g\eta) = \rho_2(U_2\frac{\partial\phi_2'}{\partial x} + \frac{\partial\phi_2'}{\partial t} + g\eta) \quad z = 0 \tag{2.12}$$

We now use the method of normal modes, assuming that an arbitrary disturbance can be resolved into independent modes of the form,

$$(\eta, \phi_1', \phi_2') = (\hat{\eta}, \hat{\phi}_1, \hat{\phi}_2)\exp[i(kx + ly) + st] \tag{2.13}$$

[$s = \sigma + i\omega$, thus, if $\sigma > 0$, the mode is unstable, if $\sigma = 0$, the mode is neutrally stable and stable (asymptotically) for $\sigma < 0$]

Thus, equations (2.7) and (2.8) yield,

$$\hat{\phi}_i = A_i e^{-\hat{k}z} + B_i e^{\hat{k}z} \text{ where } \hat{k} = \sqrt{k^2 + l^2} \tag{2.14}$$

From equations (2.9) and (2.10),

$$\hat{\phi}_1 = A_1 e^{\hat{k}z} \tag{2.15}$$

$$\hat{\phi}_2 = A_2 e^{-\hat{k}z} \tag{2.16}$$

The coefficients can be evaluated from equation (2.11) as

$$A_1 = \hat{\eta}(s + ikU_1)/\hat{k} \tag{2.17}$$

$$A_2 = -\hat{\eta}(s + ikU_2)/\hat{k} \tag{2.18}$$

From equation (2.12), we can obtain,

$$\rho_1(U_1 A_1 e^{\hat{k}z} ik + A_1 e^{\hat{k}z} s + g\hat{\eta}) =$$
$$\rho_2(U_2 A_2 e^{-\hat{k}z} ik + A_2 e^{-\hat{k}z} s + g\hat{\eta}) \tag{2.19}$$

Thus, with the substitution of the coefficients,

$$\rho_1\{(s + ikU_1)^2 + \hat{k}g\} =$$
$$\rho_2\{-(s + ikU_2)^2 + \hat{k}g\} \tag{2.20}$$

which can be written as

$$s^2(\rho_1+\rho_2)+2iks(\rho_1U_1+\rho_2U_2)+$$
$$[\hat{k}g(\rho_1-\rho_2)-k^2(\rho_1U_1^2+\rho_2U_2^2)]=0 \tag{2.21}$$

This yields

$$s=\frac{-ik(\rho_1U_1+\rho_2U_2)}{\rho_1+\rho_2}\pm\sqrt{\frac{k^2\rho_1\rho_2(U_1-U_2)^2}{(\rho_1+\rho_2)^2}-\frac{\hat{k}g(\rho_1-\rho_2)}{\rho_1+\rho_2}} \tag{2.22}$$

Conclusions

Several conclusions are of interest here,

(1)If k = 0, then

$$s=\pm i\sqrt{\frac{g\hat{k}(\rho_1-\rho_2)}{\rho_1+\rho_2}} \tag{2.23}$$

i.e., perturbations transverse to the direction of streaming are unaffected by it's presence.

(2)In every other direction, instability occurs for all wave numbers with

$$k^2>\frac{g\hat{k}(\rho_1^2-\rho_2^2)}{\rho_1\rho_2(U_1^2-U_2^2)} \tag{2.24}$$

If the wave vector $\hat{k}$ is at an angle θ to U, $k=\hat{k}\cos\theta$, instability occurs for

$$\hat{k}>\frac{g(\rho_1^2-\rho_2^2)}{\rho_1\rho_2(U_1^2-U_2^2)\cos^2\theta} \tag{2.25}$$

For a given relative velocity of the layers, instability occurs for the minimum wave number when the wave vector is in the direction of streaming, i.e.,

$$k_{min}=\frac{g(\rho_1^2-\rho_2^2)}{\rho_1\rho_2(U_1^2-U_2^2)} \tag{2.26}$$

Instability occurs for $k>k_{min}$.

This predicts the onset and development of instability, no matter how small (U_1-U_2) may be. The presence of streaming overcomes the stability of the static arrangement. This is the classic Kelvin-Helmholtz instability. Helmholtz (1868) stated this as:

Every perfectly geometrically sharp edge by which a fluid flows must tear it asunder and establish a surface of seperation, however slowly the rest of the fluid may move.

However, if the effects of surface tension are considered, stability is predicted if,

$$(U_1 - U_2)^2 < \frac{2g}{k_{min}} \frac{\rho_1^2 - \rho_2^2}{\rho_1 \rho_2} \tag{2.27}$$

where, k_{min} = minimum wave number for stability.

With this condition, we have stability for,

$$(U_1 - U_2)^2 < \frac{2}{\rho_1 \rho_2} \sqrt{Tg(\rho_1 - \rho_2)} \tag{2.28}$$

where T is the surface tension.

2.2.2 Generalized Form of Kelvin-Helmholtz Instability

From the above discussion, for the case without surface tension, it can be inferred that the onset of Kelvin-Helmholtz instability is by the crinkling of the interface by shear, and this is independent of the magnitude of the relative velocity of the two layers. A natural question to confront the reader is whether this result is entirely fortuitous, due to the sudden discontinuity in the density and velocity profiles, and not be true for continuous distributions. Thus, now, we take the case of the stabilizing effect of gravity on a continuously stratified fluid and of the destabilizing influence of shear in a generalized form of Kelvin- Helmholtz instability. We start with a basic state in dynamic equilibrium,

$$u_* = U_*(z_*) \tag{2.29}$$

$$\rho_* = \bar{\rho}_*(z_*) \tag{2.30}$$

$$p_* = (p_0)_* - g \int_{z_{1_*}}^{z_{2_*}} \bar{\rho}(z'_*)\, dz'_* \tag{2.31}$$

for $z_{1_*} \leq z_* \leq z_{2_*}$, where, z_* is the height and z_{1_*} and z_{2_*} are the horizontal boundaries of the flow. The subscript * indicates dimensional quantities. Taking L,

U and ρ_0 to be the characteristic length, velocity and density, respectively, of the basic flow and further assuming the fluid to be inviscid and density to be convected but not diffused, we non-dimensionalize the equations of motion, incompressibility and continuity to get,

$$\rho(\frac{\partial u}{\partial t} + u.\nabla u) = -\nabla p - F^{-2}\rho\vec{k} \tag{2.32}$$

$$\nabla.u = 0 \tag{2.33}$$

$$\frac{\partial \rho}{\partial t} + u.\nabla \rho = 0 \tag{2.34}$$

where F $= V/\sqrt{gL}$ is a Froude number.

Perturbations are introduced into the flow,

$$u(x,t) = U(z)\vec{i} + u'(x,t) \tag{2.35}$$

$$\rho(x,t) = \bar{\rho}(z) + \rho'(x,t) \tag{2.36}$$

$$p(x,t) = p_0 - F^{-2}\int_z \bar{\rho}(z')\,dz' + p'(x,t) \tag{2.37}$$

The form of the equations obviously permits us to take normal modes of the form,

$$\{u'(x,t), p'(x,t), \rho'(x,t)\} = \{\hat{u}(z), \hat{p}(z), \hat{\rho}(z)\}\exp[i(\alpha x + \beta y - \alpha ct)] \tag{2.38}$$

where, the real part is understood. The fact that the solutions must remain bounded as x, y $\rightarrow \pm\infty$ implies that α, β must be real; but, the wave speed c may, in general, be complex, i.e., c $= c_r + ic_i$ thus representing waves traveling in the direction $(\alpha, \beta, 0)$ with phase speed $\alpha c_r/\sqrt{\alpha^2+\beta^2}$ and grow/decay in time as $\exp(\alpha c_i t)$. Thus, $\alpha c_i > 0$ implies instability, $\alpha c_i < 0$ stability, while $\alpha c_i = 0$ implies neutral stability.

Introducing these into equations (2.32)- (2.34), and linearizing by neglecting quadratic terms of the primed quantities and using equation (2.38) we obtain,

$$i\alpha\bar{\rho}(U-c)\hat{u} + \bar{\rho}U'\hat{w} = -i\alpha\hat{p} \tag{2.39}$$

$$i\alpha\bar{\rho}(U-c)\hat{v} = -i\beta\hat{p} \tag{2.40}$$

$$i\alpha\bar{\rho}(U-c)\hat{w} = -D\hat{p} - F^{-2}\hat{\rho} \tag{2.41}$$

$$i\alpha\hat{u} + i\beta\hat{v} + D\hat{w} = 0 \tag{2.42}$$

$$i\alpha(U-c)\hat{\rho} + \bar{\rho}'\hat{w} = 0 \tag{2.43}$$

where differentiation with respect to z of a basic quantity is denoted by prime whereas that of a perturbation by D.

Thus, from equations (2.39) and (2.40),

$$\hat{u} = \frac{i\alpha\hat{p} - \bar{\rho}U'\hat{w}}{i\alpha\bar{\rho}(U-c)} \tag{2.44}$$

$$\hat{v} = -\frac{\beta\hat{p}}{\alpha\bar{\rho}(U-c)} \tag{2.45}$$

Using these in conjunction with equation (2.42), we can obtain,

$$\frac{-i\alpha\hat{p} - \bar{\rho}U'\hat{w}}{\bar{\rho}(U-c)} - \frac{i\beta^2\hat{p}}{\alpha\bar{\rho}(U-c)} + D\hat{w} = 0 \tag{2.46}$$

Eliminating $\hat{p}$ and $\hat{\rho}$, we finally arrive at,

$$(U-c)\{D^2\hat{w} - (\alpha^2+\beta^2)\hat{w}\} - U''\hat{w} - \frac{(\alpha^2+\beta^2)\bar{\rho}'}{\alpha^2F^2(U-c)\bar{\rho}}\hat{w} + \frac{\bar{\rho}'}{\bar{\rho}}\{(U-c)D\hat{w} - U'\hat{w}\} = 0 \tag{2.47}$$

Yih (1955) applied Squire's transformation to the system to show that for a three-dimensional (3-D) wave with wave number (α,β), there is a 2-D wave with the same complex velocity c, but wave number $(\sqrt{\alpha^2+\beta^2},0)$ and Froude number $\alpha F/\sqrt{\alpha^2+\beta^2}$, which thus has effectively reduced gravity but magnified growth rate $(\alpha^2+\beta^2)c_i$ and thus is more unstable.

Equation (2.47) indicates that F^{-2} occurs as a product of $-\bar{\rho}'/\bar{\rho}$, so an overall Richardson number is defined as

$$Ri = -\frac{\bar{\rho}'}{\bar{\rho}F^2} = -\frac{gL^2}{V^2}\frac{d\bar{\rho}_*}{\bar{\rho}_*\,dz_*}$$

The Brunt-Väisälä frequency (or buoyancy frequency) N_* is defined as

$$N_*^2(z_*) = -g\frac{d\bar{\rho}_*}{dz_*}/\bar{\rho}_* = RiN^2(z)V^2/L^2$$

Thus, we get,

$$\begin{aligned} RiN^2/U'^2 &= -\frac{L^2}{V^2}\frac{g}{\bar{\rho}_*}\frac{d\bar{\rho}_*}{dz_*}/(\frac{dU}{dz})^2 \\ &= -g\frac{d\bar{\rho}_*}{dz_*}/\{\bar{\rho}_*(\frac{dU_*}{dz_*})^2\} \end{aligned}$$

as the local Richardson number, J, of the flow at each height z_*, such that

$$J = N_*^2(z)/(\frac{dU_*}{dz_*})^2 \tag{2.48}$$

In many applications, $\bar{\rho}_*(z_*)$ varies more slowly with height than $U_*(z_*)$ such that $-\bar{\rho}_*'/\bar{\rho} \ll 1$; whence Ri is of the order of magnitude unity as $F \ll 1$. Thus, as in the Boussinesq approximation the last two terms of equation (2.47) are neglected; hence, the effect of variation of density is neglected in inertia but retained in buoyancy.

With this approximation and considering only 2-D waves we get,

$$\frac{d^2\hat{w}}{dz^2} = \alpha^2\hat{w} + \frac{d^2U}{dz^2}\frac{1}{U-c}\hat{w} + \frac{RiN^2}{(U-c)^{-2}}\hat{w} \tag{2.49}$$

which can be written as

$$(U-c)(D^2-\alpha^2)\phi - U''\phi + RiN^2\phi/(U-c) = 0 \tag{2.50}$$

with the corresponding boundary conditions at $z = z_1$ and z_2, which is the Taylor-Goldstein equation, where

$$\hat{u} = \partial\phi/\partial z \tag{2.51}$$

$$\hat{w} = -i\alpha\phi(z) \tag{2.52}$$

$$u' = \partial\psi'/\partial z \tag{2.53}$$

$$w' = -\partial\psi'/\partial x \tag{2.54}$$

$$\psi' = \phi(z)\exp\{i\alpha(x-ct)\} \tag{2.55}$$

Here, $\alpha \geq 0$ can be assumed without any loss of generality, and also that each unstable mode has a conjugate stable one.

Assuming $c_i \neq 0$, define

$$H = \phi/\sqrt{U-c} \tag{2.56}$$

Substituting into equation (2.50) yields,

$$D\{(U-c)DH\} - \{\alpha^2(U-c) + \frac{U''}{2} + (\frac{U'^2}{4} - RiN^2)/(U-c)\}H = 0 \tag{2.57}$$

Multiplying by the complex conjugate, H^* and integrating,

$$\int_{z_1}^{z_2}\{(U-c)\{|DH|^2 + \alpha^2|H|^2\} + \frac{1}{2}U''|H|^2 + \frac{U'^2/4 - RiN^2}{U-c}|H|^2\}\,dz = 0 \tag{2.58}$$

The imaginary part gives,

$$-c_i\int_{z_1}^{z_2}\{|DH|^2 + \alpha^2|H|^2 + (RiN^2 - U'^2/4)|H|^2/|U-c|^2\}\,dz = 0 \tag{2.59}$$

Thus,

$$\begin{aligned} 0 &> -\int_{z_1}^{z_2}|DH|^2\,dz \\ &= \int_{z_1}^{z_2}\{(RiN^2 - U'^2/4) + \alpha^2|U-c|^2\}|H|^2/|U-c|^2\,dz \end{aligned} \tag{2.60}$$

(assuming $c_i \neq 0$). Thus, the local Ri has to satisfy $RiN^2/U'^2 < 1/4$ somewhere in the field of flow for instability.

The same can also be established, although somewhat heuristically, by analyzing the energy budget; the essential mechanism of instability being the conversion of the available kinetic energy of the layers into kinetic energy of the disturbance, overcoming the potential energy needed to raise or lower the fluid when $d\bar{\rho}_*/dz_* < 0$ everywhere. Consider two neighboring fluid particles of equal volumes at heights z_* and $z_* + \delta z_*$ being interchanged.

Thus, δW = work per unit volume needed to overcome gravity = $-g\delta\bar{\rho}_*\delta z_*$.

For horizontal momentum to be conserved, the particle at z_* will have final velocity $(U_* + k\delta U_*)\vec{i}$ and the particle at $z_* + \delta z_*$ have $(U_* + (1-k)\delta U_*)\vec{i}$ as it's final velocity, where, k = some number between 0 and 1, and

$$\delta U_* = (\frac{dU_*}{dz_*})\delta z_* \tag{2.61}$$

Thus, the kinetic energy per unit volume released by the basic flow is,

$$\begin{aligned}\delta T &= \frac{1}{2}\bar{\rho}_* U_*^2 + \frac{1}{2}(\bar{\rho}_* + \delta\bar{\rho}_*)(U_* + \delta U_*)^2 \\ &\quad - \frac{1}{2}\bar{\rho}_*(U_* + k\delta U_*)^2 - \frac{1}{2}(\bar{\rho}_* + \delta\bar{\rho}_*)(U_* + (1-k)\delta U_*)^2 \qquad (2.62)\\ &= k(1-k)\bar{\rho}_*(\delta U_*)^2 + U_*\delta U_*\delta\bar{\rho}_* \qquad (2.63)\\ &\leq \frac{1}{4}(\delta U_*)^2\bar{\rho}_* + U_*\delta U_*\delta\bar{\rho}_* \qquad (2.64)\end{aligned}$$

A necessary condition for this interchange, and consequently, instabilty is $\delta W \leq \delta T$, and therefore, somewhere in the field of flow,

$$-g\frac{d\bar{\rho}_*}{dz_*} \leq \frac{1}{4}\bar{\rho}_*(\frac{dU_*}{dz_*})^2 + U_*\frac{dU_*}{dz_*}\frac{d\bar{\rho}_*}{dz_*} \qquad (2.65)$$

i.e.,

$$\frac{-g\frac{d\bar{\rho}_*}{dz_*}}{\bar{\rho}_*(\frac{dU_*}{dz_*})^2} \leq \frac{1}{4} \qquad (2.66)$$

neglecting the inertial effects of the variation of density.

Miles (1961) stated that the sufficient condition for an inviscid, continuously stratified flow to be stable to small disturbances is that the local Richardson number should exceed $\frac{1}{4}$ everywhere in the flow (a modified result is presented in Appendix B). This does not imply that the flow becomes unstable if this falls below $\frac{1}{4}$ somewhere. Counter examples have been found, for example, with a jet-like velocity profile u$\propto$ sech^2 z and an exponential density profile, in which case the flow can become unstable if $Ri_{min} < 0.214$. Hazel (1972) has demonstrated the stabilizing effect of rigid boundaries. One must consequently surmise that the entire profile (the boundary conditions, viscosity, etc.) matters in determining the critical Richardson number.

Thus, it is seen that the effect of velocity-shear on statically stable stratification can be to cause disturbances to appear at density interfaces which grow with time. Intuitively, one can sense that after a period of sustained growth, the wave should break, with the natural ramification being upward mixing of the denser fluid, i.e. entrainment.

With the preceding background of the theory of velocity-shear induced interfacial instability, we now proceed to Chapter 3 where pertinent work on the same phenomenon is reviewed. Some examples of numerical and laboratory simulations are covered to give a feel for the magnitude as well as different facets of the problem.

æ

CHAPTER 3
INSTABILITY OF STRATIFIED SHEAR FLOWS

3.1 Background

As noted in Chapter 1, shear induced instabilities are a very important factor in the generation of turbulence and mixing in stratified flows. When $\delta_s \simeq \delta$ and $d \simeq 0$ (see Figure 3.1), at sufficiently low Ri ($= \frac{g\delta_s\Delta\rho}{\rho(\Delta U)^2}$), the primary instability is of the Kelvin-Helmholtz (KH) type; however, the process of growth by pairing becomes limited by the stabilizing effects of buoyancy (Corcos and Sherman 1976) and a sufficiently large density difference will stabilize the flow.

As it is relevant in geophysical situations, the case of $\delta_s \gg \delta$, with d = 0 was studied by Holmboe (1962), who predicted a second mode of instability, now called the Holmboe mode, which has been further studied by a number of researchers, for example Hazel (1972). Theoretically, this comprises of two trains of growing interfacial waves traveling in opposite directions to the mean flow, eventually resulting in a series of sharply cusped crests protruding alternately into each layer, with wisps of fluid being ejected from these cusps (but, more often, experimental results indicate cusping only into the high speed layer which may possibly be attributed to the selective vorticity concentrations in the high speed layer). Thus, when $\delta_s/\delta \gg 1$, theoretically, there is always a range of wavenumbers which is unstable, however large Ri may be, with this second mode having maximum amplification rates at non-zero Ri.

For small Ri , transition to turbulence is by the first mode (i.e., KH) regardless of δ_s/δ values, with collapse by overturning due to the concentration of the available vorticity into discrete lumps along the interface (Thorpe 1973). This results in finer

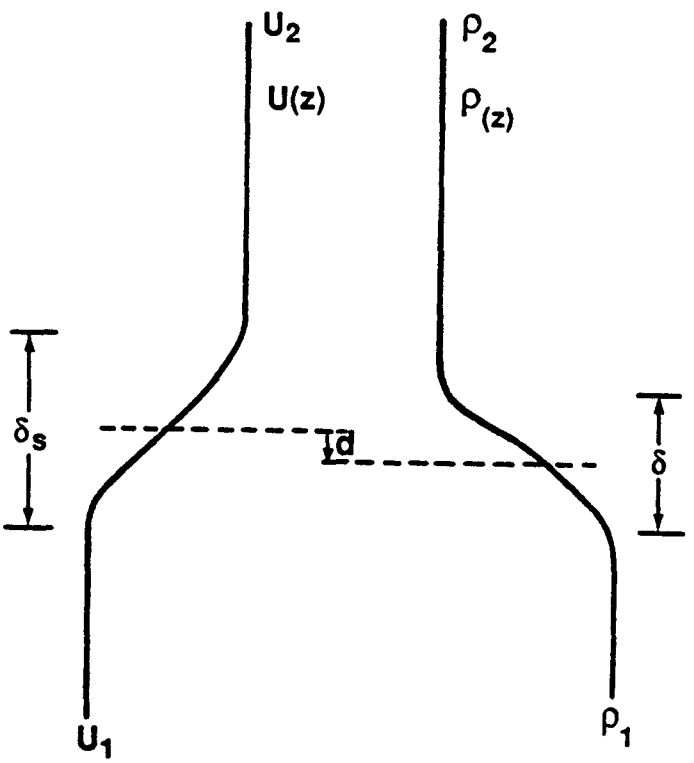

Figure 3.1: Offset Velocity and Density Profiles

scales of turbulence, and in a homogeneous fluid these lumps continue to pair with the growth of the mixed layer. However, with stratification, entrainment of fluid into the mixing layer degrades this vorticity in these lumps and this mixed layer growth eventually stops, and if the initial Ri is small, turbulence grows till length scales become large enough for buoyancy to play an important role, followed by collapse. If $\delta_s/\delta \gg 1$, this collapse is followed by mode 2 waves (Browand and Winant 1973). These seem to be like internal waves within the mixing layer, with nearly horizontal wave crests and small wavelengths (Delisi and Corcos 1973); and, finally, there is decay of the turbulence structure. Fernando (1988) mentions that turbulent patches in stratified media may be generated by the mechanism of instability (by wave-breaking and double diffusion).

Thus, stratification has this ability to destroy turbulence which may be a possible explanation for it's intermittent character, as found in nature. McLean (1985) observed longitudinal ripples on the bed while modeling deep ocean sediment transport, which he postulated to occur during deposition after high energy erosional events due to helical circulation owing to a non-uniform turbulence field. This kind of turbulence field can result because of lateral homogeneity of turbulence damping by the aforementioned density stratification. Physically, this turbulent mixing layer is destroyed by the stabilizing effect of gravitation on the largest scales of Ri.

When the initial Ri is large enough, say > 0.1, then turbulence production depends strongly on the d/δ ratio, with initial instability of the mode 2 waves. These decay by breaking at sharply peaked crests (Browand and Winant 1973), with fluid ejected into the higher speed layer as thin wisps from these crests.

3.2 Literature Review

3.2.1 Browand and Wang (1971)

Background

A velocity shear interface of thickness δ_s is considered between two horizontal streams of velocities U_1 and U_2 and densities ρ_1 and ρ_2, with the density interface of thickness δ. They define $Ri = \Delta b \delta_s / (\Delta U)^2$.

The velocity profiles agreed remarkably well with the hyperbolic function, often used in stability analysis. The difference between the stability of a sheared layer which is homogeneous and that which has a stable density interface was demonstrated.

Discussion

The effect of stratification on sheared layers is complex, with the mode unstable in the absence of stratification, called Rayleigh waves, being stabilized while a new one, the Holmboe mode is now unstable. The mode destabilized by gravity has a non-zero wave speed when riding at the mean velocity $(U_1 + U_2)/2$. In these co-ordinates, the disturbance is assumed to consist of one wave traveling upstream and one traveling downstream, with the interface a standing wave of increasing amplitude.

Disturbances in the case of a homogeneous shear layer can be thought of as two almost independent distortions of the upper and lower boundaries of the constant vorticity region. Short wave length disturbances are totally independent. The amplitude of the disturbance oscillates as the two distortions alternately reinforce and obstruct. However, long wavelength disturbances influence each other to such an extent that "slippage" of the upper and lower distortions can be stopped. The relative phase is fixed in the position most favorable for growth (PFMMG) of the perturbation. In the stratified case, additional vorticity is generated by the distor-

tion of the central interface. This baroclinic vorticity is responsible for inhibiting instability at low Richardson numbers (Rayleigh waves); however, at high Ri, stratification alters the slippage of the distortions such that the wave lingers more at the PFMMG than in unfavorable regions (Holmboe waves).

In the regions of instability of Rayleigh waves, both Holmboe and Rayleigh waves are indistinguishable, both being phase locked, and non-linear growth is by roll-up or overturning. Previously well distributed vorticity is now concentrated into discrete lumps along the interface and breaking is violent.

In regions where Holmboe waves are unstable, no roll-up occurs. Interface displacement simply grows in magnitude with each succeding oscillation, ultimately breaking at the crests, which may be on both sides or not, according to as the excitation is unforced or not, respectively.

3.2.2 Smyth, Klaassen and Peltier (1987)

These investigators performed numerical simulations of the evolution of Holmboe waves. A series of simulations using progressively lower levels of stratification led to Kelvin - Helmholtz (KH) waves. The effect of strong statification on KH waves depends on the ratio of the vertical distances over which the density and flow velocity, i.e., δ and δ_s , change.

- If $\delta \geq \delta_s$, increasing stratification stabilizes the flow.
- If $\delta < \delta_s/2$, increasing stratification causes the KH wave be replaced by Holmboe type oscillatory waves.

From linear theory, the relationship between KH and Holmboe type instabilities can be shown to be equivalent to a damped oscillator, governed by,

$$A''(t) + bA'(t) + cA(t) = 0$$

Stratification, represented by c, provides the restoring force. Shear, represented by b, serves to transfer energy into or out of the oscillation.

Solutions are of the form $A \sim e^{\sigma t}$, where $\sigma = \sigma_r + i\sigma_i$, subscripts denoting real and imaginary parts respectively. If $\sigma_i = 0$, we have a monotonically growing disturbance, i.e., KH waves. However, if c/b^2, which is analogous to the bulk Richardson number, grows beyond a certain value, this train gives way to oscillatory Holmboe waves.

A linear analysis of the governing hydrodynamic equations was performed to determine, for a given level of stratification and Ri (with δ_s being the length scale), the value of α, the wave number, which has maximum growth rate, σ_r, to determine the horizontal wave length to impose on the non-linear model.

The plot of $\sigma(\alpha, Ri)$ showed that, for small values of $Ri(< 0.3)$, the fastest growing modes had $\sigma_i = 0$; while for higher Richarson numbers, σ_i had non-zero values, i.e, Holmboe instability. Two points were taken from the Holmboe regime and one from the KH regime for non-linear analysis. By analysing the evolution of the non- dimensional perturbation kinetic energy for the three points they confirmed the nature of the instabilities predicted by the linear analysis : slow exponential growth coupled with fast oscillations characterising disturbances in the Holmboe regime and monotonically growing waves in the KH regime.

Holmboe waves have two components, with equal growth rates and equal but oppositely directed phase speeds. The position most favorable for growth (PMFFG) is just before the "in-phase" configuration in accordance with Holmboe (1962). In the "in- phase" configuration, the kinetic energy is maximized. The phase speed is maximum just beyond this "in-phase" position. This implies that as the level of stratification decreases, the maximum phase speed increases relative to the cycle averaged speed, resulting in a greater time spent in the PMFFG and thus effecting increasing growth rates. When this level of stratification is further decreased, the phase speed at the PMFFG should vanish, with phase locking of the two components. They should now rotate as a unit and grow into intertwined fingers of heavy

and light fluid as in KH waves.

With decreased stratification in the Holmboe regime, growth rates and oscillation frequency reduced as predicted, and also, the phase speed increased after leaving the "in-phase" position. With evolution, thin plumes of fluid were ejected from the peaks of the waves, primarily after passing the "in-phase" configuration. The KH regime simulation, too, was in accordance with linear predictions.

3.2.3 Lawrence, Lasheras and Browand (1987)

Two layers of different velocities and densities were seperated by interfaces of thicknesses δ_s and δ, respectively. The centers of the two interfaces were seperated by a distance d.

Theoretical Analysis

An eigenvalue relation was derived from the Taylor- Goldstein equation and stability diagrams are plotted of Ri vs. α, for different values of ϵ, where, $Ri = \frac{\Delta b \delta_s}{(\Delta U)^2}$, $\alpha = k\delta_s =$ instability wave number, $\epsilon = 2d/\delta_s$, $\Delta b = \frac{\rho_1 - \rho_2}{\rho_0}$, $\Delta U = |U_1 - U_2|$, $k = 2\pi/\lambda$, and $\lambda =$ wavelength .

With $\epsilon = 0$, there were two modes of instability : a non-dispersive Kelvin - Helmholtz type for $Ri < 0.07$ and a dispersive one, the Holmboe type, for all (positive) Ri. In the overlap region, $0 < Ri < 0.07$, KH had higher amplification rates. For $\epsilon > 0$, the KH mode as well is dispersive and has higher growth rates. For $\epsilon > 1$, the Holmboe mode disappeared.

Experimental Observations

For $\epsilon > 0$, concentrated spanwise vorticity was observed above the interface, in the high speed layer only (and none in the lower low speed layer), causing interfacial cusping into the upper layer. Initial instability was two dimensional. As Ri decreased, the wavelength of the disturbances increased. At lower Ri, disturbances developed considerable three dimensionality, with wave breaking, similar to KH billows. This billowing was only in small wisps, demonstrating the inhibiting effect of

buoyancy. With increasing Ri, at fixed ϵ, this tendency decreased and thin wisps were lifted almost vertically into the upper layer. Instabilities were observed to pair in the same manner as KH instabilities in unstratified fluid, with wisps ejected, just after this pairing.

3.2.4 Narimousa and Fernando (1987)

The investigators discuss the effects of velocity induced shear at the density interface of a two-fluid system. One of their most important conclusions has been regarding the entrainment- Richardson number relationship : $E_u \propto (Ri_u^{-n})$, where, E_u is an entrainment coefficient $= u_e/u$, $u_e =$ entrainment velocity, $u =$ scaling velocity, $Ri =$ Richardson number $= \Delta b h/u^2$, $\Delta b =$ interfacial buoyancy jump, $h =$ mixed layer depth, and $n =$ a coefficient.

The investigators used a recirculating flume, which was free of the rotating screen of the more popular annular flume experiments. Their two-fluid system consisted of initially fresh and salt water layers. The mixed layer (of initially fresh water) was selectively driven over the heavier quiescent fluid by using a disk pump, developed by Odell and Kovasznay (1971). The velocity of the mixed layer was varied betwen 5 - 15 cm/s using variable pump rotation rates. Shear layer velocity profile appeared linear while that in the viscous diffusive momentum layer resembled Couette flow profiles.

For moderately high Richardson numbers, $Ri_u > 5$, the density interface was found to be topped by a thin layer of thickness δ_I, with a weak density gradient which had not yet got well mixed. This partially mixed fluid results owing to the fact that energy of the eddies is not strong enough to entrain the fluid from the stable interfacial layer, and mixing can only occur by wave breaking resulting from the mixed layer turbulence at higher Richardson numbers, i.e., eddies assist entrainment in two stages, from the interface to the intermediate layer and from there into the mixed layer.

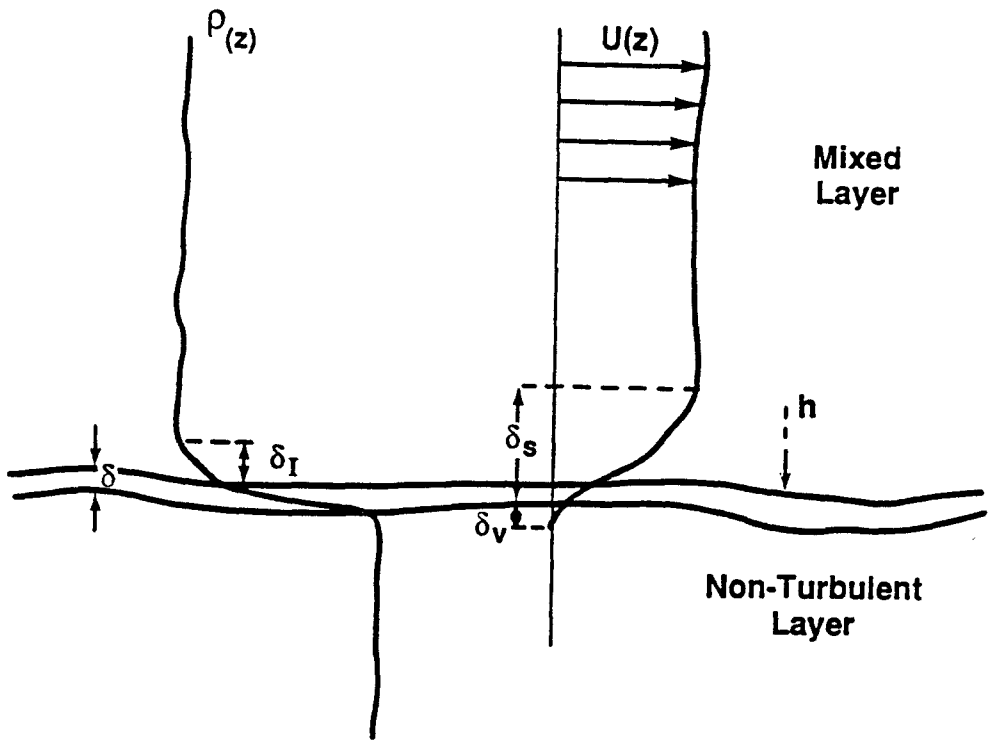

Figure 3.2: Physical description of the complete flow configuration, with density and velocity profiles (adapted from Narimousa and Fernando 1987.

Fluid above this layer was homogeneous. At low Ri_u, with high rates of entrainment, the intermediate layer was absent. The entrainment interface consisted of regularly spaced billows with high spatial density gradients within, with their centers having small scale irregularities which could be the effect of local instability regions due to the entrainment of heavy and light fluid into the core. However, the final stage of mixing within these billows was fairly slow, with breakdowns into regions containing small scale structures which may be due to the interaction of two adjacent vortices. With increasing Ri_u, the frequency of billows progressively decreased and entrainment was dominated by a wave breaking process, with wisps of fluid being ejected into the upper layer. This kind of behavior was seen over a whole range of $Ri_u (5 < Ri_u < 20)$, with decreasing frequency as Ri_u increased. Also, large amplitude non-breaking solitary waves were seen over $Ri_u = 10 - 20$.

The shear layer is very important as it is reponsible for the turbulent kinetic energy of entrainment and thereby controls the size of the energy containing eddies at the interface. The investigators found that δ_s/h was independent of Ri_u (and about 0.2) indicating that the size of the eddies should be scaled by h.

The average measured value of δ/h was also independent of Ri_u, and around 0.04-0.08. This ratio was also confirmed by another interpretation of data as follows:

Observing that the buoyancy in the mixed layer and the gradient in the interface are constant,

$$b(z) = b_\infty + \Delta b(z - h - \delta)/(\delta) \text{ for } (h < z < h + \delta) \tag{3.1}$$

where, $b(z)$ = mean buoyancy at elevation z, b_∞ = buoyancy of lower unperturbed layer, and z is positive down from the free surface.

Assuming horizontal homogeneity, Long (1978) integrated the buoyancy conservation equation,

$$\frac{\partial b}{\partial t} = \frac{\partial q}{\partial z} \tag{3.2}$$

where, $q(z) = -\overline{bw}$ = buoyancy flux; b and w being the values of buoyancy and vertical velocity fluctuations, respectively.

This yielded,

$$q(z) = q_2 z/h \quad (0 < z < h) \tag{3.3}$$

$$q_2 = -h\frac{d(\Delta b)}{dt} \tag{3.4}$$

$$q(z) = q_2 + (\frac{\tau^2}{2\delta} - \tau)\frac{d(\Delta b)}{dt} - \frac{\Delta b \tau^2}{\delta^2}\frac{d\delta}{dt} - \frac{\Delta b}{\delta}\tau\frac{dh}{dt} \quad (h < z < h + \delta) \tag{3.5}$$

where, q_2 = buoyancy flux at the entrainment interface, and τ = z - h.

As $q(h + \delta) = 0$, it is possible to obtain

$$\frac{d\{\Delta b(h + \delta/2)\}}{dt} = 0 \tag{3.6}$$

By defining a characteristic velocity scale based on the initial buoyancy jump and the depth of the initially homogenous layer, i.e.,

$$V_0^2 = h_0 \Delta b_0$$

and defining $\delta = \alpha h$ one finally arrives at

$$h(1 + \alpha/2) = V_0^2/\Delta b \tag{3.7}$$

Plotting this equation showed $\delta \sim 0.06h$.

Energy Budget Analysis

Analysis of the energy budget yielded the result that buoyancy flux, turbulent energy production and dissipation terms were of the same order and that $E \sim Ri_u^{-1}$.

Wave amplitudes at the interface, δ_w, scaled by h were of the order of $Ri_u^{-1/2}$. This may possibly be due to the energy containing eddies impinging on the interface. The vertical kinetic energy of the eddies = w_1^2 (where w_1 is the rms fluctuation of the vertical velocity). Then the generated potential energy of the waves $\sim N^2\delta_w$. Thus, $\delta_w \sim w_1/N$, where N = $(\Delta b/\delta)^{1/2}$ = boundary frequency of the interfacial

layer.

$$\delta \sim h \tag{3.8}$$

$$w_1 \sim \Delta u \tag{3.9}$$

Hence,

$$\frac{\delta_w}{h} \sim Ri_u^{-1/2} \tag{3.10}$$

Summary

(1)During entrainment, two layers, the density interfacial layer and the shear layer, having direct bearing on the entrainment process developed and increased linearly, independent of Ri_u.

(2)Billows, formation and breakdown of large ordered vortices cause mixing at low Ri_u, while breaking waves cause it at higher Ri_u.

(3)Wave amplitudes scaled well with the size of the energy containing eddies of the size of the mixed layer.

(4)The rates of work done against buoyancy forces, kinetic energy dissipation and shear production of turbulent kinetic energy were of the same order.

3.3 Conclusions

The preceding discussion documents some of the modes of interfacial instability which are possible. The mode of instability is dependent on the stratification and the ratio of the thicknesses of the shear layer and the density interface. When $\delta_s/\delta \gg 1$, increasing stratification causes monotonically growing Kelvin-Helmholtz waves to be replaced by the oscillatory Holmboe mode. The physical nature of the modes differs as well, in that Kelvin-Helmholtz waves are associated with billowing and lumping (and pairing) of vorticity near the interface, while Holmboe waves are characterized by a series of non-linearly crested waves cusping generally into the high speed layer only. Billowing as well as cusping into the high speed layer were observed in laboratory experiments by Narimousa and Fernando (1987) with the transition

in the mode of instability occuring with increasing Richardson number. Moore and Long's (1971) experiments to determine entrainment rates in velocity-sheared salt-stratified systems (see Chapter 4) also describe some of these phenomena in detail. In effect, it can be concluded that velocity-shear has a destabilizing effect on stable stratification and can cause upward mixing of the heavier fluid. This effect of the growth and breakdown of instabilities is examined in the next chapter.

CHAPTER 4
ENTRAINMENT IN STRATIFIED SHEAR FLOWS

4.1 General Aspects

The effect of interfacial instabilities in causing entrainment across the (statically) stable density interface is considered in this chapter. As a considerable amount of worthwhile and interesting work has been done on both shear flows and flows without mean shear, a complete review is beyond the current scope. Thus, only directly pertinent studies as regards shear flows are reviewed. Moore and Long (1971) discuss their results with respect to those obtained by previous investigators and Long (1974) theoretically examines many of these results, thereby making this literature especially riveting. A recent experimental study by Narimousa, Long and Kitaigorodskii (1986) is also reviewed. Not much published work is available specifically regarding vertical entrainment of fluid muds, and thus the study using kaolinite by Wolanski, Asaeda and Imberger (1989) is reviewed in spite of it being for a mean-shear free environment.

4.2 Moore and Long (1971)

The experiments were run in a racetrack shaped flume with a system of holes and slits in the floor and in the ceiling, allowing fluid injection and withdrawal to produce required steady state horizontally homogeneous shearing flows. Their steady state was defined as keeping the level of the density inflexion point constant.

In the steady state two-layer experiments, the density and velocity profiles were kept constant by adjusting the flow rates and replenishing salt to the lower saline layer. This amount of salt per unit time, on dividing by the horizontal cross section

area of the flow tank, gave the salt mass flux.

In the entrainment experiments, the tank was filled with fluid with a linear density gradient and then circulation of either fresh or salt water was started and the density profile observed as a function of time.

4.2.1 Results of Two Layer Steady State Experiments

The investigators' overall Richardson number was defined as, $Ri_o = \hat{H}\Delta b/(2\Delta u)$ where, $\hat{H}$ = total depth, Δb = buoyancy difference between the top and bottom layers of fluid, and $2\Delta U$ = velocity difference between the top and bottom layers of fluid. Also, q = buoyancy flux, and, $Q = q/\Delta b(2\Delta U)$ = non- dimensional buoyancy flux.

A layer of thickness δ_s, with a velocity gradient, seperating two homogeneous layers of depths h each, developed. At low Ri_o, δ_s was very large and decreased with increasing Ri_o, until it ultimately became quite small.

For values of Ri_o greater than about three, turbulence in each homogeneous layer caused erosion to a considerable extent of the layer over which the density gradient initially manifested. The interface was clearly visible. The surface of the interface was irregular in shape (with amplitudes $\sim$ 0.5 cm, wavelength $\sim 3-4$ cm and width $\sim$ 1 cm) with wisps of fluid being detached from the crests of disturbances, this phenmenon being more observable for disturbances cusping into the lower density layer. The speed of these waves was less than of the homogeneous layer above. These grew in amplitude and then simply disappeared with a wisp of fluid ejected from the tip, indicating that the original disturbance may well have been caused by eddies scouring the interface, with it's "roller action" drawing dense fluid up into a crest before it sharpened and was sheared off.

For values $1.5 < Ri_o < 3.0$, the interface was less sharp and more diffuse (with δ_s increasing). The thickness of the region with the density gradient, δ, also increased, as did the salt mass flux. Mixing now seemed to be more due to

internal wave breaking. For $Ri_o < 1.0$, very large eddies extended through the diffused interface. For low values of Ri, $\delta_s \simeq \delta$ while for higher values of Ri_o, $\delta_s > \delta$. Richardson number, Ri_{o_δ}, defined using the average density gradient and average velocity gradient over δ, had a value close to one.

Plotting the non-dimensional buoyancy flux with Ri_o yielded the functional relationship

$$Q = C_1/Ri_0 \tag{4.1}$$

with C_1, which may be weakly dependent on kinematic viscosity and diffusivity, having a value $\sim 8 \times 10^{-4}$.

Other researchers have obtained relationships between E and Ri, where

$$E = u_e/u \tag{4.2}$$

with the entrainment velocity u_e defined as the normal velocity of the interface, or for steady flow experiments, the volume flow rate of the fluid being entrained divided by the cross sectional area over which this is occuring, u = some representative velocity and Ri = Richardson number computed for that particular experiment, with $\Delta\rho$ always representing the density jump between the turbulent homogeneous layer and the fluid being entrained.

Rouse and Dodu (1955) used a two layer fluid system with turbulence being generated by a mechanical agitator and pointed out that if the entrainment rate is proportional to Ri^{-1}, the implication is that the rate of change of potential energy due to entrainment is proportional to the rate of production of turbulent energy by the agitator.

Ellison and Turner (1959) discussed entrainment rates of a layer of salt water of thickness D flowing with velocity $\bar{u}$ under a layer of fresh water. Defining $Ri = \Delta bD/\bar{u}^2$, they obtained $E \sim Ri^{-1}$ for $Ri \leq 1$.

Lofquist (1960) got a similar relationship for $Ri < 1$, but his data were scattered

for $Ri > 1$, with a faster decrease in entrainment rates than is indicated by $E \sim Ri^{-1}$.

Turner (1968) studied mixing rates across a density interface with turbulence being generated on either or both sides by a mechanical agitator and obtained $E \sim Ri^{-1}$ for $Ri < 1$, but $E \sim Ri^{-3/2}$ for $Ri > 1$.

Kato and Phillips (1969) applied a constant shear stress $\tau = \rho u_*^2$ at the upper surface of a linearly stratified fluid and obtained $E \sim Ri_*^{-1}$, with values of Ri_* equivalent to $Ri_o < 1$. These investigators also demonstrated that the entrainment coefficient E represented a time rate of change of potential energy per unit mass V_1, in non- dimensional terms, i.e.,

$$\frac{2\rho_0}{g\Delta\rho u_*}\frac{dV_1}{dt} = \frac{u_e}{u_*} = E = KRi_*^{-1} \tag{4.3}$$

with, $Ri_* = g\frac{\Delta\rho}{\rho_0}h/u_*^2$ and K is some constant.

Moore and Long (1971) used this basis to compare their functional relationship with other researchers and showed that the non-dimensional flux is essentially the same as an entrainment coefficient. Another way of showing this relationship is as follows :

If the injection-withdrawal system at the top is turned off and the interface allowed to rise a distance dh = u_e dt, then [mass(t + dt) − mass(t)] = mass added at the bottom = dm.

Letting lower density = $\rho_1 + \Delta\rho_1/2$ and upper density = $\rho_1 - \Delta\rho_1/2$,

$$\begin{aligned}&(\rho_1 + \frac{1}{2}\Delta\rho_1)(\hat{H}/2 + dh)A + (\rho_1 - \frac{1}{2}\Delta\rho_1)(\hat{H}/2 - dh)A \\ &-(\rho_1 + \frac{1}{2}\Delta\rho_1)(\hat{H}/2)A - (\rho_1 - \frac{1}{2}\Delta\rho_1)(\hat{H}/2)A \\ &= dm\end{aligned} \tag{4.4}$$

Thus,

$$\begin{aligned}u_e &= dh/dt \\ &= (1/\Delta\rho_1 A)dm/dt\end{aligned} \tag{4.5}$$

Therefore,

$$u_e \Delta b = q \tag{4.6}$$

If u_e is defined thus for the steady state experiment, too, we get,

$$Q \equiv E \tag{4.7}$$

Thus, $E \sim Q \sim Ri_o^{-1}$ should be valid over $0 < Ri_o < 30$, as evidenced by the Moore and Long experiments. Lofquist's results maybe attributed to the horizontal inhomogeniety of his experiments, while Turner's maybe due to the absense of a mean velocity to his flow, his method of definition of the Richardson number, or the absence of what he calls fine structure in his experiments.

These relationships were considered in terms of energy changes and it was shown that the rate of change of potential energy of the system or the buoyancy flux and the rate of dissipation of kinetic energy per unit volume were of the same order.

4.2.2 Results of Entrainment Experiments

The initially linearly stratified fluid was eroded and replaced by a homogeneous layer of depth h(t), when the injection- withdrawal system was applied to only one side of the channel. The results showed that $h^3 \propto t$, similar to Kato and Phillips (1969).

4.2.3 Summary

Over the range of Richardson numbers studied, results showed that the existence of turbulent layers on either side of a region with a density gradient caused erosion of this region to occur, with the formation of two homogeneous layers seperated by a layer with strong density and velocity gradients. The gradient Richardson number of this transition layer tended to have a value of order one. The non-dimensional buoyancy flux Q was functionally related to the overall Richardson number, Ri_o, by $Q \sim Ri_o^{-1}$ for $0 < Ri_o < 30$. Entrainment experiments of an initially linearly

stratified fluid with the application of shear on one side resulted in the formation of a homogeneous layer seperated by an interface from the stratified layer,with $h^3(t) \propto t$.

4.3 Long (1974)

Long critically analyzed mixing processes across density interfaces including cases without and with shear, which have been shown by previous investigators to have different relationships with an overall Richardson number, Ri_*, based on the buoyancy jump across the interface, the depth of the homogeneous layer and the intensity of turbulence at the source.

At large Reynolds (Re) and Peclet (Pe) numbers, the fluxes of heat or salt and the entrainment velocity appear to be proportional to minus one and minus three halves powers of Ri_* for flows with and without mean shear respectively, where the higher entrainment rate for shear flows is attributed to the decrease of rms velocities near the interface for increasing Ri_* for cases of zero shear. Conforming to our area of interest, this discussion will be restricted to the cases with mean shear.

Kato and Phillips (1969) applied a constant shear stress $\tau = \rho u_*^2$ at the surface of initially linearly stratified fluid in an annular flume using a rotating screen. This resulted in the development of an upper homogeneous layer and lower stratified fluid with an interfacial buoyancy jump Δb. Defining the rate of downward propagation of this interface as u_e, the investigators arrived at

$$u_e/u_* = K_1 Ri_*^{-1} \tag{4.8}$$

with, $Ri_* = h\Delta b/u_*^2$, h = depth of the homogeneous layer and K_1 is some constant.

They also found that U/u_* increased with time, where U is the speed of the screen, with u_* held constant. A simple analysis also reveals this quantity to be independent of the Richardson number.

In Moore and Long's (1971) experiments in a race track shaped flume with salt

and fresh water, buoyancy flux q was measured at steady state, yielding

$$q = K_2(\Delta u)^3/h \tag{4.9}$$

with Δu being the mean velocity difference of the two layers and K_2 is some constant. Defining the entrainment velocity by, $u_e \Delta b = q$, this yields equation (4.8) on making the plausible assumption that $\Delta u/u_*$ is independent of Ri_*, where ρu_*^2 is the constant momentum flux in the tank.

The theory (Turner 1973) that erosion of the interface should depend on the properties of turbulence near the interface (and not at the source), especially on the rms velocity scale u_1 and the integral length scale l_1 near the interface proposes a relationship of the form

$$u_e/u_1 = f(Ri) \tag{4.10}$$

with, $Ri = l_1 \Delta b/u_1^2$ assuming no dependence on any other quantities, and large Re and Pe.

Now, we have,

$$\frac{\partial \tau}{\partial z} = \frac{\partial \bar{u}}{\partial t} \tag{4.11}$$

with $\bar{u}$ as the mean horizontal velocity at depth z.

For the Moore and Long steady state experiments,

$$\frac{\partial \tau}{\partial z} = 0$$

As $\tau = -\rho \overline{u'w'}$ and the correlation coefficient is of order one in the homogeneous layers, thus, $u_* = \sqrt{\tau/\rho}$ is proportional to u_1 and $l_1 \sim h$. Thus,

$$u_e/u_1 = K_3 Ri^{-1} \tag{4.12}$$

where K_3 is a constant. The energy equation for these experiments is,

$$\frac{\partial}{\partial t}(\overline{c'^2}/2) = -\frac{\partial}{\partial z}[w'\overline{(c'^2/2 + p'/\rho_0)}] + \tau \bar{u}_z + q - \epsilon \tag{4.13}$$

where, c' = turbulent speed, p' = turbulent pressure, and ϵ = dissipation function.

Now, the velocity difference is proporional to $\sqrt{\tau}$ and the two energy source terms as well as the dissipation function are of order u_1^3/h or u_1^3/l_1 near the interface. Assuming that $q \sim u_e \Delta b$ is of the same order, one again arrives at

$$u_e/u_1 \sim Ri^{-1}$$

as in equation (4.12).

The shearing experiments indicate that

$$q \sim u_1^3/h \sim u_*^3/h \tag{4.14}$$

In the homogeneous layer near the interface, $q \sim u_1 b_1$ where b_1 is the rms buoyancy fluctuation. With the assumption that this correlation is of order one, we obtain that $u_1^2/(b_1 h) \sim 1$, thus, the kinetic energy and the available potential energy, $b_1 h_1$, are of the same order.

Long thus interprets the experiments to indicate that turbulence causes potential energy to increase at a rate proportional to the rate at which kinetic energy is supplied to the region of the interface and not necessarily to generation at the source. A plausible unifying arguement leads to the conclusion that entrainment rates in cases with or without shear are proportional to Ri^{-1} defined on the buoyancy jump and velocities and lengths characteristic of turbulence near the interface.

4.4 Narimousa, Long and Kitaigorodskii (1986)

The flume and pump section in this study were the same as used by Narimousa and Fernando (1987). Experiments were run with two kinds of systems : a linearly stratified system and a two layered fluid system. We will confine our discussion to the latter which comprises of fresh water over salt water.

During entrainment, interfacial Kelvin - Helmholtz instabilities and wave breaking were easily observed. At low Richardson numbers (Ri), turbulence caused the disturbances to be highly irregular, however, this irregularity decreased as Ri grew and finally internal waves developed and occupied the entire interfacial layer. These

instabilities (disturbances) were larger for higher pump speeds and smaller density jumps.

These investigators attempted to find a relationship between E_*, where the entrainment velocity was scaled by the friction velocity u_*, and Ri_*, based on u_* as well, i.e.,

$$E_* = u_e/u_* \tag{4.15}$$

$$Ri_* = h\Delta b/u_*^2 \tag{4.16}$$

Measurements were made of the mean mixed layer velocity, U, the mixed layer depth, h, and the entrainment velocity u_e, while the friction velocity u_* was deduced from the mean momentum balance equation for homogeneous turbulent shear flow. Plots of h vs.t revealed that u_e = dh/dt was constant.

4.4.1 Deduction of u_*

The streamwise momentum equation for the mixed layer, the interface and a thin layer below it where the velocity drops to zero, is

$$d(Uh)/dt = u_*^2 - w_*^2 h/W \tag{4.17}$$

where u_* is identified with the pressure gradient force and Reynolds stress force accelerating the flow due to pump action and is the friction velocity of the pump; while w_* is the friction velocity of the side walls, W being the width of the side walls. The second term accounts for the retarding action of the side walls.

The Blasius resistance formula for turbulent channel flow is,

$$U/w_* = 8.74(Ww_*/2\nu)^{1/7} \tag{4.18}$$

$$\text{i.e., } w_* = 0.15U^{7/8}(2\nu/W)^{1/8} \tag{4.19}$$

$$\text{also, } \frac{d(Uh)}{dt} = \frac{\partial(Uh)}{\partial h}\frac{\partial h}{\partial t} = U_c u_e \tag{4.20}$$

Thus,

$$u_*^2 = U_c u_e + \{0.15U^{7/8}(\frac{2\nu}{W})^{1/8}\}^2 h/W \tag{4.21}$$

As $U_c(= \frac{\partial(Uh)}{\partial h})$ was obtained from graphs, u_* was easily calculated, and found to increase very slowly with h.

The measured $S = Uh$, on being plotted against h had two distinct regions, initially increasing linearly and then remaining constant, leading to the interesting observation that U decreases with h, first slowly and then faster as the pump term is balanced by the wall friction term. Experimentally, it was determined that $U \sim 10.65u_*$.

4.4.2 Entrainment Rates Based on u_*

The investigators start out with the assumption that $h\Delta b$ is constant, in slight contrast to Narimousa and Fernando (1987) who had

$$h_0\Delta b_0 = h\Delta b(1.03) \tag{4.22}$$

which may be due to the fact that the region of the thin density interface was not considered while employing the buoyancy conservation equation. This enabled them to develop plots of E_* vs. Ri_*.

No simple unifying relationship was found over the entire range of Ri_*, but for subranges they found,

$$E_* \simeq 0.65Ri_*^{-1/2} \quad 15 < Ri_* < 150 \tag{4.23}$$

$$E_* \simeq 7Ri_*^{-1} \quad 150 < Ri_* < 800 \tag{4.24}$$

$$E_* \simeq 5Ri_*^{-3/2} \quad Ri_* > 150 \tag{4.25}$$

This can be attributed to the difference in the very nature of the entrainment process over the three ranges. Initially, the mixed layer as well as the base of the mixed layer are fully turbulent; the high turbulent shear and weak density jumps result in the eddies of the mixed layer directly producing entrainment; in

the next range, the interface becomes less chaotic and Kelvin- Helmholtz type of instabilities occur which are less efficient in causing entrainment. Finally, due to even lesser shear, entrainment decreases further, and this is similar to previous shear free experiments (oscillating grid type), where Long (1978) obtained $E \sim Ri_*^{-7/4}$, which is close to the one obtained here.

4.5 Wolanski, Asaeda and Imberger (1989)

Turbulence was generated in a plexiglass cylinder using oscillating grids along it's walls. The cylinder was filled with a fluid mud mixture of kaolinite and tap water, with initial concentrations always greater than 40 g/l. The grids were stopped after fully mixing the fluid mud. A lutocline formed, seperating the clear, upper layer from a turbid bottom layer, and moved down with a constant velocity w_{fo}, which depends on the suspended sediment concentration. As the oscillation was started again, the fall velocity w_f reduced to less than w_{fo}. There was no mixing for stroke frequencies $\omega < \omega_c$, the critical frequency at which billowing and wisp formations occured. In this frequency range, w_f/w_{fo} decreased for increasing values of ω, which can be attributed to the break-up by turbulence of the clay flocs. At $\omega = \omega_c$, there was active mixing across the interface, which eroded by moving downwards at a velocity greater than w_{fo}, thereby implying the presence of a higher intensity of turbulence in the upper layer. However, very soon, the fall velocity decreased to below w_{fo} again as a balance prevailed the upward turbulent entrainment and the downward gravity settling at the lutocline, with no more erosion of the lutocline.

For $\omega > \omega_c$, the lutocline was convoluted with large internal waves cusping into the upper layer where the intensity of turbulence was lower due to sediment induced dissipation. The height to which the fluid was entrained increased with increasing stroke frequency. Also, the onset of turbulence occured at almost the same value of the Richardon number for all the experiments.

Thus, similar to heat and salt stratified experiments, buoyancy effects are dom-

inant in inhibiting mixing across the lutocline. However, an additional feature affecting the process is the extraction of turbulent kinetic energy by the sediment to counteract the buoyancy flux due to sediment fall velocity, which, here, causes a collapse of turbulence in the bottom layer with resultant erosion of the lutocline only from the top. It must be mentioned that Wolanski and Brush (1975) found, in oscillating grid type of experiments, that the entrainment rate decreased much faster with increasing Richardson numbers than was the case with salt or heat stratified experiments.

The dependence of the fall velocity on the suspended sediment concentration served to limit the height of entrainment into the top layer and also stopped lutocline erosion after an initial period of active mixing, which is what E and Hopfinger (1987) as well had observed.

4.6 Conclusions

The preceding review of flows with mean shear show that many investigators have found relations of the form $E \propto Ri^{-1}$ for salt-stratified systems, although the range of validity of this relation varies according to the method of defining the Richardson number (see, for instance, Appendix B). Moore and Long (1971) related the non-dimensional buoyancy flux, Q, to the Richardson number according to a similar ($Q \propto Ri^{-1}$) relation and showed that the entrainment coefficient, E is equivalent to Q. Narimousa et al. (1986) arrived at different entrainment relations for (three) sub-ranges of the Richardson number defined on the basis of the friction velocity u_*. The exponent in the $E_* \propto Ri_*^{-n}$ increased with increasing Richardson number, thus resulting in decreasing rates of entrainment with increasing Richardson number, which they attributed to the difference in the very nature of the entrainment processes over the sub-ranges. Wolanski et al. (1989) demonstrated that the behavior of sediment particles or aggregates is different from salt-stratified systems because of greater dissipation of turbulent kinetic energy to counteract the

sediment fall velocity thereby implying a lesser rate of entrainment for sediment-stratified systems, which is the focal point of the present investigation.

CHAPTER 5
METHODOLOGY

5.1 Apparatus

Turbulence generated by grid stirring has been the most popular mode of laboratory studies of dynamics of stratified systems. In a two-layered system seperated by a density interface, the grid is placed in either layer or there might be a system of grids placed in vertical succession and extending into both layers. It can be shown that the grid may be replaced by a virtual source of energy at a horizontal plane, the "action" of the source being determined by a single "action parameter" (Long 1978) having the dimensions of viscosity and proportional to the constant eddy viscosity in the turbulent fluid above the source. However, the issue of entrainment of fluid muds in estuarine situations is obviously the result of current-shear induced turbulence. Thus, it appears more prudent and realistic to simulate this phenomenon with a laboratory apparatus which can produce the required turbulent kinetic energy for mixing by velocity shear.

In this respect, most previous experimenters have used flumes with annular geometries, with a rotating screen applying shear stress at the surface of the stratified fluid within it (Kato and Phillips 1969; Kantha, Phillips and Azad 1977; Deardorff and Willis 1982). This annular flume has the advantage of being free of end walls and thus avoids undesirable recirculating flow (as in some previous surface shear free experiments with salt and fresh water of Ellison and Turner 1959, and Chu and Baddour 1984). But, this kind of arrangement seems affected by secondary circulations in the radial direction (Scranton and Lindberg 1983) causing substantial interfacial tilting. Deardorff and Yoon (1984), after an in-depth study concluded

that the cause for this tilting lies in the uneven angular momentum distibution across the annulus due to the solid body rotation of the screen. The fluid possses a mean velocity towards the outside resulting in higher entrainment rates at the outer wall relative to the inner wall.

The experiments were carried out in a specially designed recirculating flume (see Figures 5.1, 5.2 and 5.3) which basically consists of two sections, the pump and the observation sections, joined together by two semi-circular annuli. This kind of flume has been used by previous experimenters (for example, Moore and Long 1971; Narimousa, Long and Kitaigorodskii 1986) and is free of the effects of end walls and that of a rotating screen. Some secondary circulation is introduced in the process of bending the flow; however, this is possibly to be minimized by the large radius of curvature and the relatively long straight section used for observations. Here, it might be noted that in some experiments of this general nature, secondary circulations are not undesirable (even though the geometric dimensions of the apparatus will dictate their transverse length scales), since turbulent geophysical flows also contain them (e.g., longitudinal rolls or Langmuir cells), albeit with independent preferred wave numbers. Although the effect of streamline curvature is not too well understood, the effects of variation in transverse length scales does not appear to cause substantial variation in entrainment (Scranton and Lindberg 1983).

The flume was entirely made of plexiglass to enable visualization of the flow and other desired parameters. Except for the walls of the two semi-circular sections, the plexiglass used was 1.25 cm thick everywhere, including the bed and the floor of the flume. The walls of the semi-circular section were 0.32 cm thick, this merely being expedient to afford ease of bending to the design radius of curvature. The flume was 61 cm over the floor throughout. The entire unit was placed on a specially built table.

A 'bed' was constructed first and placed on the table. The floor of the flume

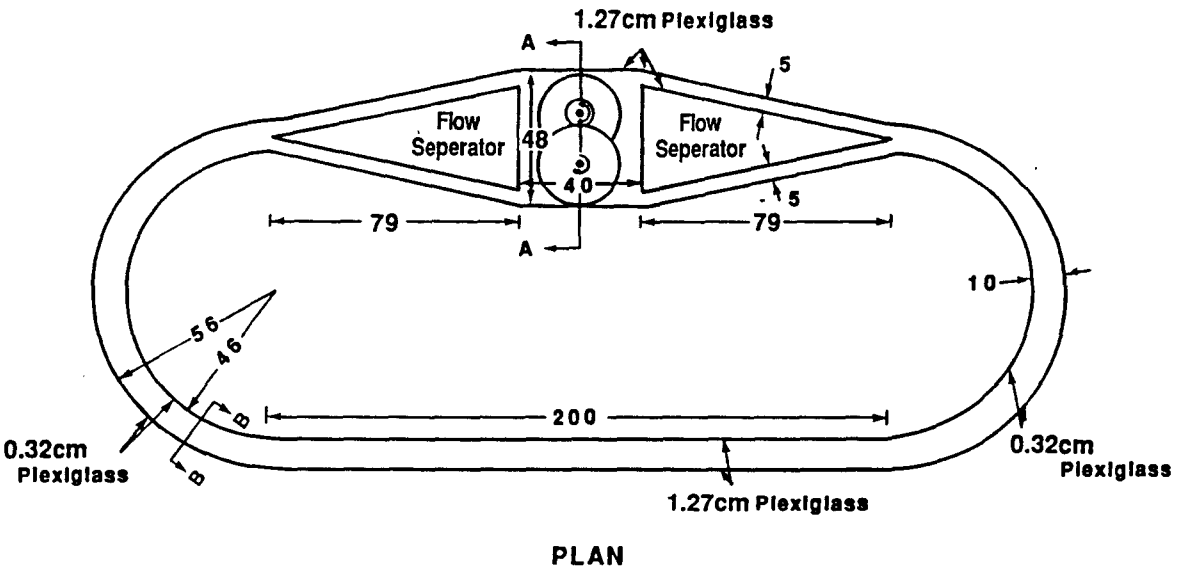

Figure 5.1: Recirculating flume of plexiglass used in the present investigation (dimensions in centimeters).

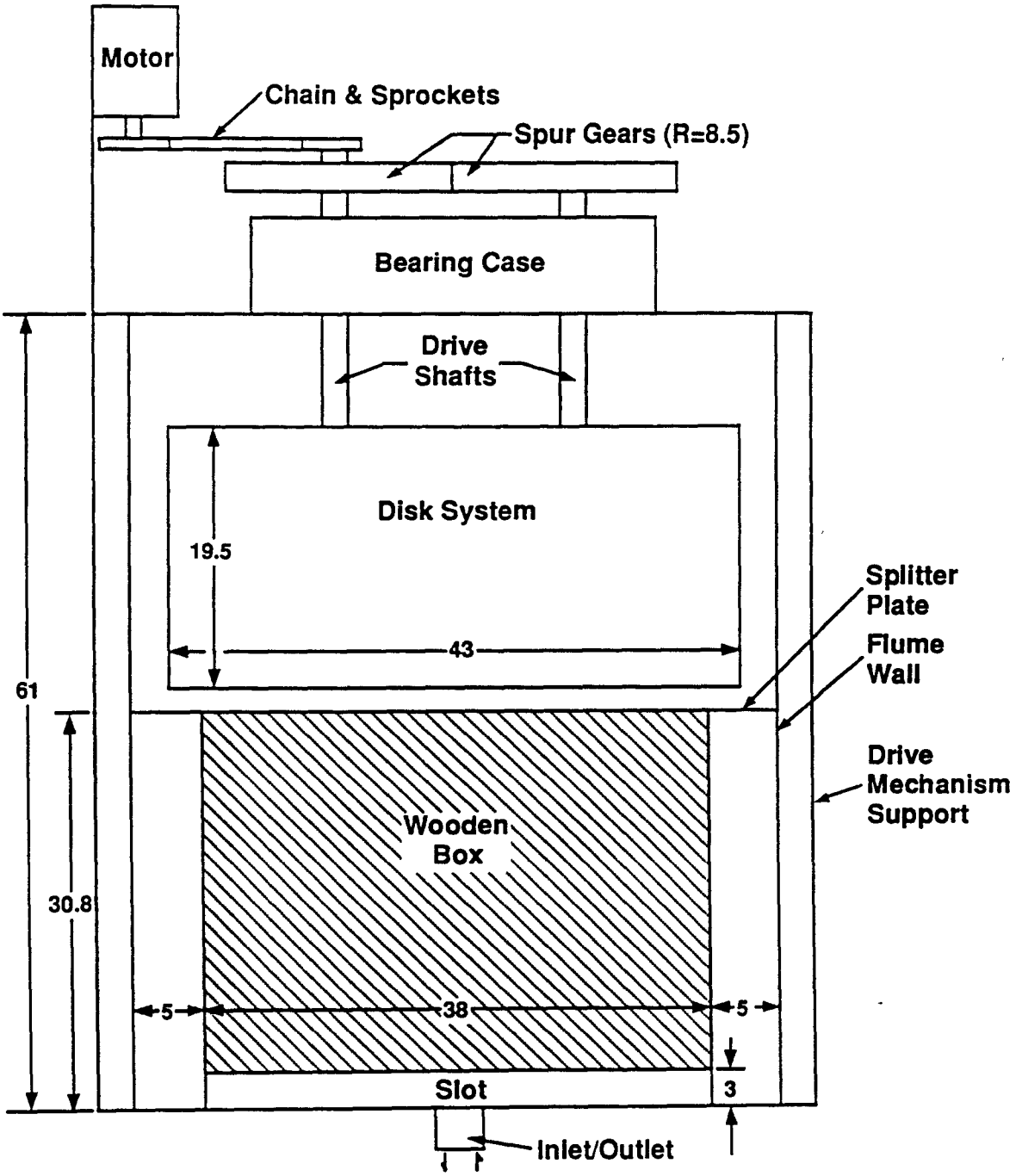

Figure 5.2: Section A-A of the flume, from Figure 5.1 (dimensions in centimeters).

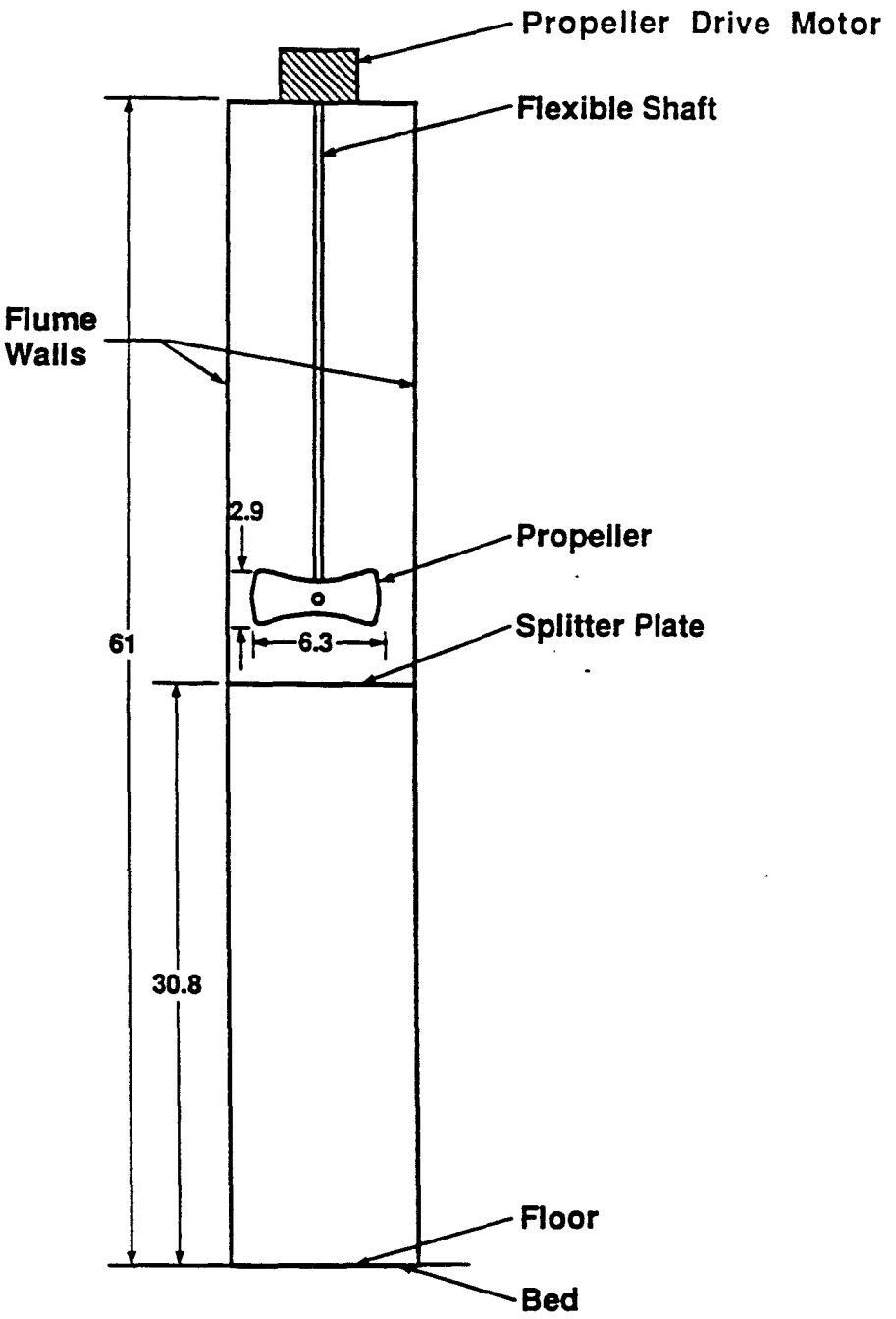

Figure 5.3: Section B-B of the flume, from Figure 5.1 (dimensions in centimeters).

was bolted and glued onto this. Next, the walls were cut, and bolted and sealed to this floor. The walls were supported with 20 cm high and 5 cm wide sections at periodic intervals and also connected with brackets at the top. Joints were sealed with gussets and rubber to prevent any leakage.

The required turbulent shear flow was obtained by using a disk pump (see Figure 5.4), first introduced by Odell and Kovasznay (1971), to selectively drive the upper fresh water layer over the quiescent fluid mud.

The width of the flume was 10 cm everywhere, except at the pump section. The disks of the pump were between walls 47.5 cm apart. To maintain a constant cross-section of flow as much as possible, flow seperator sections (triangular in plan, of dimensions $73.7 \times 73.7 \times 31.8$ cm) were placed both up and downstream of the pump, which created two channels of 5 cm width each on either side of the pump. These channels guide and blend the flow into the semi- circular section in front of the pump, while upstream of the pump, these split and guide the flow onto the pump. The flow seperators were of the same height as the flume, i.e., 61 cm. Also, the two flow seperator sections were connected by a weighted wooden box of height 30.8 cm which served to maintain the required 5 cm width. The hole of the intake valve for fluid mud was directly under a transverse slot (of dimensions $38 \times 13 \times 3$ cm) at the bottom of this box. The entire pump section had vertical supports at every 40 cm.

The radius of curvature of the curved section was ~ 51 cm. Here, supports were put at closely spaced intervals of 25 cm, to take into account the additional stresses due to bending. The observation section was completely straight and 200 cm long. Small holes were drilled into the outer wall of the observation section, near the entrance (in the flow direction) to the observation section and thin, flexible pipes were inserted into them, taking care that they did not intrude into the interior of the flume. The other ends of these pipes were closed with metal clips. These holes

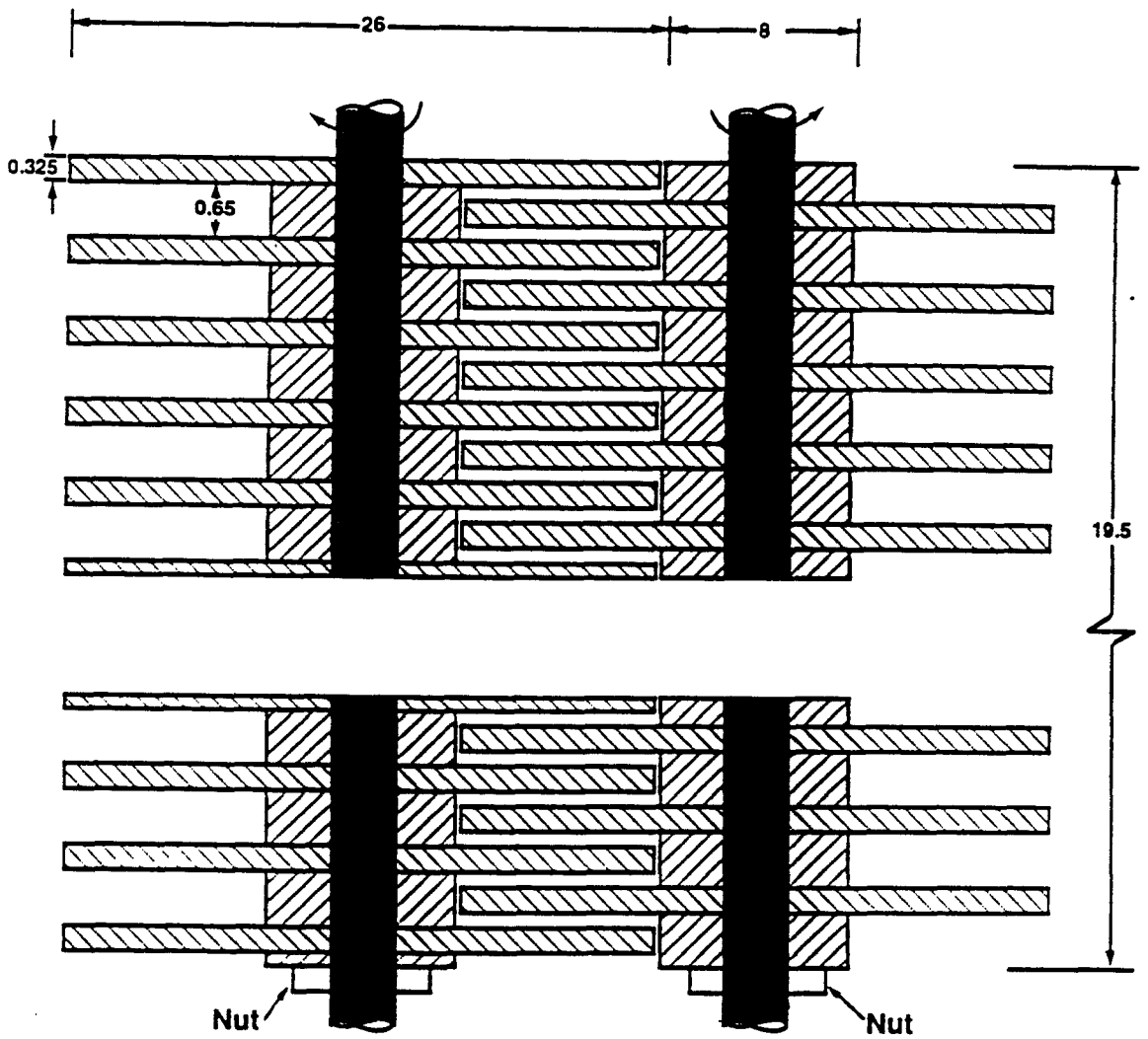

Figure 5.4: Details of the disk pump system used in the present investigation (dimensions in centimeters).

were at closely spaced vertical intervals–1-4 cm apart. This was done to extract samples of fluid mud for the estimation of concentration profiles (as a function of time). At the center of the outer wall of the observation section, a 38 × 56 cm size grid of 2 cm mesh on a transparency was pasted to record the rate of progress of injected dye-lines. The entire flume had brackets at the top, every 10 cm, to tie the walls together.

A Sony Betamax video recording system was set up about 1 m from the observation section of the flume such that the line of vision of the camera was normal to the sidewall of this section. The camera was focussed onto the grid at the center of the wall. Two powerful (1000 W) lamps were set behind the camera to provide the requisite illumination for recording.

The reason for a disk pump was that it could produce quite homogeneous horizontal streaming of the flow. The pump imparted only a horizontal component of velocity to the fluid. The disks of the disk pump were of two different diameters, 8 and 26 cm, which were alternately stacked on each of the shafts. The larger disks were 0.325 cm thick, while the smaller ones were 0.65 cm thick. These shafts were so positioned that a large disk of one shaft meshed with the smaller of the other and so on. Thus, the two stacks meshed, leaving almost no space in between them, but creating gaps at the outer edges, between the larger disks. When the two shafts were driven in opposite directions by a 1/8th h.p. Dayton Permament Magnet Gearmotor (F/L rpm 50, F/L torque 130 inch- pounds) via a chain and sprockets arrangement, fluid was pulled around the outer channels by the viscous drag of the larger disks and ejected as horizontal jets from within these gaps. The disks were sand-blasted to improve surface roughness to increase the efficiency of the pump by increasing drag. With the disk pump in place, the bottom-most disk of the pump was just above the elevation of the splitter plate (described next).

Preliminary calibration tests were performed with a homogeneous fluid to test

the range of velocities obtainable with this pump. As the maximum mean velocity obtained was only about 9 cm/s, it was decided to augment the velocity with the assistance of a screw propeller. This propeller was placed (the axis of the propeller was $\sim$ 2 cm above the level of the splitter plate which is described below) in the curved section downstream of the pump and before the entrance to the observation section (Section B-B, Figure 5.3), and driven by a motor placed outside via a flexible shaft. The result was quite satisfactory with the maximum obtainable velocity with the two-layered system of fluid mud and water in place being $\sim$ 14 cm/s. Also, the horizontal homogeneity of the flow was not disturbed. To impart additional horizontal homogeniety to the streamlines, a sidewall-to-sidewall thin metal splitter plate was constructed in a horizontal plane 30.8 cms from the floor and this splitter plate covered the entire pump section (which is the only region with a width greater than 10 cm and having the flow seperators and the disk pump) and the entire curved section downstream of the pump. This also served to prevent any suction effects either due to the disk pump or the propeller (which together are referred as the pump system hereafter) from affecting into the fluid mud below.

5.2 Procedure

Each experimental Run was divided into intervals of $\sim$ 8-20 (generally $\sim$ 10) minutes each. At the end of each interval, the required measurements were "instantaneously" made, and these were considered to be the representative conditions for that interval. It must be mentioned is that in the case of experiments with salt-stratified systems, the sole cause for the deepening of the mixed-layer is turbulent entrainment across the density interface. In a velocity-sheared two-layered system of fluid mud and water, the rate of propagation of the visual density interface (i.e., the rate of change of depth of the mixed-layer) is not the result of vertical entrainment of fluid mud alone, but is also due to the settling characteristic of fluid mud below the level of the interface. Thus, in this case, one cannot easily quantify

turbulent entrainment in terms of changes of the mixed- layer depth. Therefore, a more direct approach was adopted. The most basic effect of the turbulent kinetic energy of the system is mass/buoyancy transfer across the interface. It therefore appears to be the most logical quantity to measure and relate to a suitably defined Richardson number.

From an estimate of the initial depth of the mixed layer, the flume was first filled with the requisite pre-determined height of tap water. Two types of test sediment were considered–kaolinite and bentonite (see Appendix A), with the objective of determining the effect of varying degrees of cohesion on entrainment rates. Bentonite, a montmorillonitic clay, is highly cohesive (and thixotropic) whereas kaolinite is not as cohesive and properties of bentonite aggregates are not as uniform as that of kaolinite. Sediment was well-mixed with tap water (for composition of tap water, see Dixit 1982) in a vertical, steel cylinder of 77 cm diameter with the aid of a Ingersoll-Rand two-stage 10 h.p. air compressor with a maximum discharge rate of 14.0 kg/cm^2. The compressed air was introduced into this vertical mixing tank at a high flow rate through tiny holes in a T-shaped PVC pipe section placed at the bottom of the cylinder. This agitation was continued long enough until the fluid mud was well mixed and quite homogeneous. In the case of kaolinite, the sediment-water mixture was thoroughly agitated for at least an hour which provided quite "homogeneous" mixing, while bentonite was not as tractable in this respect. Bentonite, which is highly thixotropic, formed lumps with a wide range of sizes (of upto $\sim$ 20 cm diameter) even when the sediment was introduced at a slow rate into agitated tap-water. These lumps were dry inside although covered by a wet "skin". The mixture was allowed to equilibrate for $\sim$ 5 days with periodic agitation (upto $\sim$ 6 hours every day) before a fairly uniform, workable mixture resulted.

The well-mixed fluid mud was instantaneously pumped into a horizontal cylindrical feeder tank above the elevation of the flume. This fluid mud was then in-

troduced into the flume through the intake valve at the flume bottom. The mud entered the flume with a vertical (upward) velocity at the position of the slot at the bottom of the wooden box and on encountering the wooden obstruction turned at right angles and flowed horizontally into the bottom of the flume, displacing the lighter tap water upwards. With all stops open, the filling rate was about 2.5 cms per minute per unit area of the flume. The time required to fill the flume with the requisite volume of fluid mud was $\sim$ 15 minutes. In the first three experimental runs, the filling rate was slightly slower, while in the remaining runs the resulting fluid mud layer underneath water was essentially homogeneous initially (except very near the bottom). The interface was always positioned so that it was just under the level of the splitter plate such that the internal boundary to the diffusion of momentum (Narimousa and Fernando 1987) formed by the interface, and the physical boundary of the horizontal splitter plate would be almost continuous. In all the runs, the method of filling fluid mud under water always resulted in the formation of a diffuse intermediate layer (of thickness $\sim$ 5-7 cms) just above the interface. The density of this layer was found to be minimal ($\sim 10^{-5}$ g/cm^3) and this layer completely eroded within 1-1.5 minutes after starting the run.

As soon as the two-layered system was in place, the depth of the mixed layer, h, was noted, and samples ($\sim$ 10 cm^3 each) of fluid mud, at discrete vertical intervals ($\sim$ 5 cms), were withdrawn via the flexible tubes in the outer wall of the observation section of the flume to obtain the initial concentration profile (across depth). These samples were directly withdrawn into small (capacity $\sim$ 60 cm^3 each), clean glass bottles which were then tightly capped. The elevation of the position (from the bottom of the flume) from which the sample had been taken was marked on the corresponding bottle. The time was also noted. As the instantaneous concentration profile was required, it was not considered expedient to spend more than 1-1.5 minutes for sampling, by which the number of samples was limited to a maximum

of six each time. The video recording system was turned on (to record the entire experiment) and the experiment was begun by starting the pump system (the disk pump and the propeller were started simultaneously) to rotate at a predetermined rotation rate (which, in conjunction with varying buoyancy jumps across the interface, provided a wide range of Richardson numbers $\sim 4 - 32$). The rotation rate of the disk pump was always at the maximum, while the rotation rate of the propeller was adjusted such that the pump system could produce the desired predecided mean initial velocity in the mixed-layer.

After the experimental run was in progress, with velocity- shear causing fluid mud entrainment across the density interface through massive undulations convoluting the interface, sets of samples, for gravimetric analysis, were systematically withdrawn at discrete time intervals ($\sim$ 10 minutes). Consecutively, dye lines were also injected to get the corresponding velocity profile for that interval. The depth of the mixed layer was noted.

Dye-lines (of diluted rhodomine such that it would be almost neutrally buoyant in water) were injected into the flow and their movement across the grid was recorded by the video camera. A syringe with a long needle ($\sim$ 35 cm) was used for this purpose. The needle was introduced vertically into the observation section through a slot in a bracket tying the sidewalls together at the top. The needle was aligned with the upstream vertical edge of the grid and it's end was well within the lower layer of fluid mud. The plunger was depressed and the spewing needle was "instantaneously" pulled out leaving a clearly visible dye-line (which became diffuse with downstream progress). The velocity profile could be easily determined by measuring the rate of downstream progress of this injected dye-line. For each interval, dye-lines were injected at least twice (and frequently three times) and averaged to get a more accurate velocity profile. A problem which could not be circumvented was that, below the level of the visual density interface, the turbidity of fluid mud

prevented visualization of the dye-line. However, Narimousa and Fernando (1987), using a similar flume and pump system, found that the velocity rapidly decreased to a very insignificant value at the interior of a density interface of finite thickness, $\delta \sim 0.06\times$ (depth of mixed layer). Thus, the contribution of this portion to the mean overall velocity was assumed to be negligible. In the present investigation as well, visual observation seemed to be in conformance with this argument. The resulting velocity profile was integrated, and knowing the depth of the mixed layer, the representative mean velocity for the interval could be obtained. Temerature recordings of the mixed-layer were also made throughout the course of some of the runs which showed that the increase of temperature of the mixed-layer by the end of a run was not more than 2 °C (mean temperature was $\sim$ 17°C.

The recording of the experiment (on the video recording system) was played back to obtain the rate of progress of injected dye-lines. The representative velocity distribution was thus obtained. This was drawn on a graph-paper to measure the area which further gave the mean representative velocity for each interval. The point of inflection of the velocity profiles (see Figure 3.2) were also noted as the velocity-gradient is responsible for the shear production causing entrainment. The vertical distance of this point from the interface was designated δ_s.

For the purpose of gravimetric analysis, Millipore Filtering System was used in conjunction with a small, vacuum pump (which could produce a vacuum of upto 65 cms of Hg). Millispore filters (Filter Type HA, Pore Size 0.45 μm) were first dried in an oven at a temperature of 50 ^{0}C for at least 3 hours. These were then removed from the oven and allowed to equilibrate in a room (whose temperature and relative humidity were monitored with an air-conditioning unit) for a minimum of 8 hours. These filters were then weighed in the same room on a Mettler balance (Type H80) which was accurate upto 1 mg. These pre-weighed filters were then used to dewater known volumes of sediment samples. In the case of bentonite, the sample

volume that could be used for this process of dewatering was only 0.5 cm^3 as the filters got clogged with the sediment particles for greater volumes of fluid mud. To improve accuracy in obtaining concentration profiles for bentonite, this procedure of dewatering was done for at least three sub-samples for each base sample wihdrawn from any elevation of the flume at any time, and these were averaged.

The filtrate was allowed to remain on the paper which was then heated in the oven again (at 50 ^0C for at least 6 hours) to remove the last vestiges of water. The dried filter paper with dry sediment on it was again equilibrated in the same monitored room and then weighed on the Mettler balance from which the mass of sediment in a known volume of sample was easily obtained. This procedure was carried out for all the samples, and, thus, the concentration profile of fluid mud was known for each interval. Knowing the depth of the fluid mud, the mass flux (and hence, the buoyancy flux) across the interface could be calculated.

CHAPTER 6
RESULTS AND ANALYSIS

6.1 Definition of Richardson Number

Vertical mixing across a density interface is dependent on the local Richardson number (Turner 1986), e.g., the gradient Richardson number across the interface in terms of the velocity and density differences across the interface. However, measurement of the local Richardson number is generally difficult (the thickness of the interface needs to be determined) and a common procedure is to define an overall Richardson number. The most suitable definition in the present case as well is such an overall Richardson number in terms of the depth of the mixed layer and the buoyancy jump across the interface. The depth of the mixed layer controls the length-scale of the energy-containing eddies, with the interface acting as an internal boundary. Regarding the velocity- scale, most of the previous researchers tend to identify with the friction velocity, u_*. In flume experiments without rotating screens, it can be seen that most of the turbulence is produced at the density interface and the side-walls (Narimousa and Fernando 1987). However, in wall bounded flows, most of the sidewall induced turbulence dissipates near the walls itself and only a small portion diffuses outwards (Hinze 1975, p. 648). This is also confirmed by Jones and Mulhearn (1983). Thus, most of the energy required for turbulent mixing is a direct result of shear production at the interface and the most important scaling velocity should be the velocity difference between the two layers, ΔU (e.g., Ellison and Turner 1959, Lofquist 1960, Moore and Long 1971). In the present case, the velocity of fluid mud at and below the level of the density interface was considered negligible (although it could not be expressly measured, visual observations seemed

to confirm the fact) as in Narimousa and Fernado (1987). Thus, the mean velocity of the mixed-layer was taken as the most representative velocity scale. With this, the Richardson number is defined as

$$Ri_u = g\frac{h\Delta b}{\bar{u}^2} \tag{6.1}$$

with the interfacial buoyancy jump being

$$\Delta b = g\frac{\rho_2 - \bar{\rho}_1}{\bar{\rho}_1} \tag{6.2}$$

where $\bar{\rho}_1$ is the mean mixed-layer density and ρ_2 is the density of fluid mud at the level of the density interface.

6.2 Initial Conditions

The initial conditions for all the experimental Runs are listed in Table 6.1 (for a physical description of the flow configuration, refer to Figure 3.2). The associated terminology is as follows:

M_2	=	mass per unit area of fluid mud
h	=	depth of mixed layer
H	=	depth of fluid mud
$\bar{C}_2$	=	mean concentration of fluid mud
C_2	=	concentration of fluid mud at the level of the interface
$\bar{u}$	=	mean velocity of the mixed layer
Δb	=	buoyancy step across the interface

The subscript 0 denotes initial conditions. It must be noted that in Runs 4-10, the pump system was kept at some fixed (by not altering the speed controls) rotation rate (the rate was tuned such that a pre- determined mean velocity could be achieved in the mixed-layer) throughout the course of the each run, the velocity profiles being allowed to evolve with time, while the speed settings of the pump system (specifically, only the propeller) was varied during the course of the experiment for the remaining runs. The initial values of the mean velocity were in the range 7.4-13.1 cm/s. However, in the first three runs, mean velocity values even exceeded these initial values as the rotation rate of the pump system was increased. In Runs

Table 6.1: Initial conditions of all Runs

RUN NUMBER	$(M_2)_0$ g/cm^2	h_0 cm	H_0 cm	$(C_2)_0$ g/l	$(C_2)_0$ g/l	$(\bar{u})_0$ cm/s	$(\Delta b)_0$ cm/s^2
1	1.1685	32.2	19.8	59.0	29.0	7.4	17.7
2	3.0625	28.8	26.5	115.6	94.5	7.5	57.7
3	3.2375	26.0	25.0	129.5	110.0	11.8	67.2
4	2.5410	26.5	29.5	86.1	76.0	13.1	46.4
5	2.3450	25.3	27.7	84.7	76.0	11.9	46.4
6	1.6125	22.2	28.5	56.6	35.0	9.5	21.4
7	1.2450	28.0	27.0	46.1	30.0	11.0	18.3
8	1.9918	25.0	31.2	63.8	50.0	13.0	30.5
9	2.2350	23.6	28.2	79.3	62.0	9.6	37.9
10	1.0154	24.5	29.5	34.4	30.5	9.2	18.6
11	1.0800	23.6	28.0	38.6	28.0	9.9	17.1

1-9, kaolinite was the constituent sediment of fluid mud while the fluid mud was of bentonite for Runs 10 and 11. The initial mean concentration of fluid mud was in the range 45-130 g/l which corresponded to bulk density range of $\sim$ 1.03-1.08 g/cm^3. The upper limit of this range was imposed by the performance capabilities of the pump system so as to obtain reasonable (for which entrainment was possible) values of the Richardson number . In the case of bentonite, higher values of mean initial concentration could not be used because of difficulty in obtaining a fairly uniform, well-mixed suspension.

6.3 Evolution of Characteristic Profiles

A typical time-evolution of the concentration profile below the level of the density interface is shown in Figure 6.1. The data are for Run 9 with kaolinite as the constituent sediment of fluid mud. Initially, i.e. at t = 0, the fluid mud was essentially quite well-mixed (with generally mild lutoclines) with obviously the steepest gradient at the interface. Although the interface is shown to have an infinite gradient, it is a well-known fact that in similar and geophysical situations, the interface is a region of thin but finite thickness (of the order of 1/20th the thickness of the mixed layer) with a steep density gradient, see Narimousa and Fernando (1987). The settling characteristic of the suspension caused a lutocline to develop for about 5 cm directly below this interface. The bottom 8 cm show a slightly steep lutocline as well, which might be due to settling. With the passage of time, the interface sharpens in the sense that the lutocline below it disappears. The concentration of fluid mud at the level of the interface generally increases with time (except for the profile at t = 21 minutes, which could be due to the local settling rate being more than the rate of scour of the interface due to entrainment, temporarily). The bulk concentration of the fluid mud always increased with time as the mud settled. The major lutocline progressively steepened. It must also be noted that the mean concentration of the mixed layer is simultaneously increasingly as well. However, as

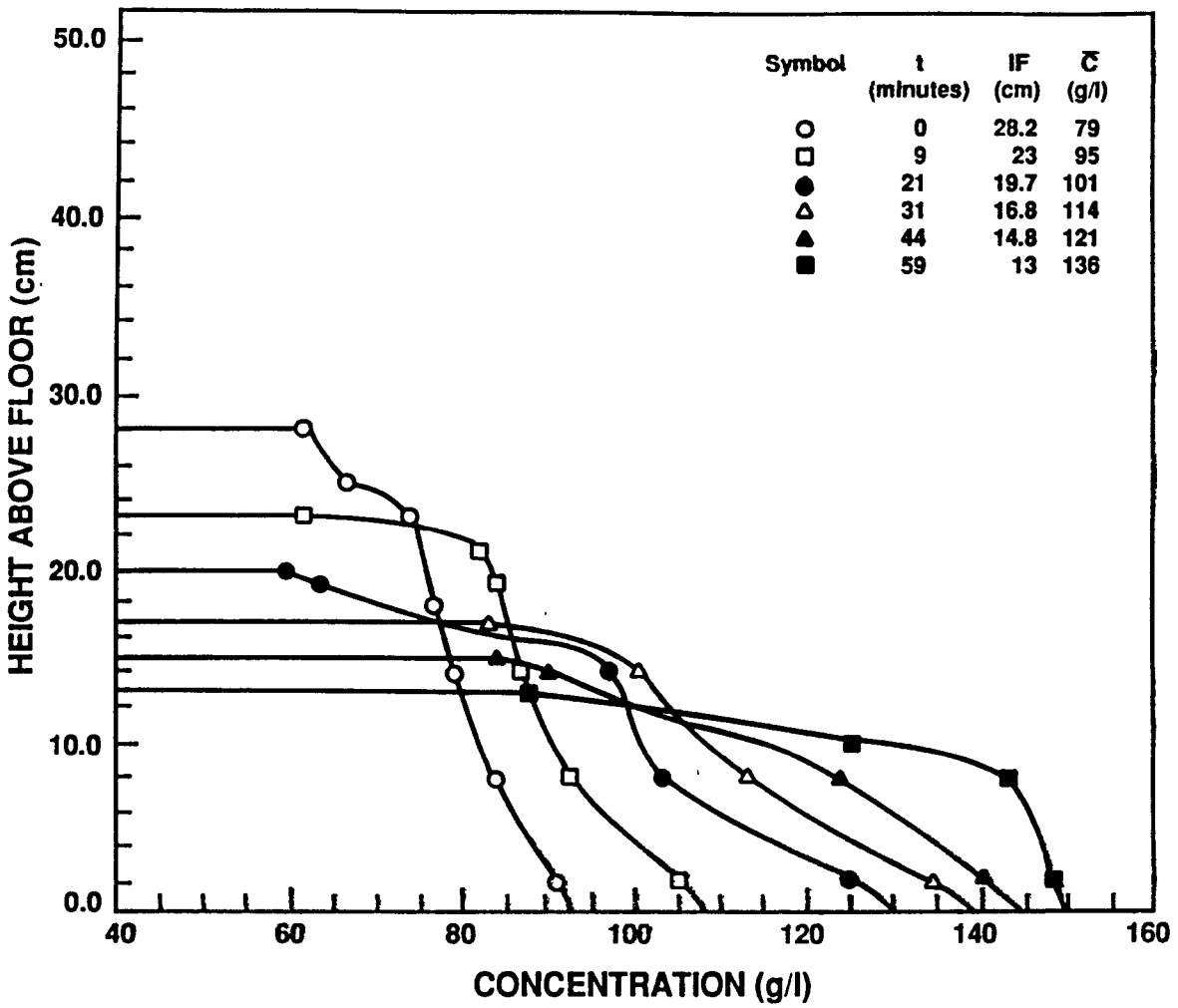

Figure 6.1: Sequence of concentration profiles of Run 9 with kaolinite depicting the evolution of concentration with time. IF denotes interface.

will be seen later, the buoyancy jump across the interface generally increased with time (except for the second interval t = 9 to t = 21 minutes, when it appeared to decrease). Entrainment progressed until the buoyancy jump became strong enough to overcome the excess (after dissipation) turbulent kinetic-energy which tended to increase the potential energy of the system by causing entranment, at which point the entrainment apparently decreased a lot.

Figure 6.2 shows the typical evolution of velocity profiles in the mixed layer for Run 6 (with kaolinite). Initially, the profile was homogeneous without any gradient at all in the mixed-layer, i.e. an apparent step velocity profile resulting in the case of a vortex sheet discussed in Section 2.2.1. There was much entrainment at these earliest times with massive convolutions covering the entire extent of the interface. Closer examination revealed that the (thin, but finite) interface might itself be turbulent at these times. Initially, the mean velocity of the mixed-layer increased very rapidly with time as the inertia of the system was being overcome. This generally took between 3 to 4 minutes, by which time the mean velocity peaked. Next, the mean velocity of the mixed-layer slowly decreased with time which might be due to three reasons : (1) with the passage of time during the course of a run, with entrainment (and settling), the elevation of the interface decreased, and progressively more and more volume of fluid was being driven (considering the interface to act as an internal boundary to the diffusion of momentum) by the pump system which had a constant energy input; however, calculations to check conservation of mass ($h\bar{u}$) and momentum ($h\bar{u}^2$) for each run revealed discrepencies indicating that more accurate measurements of velocity profiles need to be made if these quantities (mass and momentum for each run) need to be accurately estimated, (2) sidewall friction may not always be negligible, and (3) as the mixed-layer concentration increased with time (due to mass flux into it), there was consequently increasing dissipation of turbulent kinetic energy in the mixed-layer to counteract the downward buoyancy

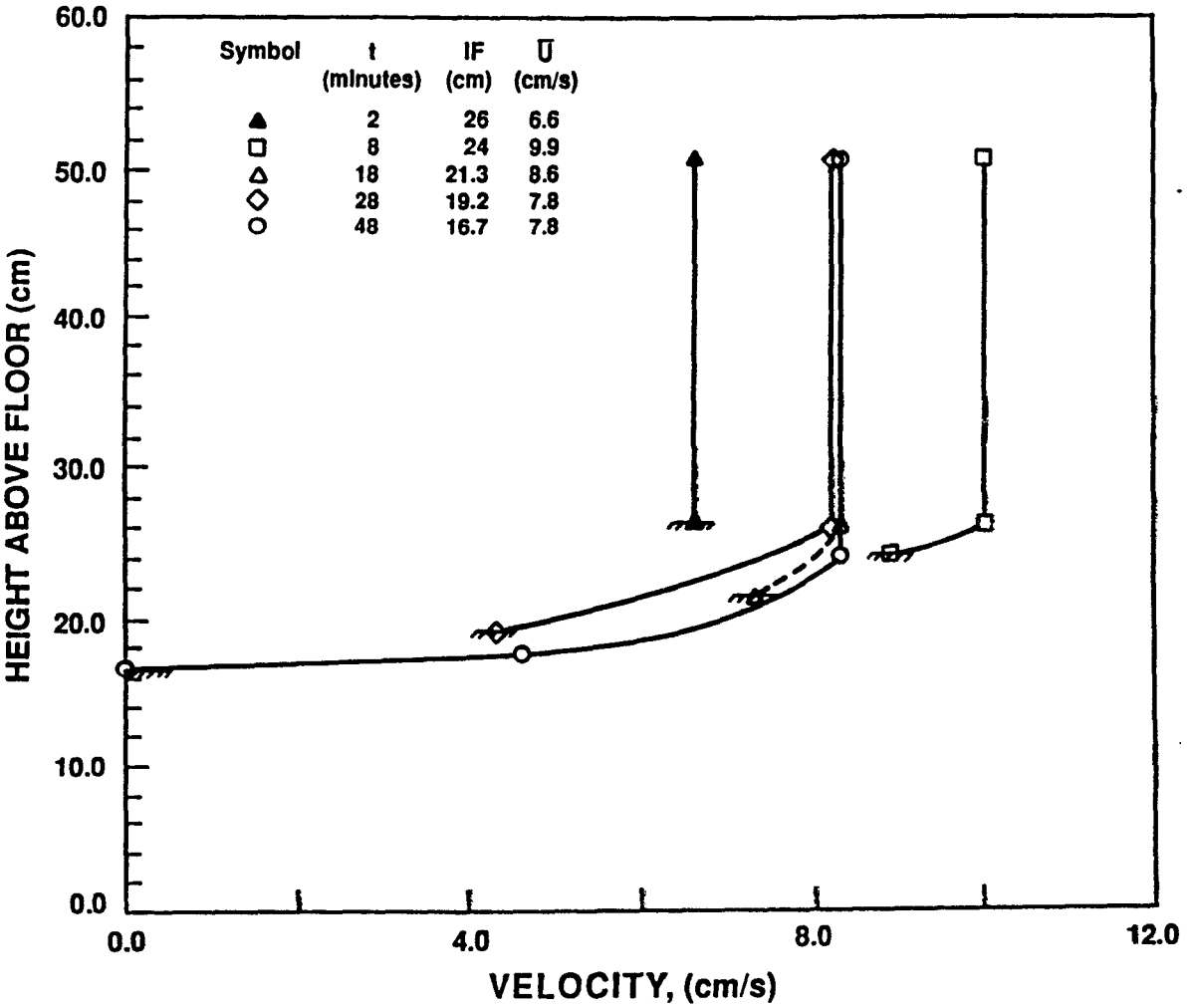

Figure 6.2: Evolution of the velocity profile in the mixed-layer for Run 6 with kaolinite. IF denotes interface.

flux due to the sediment particle's fall velocity (see also Wolanski et al. 1989). This can be considered in terms of the energy equation (see Abraham 1988)

$$\frac{dK}{dt} = \overline{u'w'}\frac{\partial \bar{u}}{\partial z} - \frac{g}{\rho}\overline{w'\rho'} - \epsilon \tag{6.3}$$

with the primes denoting turbulent fluctuations, K the turbulent kinetic energy and ϵ the dissipation function. Assuming the turbulence to be in local balance, diffusive transport is neglected and $\frac{dK}{dt} = 0$. Thus,

$$\overline{u'w'}\frac{\partial \bar{u}}{\partial z} = \frac{g}{\rho}\overline{w'\rho'} + \epsilon \tag{6.4}$$

whence the production term of kinetic energy is balanced by the buoyancy term (which is the conversion of input energy into the potential energy of the system) and the dissipation function. Hence, at constant input of kinetic energy, as the buoyancy term decreases, the dissipation of energy increases. Thus, with the passage of time, at fixed input of energy due to the pump system, the available energy to effect entrainment decreased. Visually, this resulted in decreased amplitudes of the waves at the interface. Figure 6.3 shows that the mixed-layer depth (for Run 10 with bentonite as the constituent sediment of fluid mud) increased very rapidly with time initially, but slowed down after $\sim$ 20 minutes. Figure 6.4 is more illustraive as it plots the rate of change of the mixed-layer depth against time (obtained by differentiating the curve fitted in Figure 6.3). As expected, the curve asymptotes towards zero after about $\sim$25 minutes.

6.4 Shear Layer

The shear layer is obviously very important as it is directly responsible for overcoming the static stability of the two-layer system (of fluid mud and water) and causing mixing. The vertical distance, between the point where the velocity profile deviates from the vertical in the mixed layer to the the level of the interface, was taken to be the thickness of the shear layer, δ_s (refer to Figure 3.2) (although the velocity may decrease to zero inside the thin interface). At the start of each run

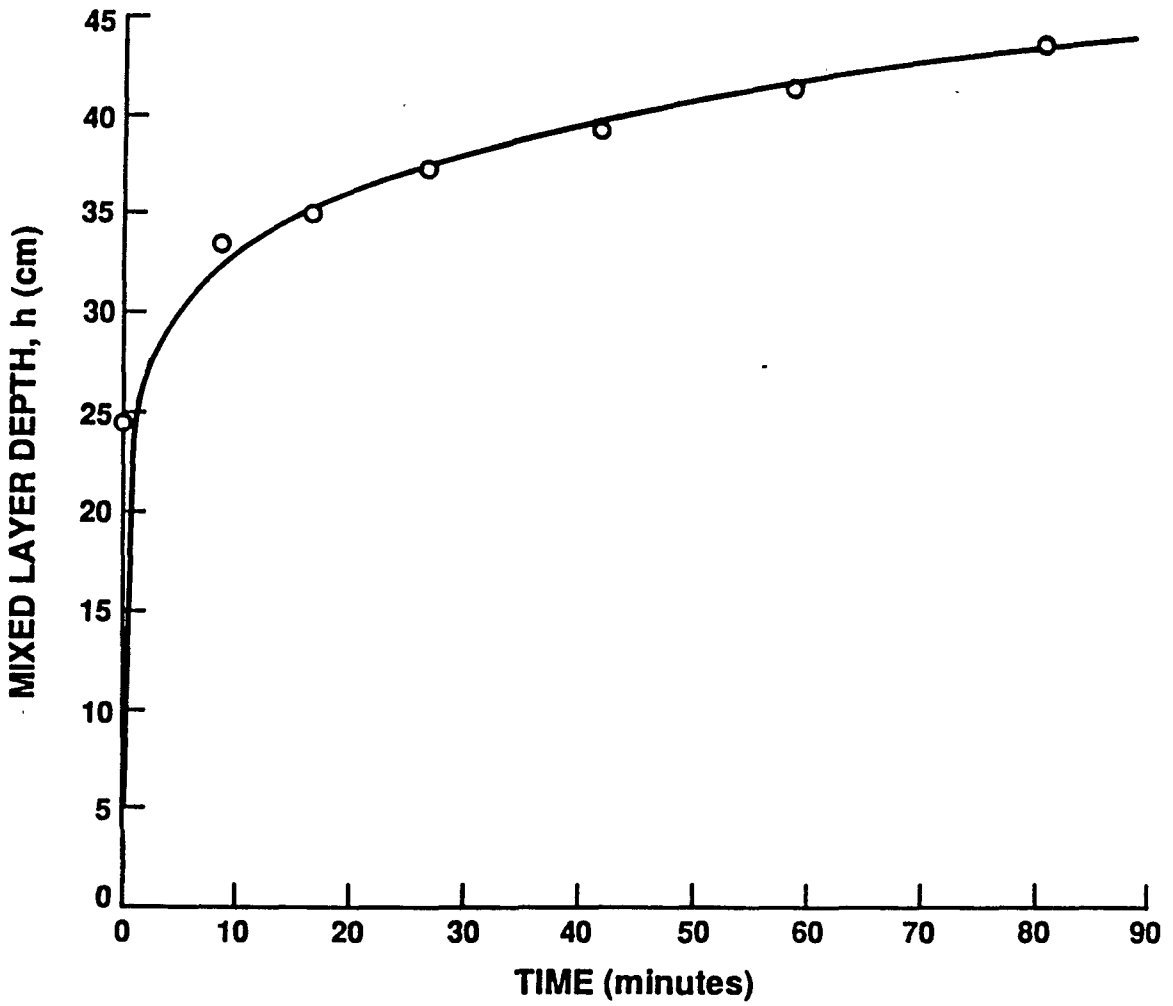

Figure 6.3: Change in the mixed-layer depth with time for Run 10 with bentonite.

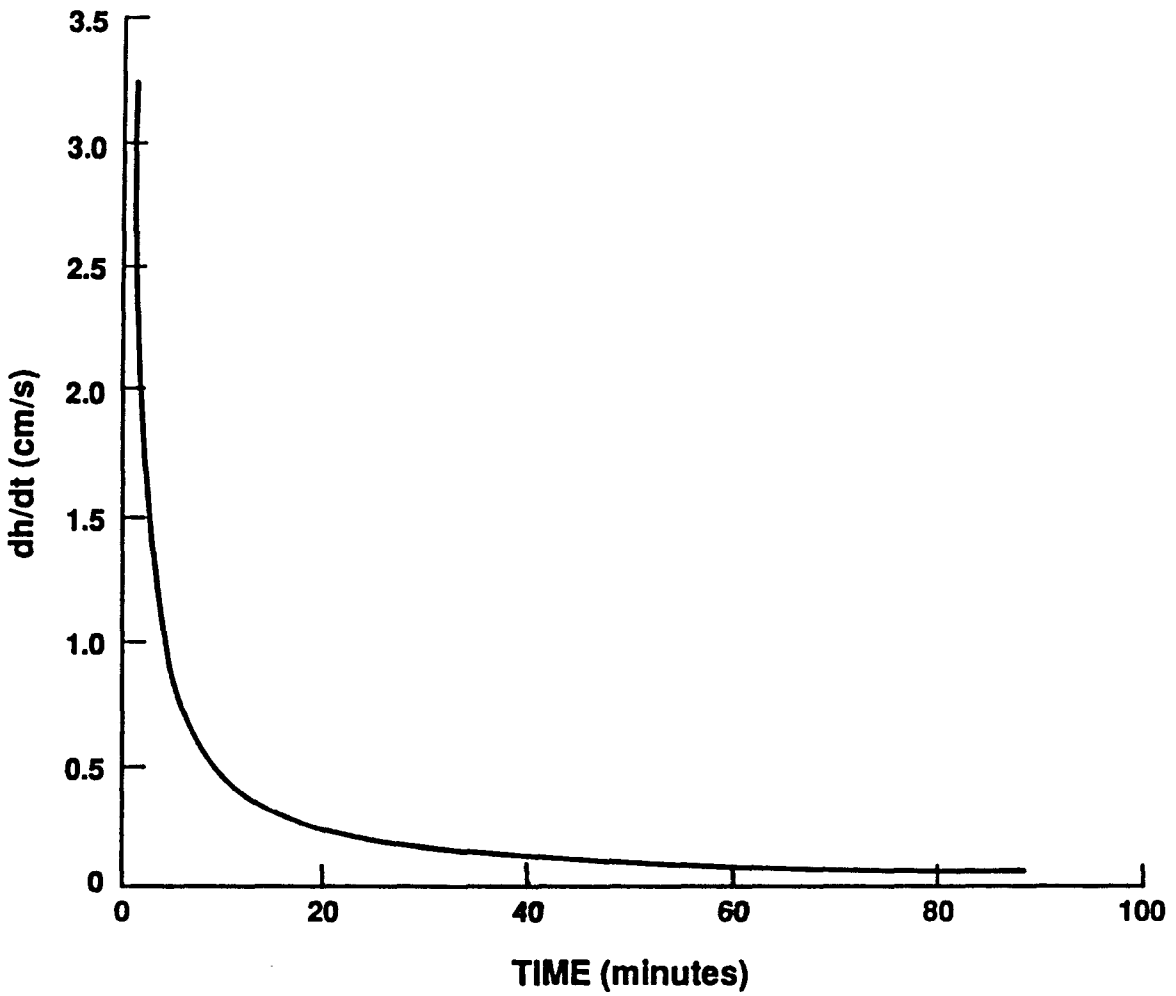

Figure 6.4: Rate of change of mixed-layer depth in Run 10 with bentonite.

when, initially, the upper mixed layer was equilibrating to the energy input of the pump system, the interface appeared to be in turbulent motion, but the velocity below the level of the visual interface could not be determined. Above it, the mixed layer was fully turbulent and dye injection showed an apparent step velocity profile with the vortex sheet at the interface. Actually, as mentioned before, it might be more realistic to assume the thin density interface (Narimousa and Fernando 1987) to have a steep density gradient. This appears to be most plausible as the interface, at those times, was convulsed by massive undulations – of heights of the order of ~ 6-8 cms – causing much mixing. The effect of the splitter plate in causing additional entrainment was also visible. Thus, the first interval of each run was not considered while plotting data in Figure 6.5 where the data are from all the runs (i.e., for both kaolinite and bentonite) have been included. Unfortunately, the data are quite scattered for any definitive conclusions to be made. The values of δ_s range from $\sim 0.18 - 0.34$ h. To avoid illusionary appearances on account of disparate scales of the axes, the same was also plotted on a log- log scale (see Figure 6.6) which indicates that the δ_s may be $\sim 0.23h$ for $4 < Ri_u < 20$ with a slight increase beyond 20. Long (1973) reported that Moore and Long's (1971) data indicated $\delta_s/h \sim Ri_u^{-0.5}$ while Narimousa and Fernando (1987) found the non-dimensional shear layer thickness to be independent of Richardson number and about 0.2. In the present case, the scatter of data may not actually be very surprising, as (1) the diffusion of momentum into and maybe even below the level of the interface may not always have been totally negligible, and (2) the conditions for two different runs were not exactly duplicated for the same Richardson number, e.g., a value of $Ri_u = 10$ may have been obtained in the second time interval of a run while it may have occured in the later intervals of the other. There will be greater dissipation of kinetic energy in the second case in trying to counteract the settling tendency of more sediment particles, as the concentration of the mixed layer increases with

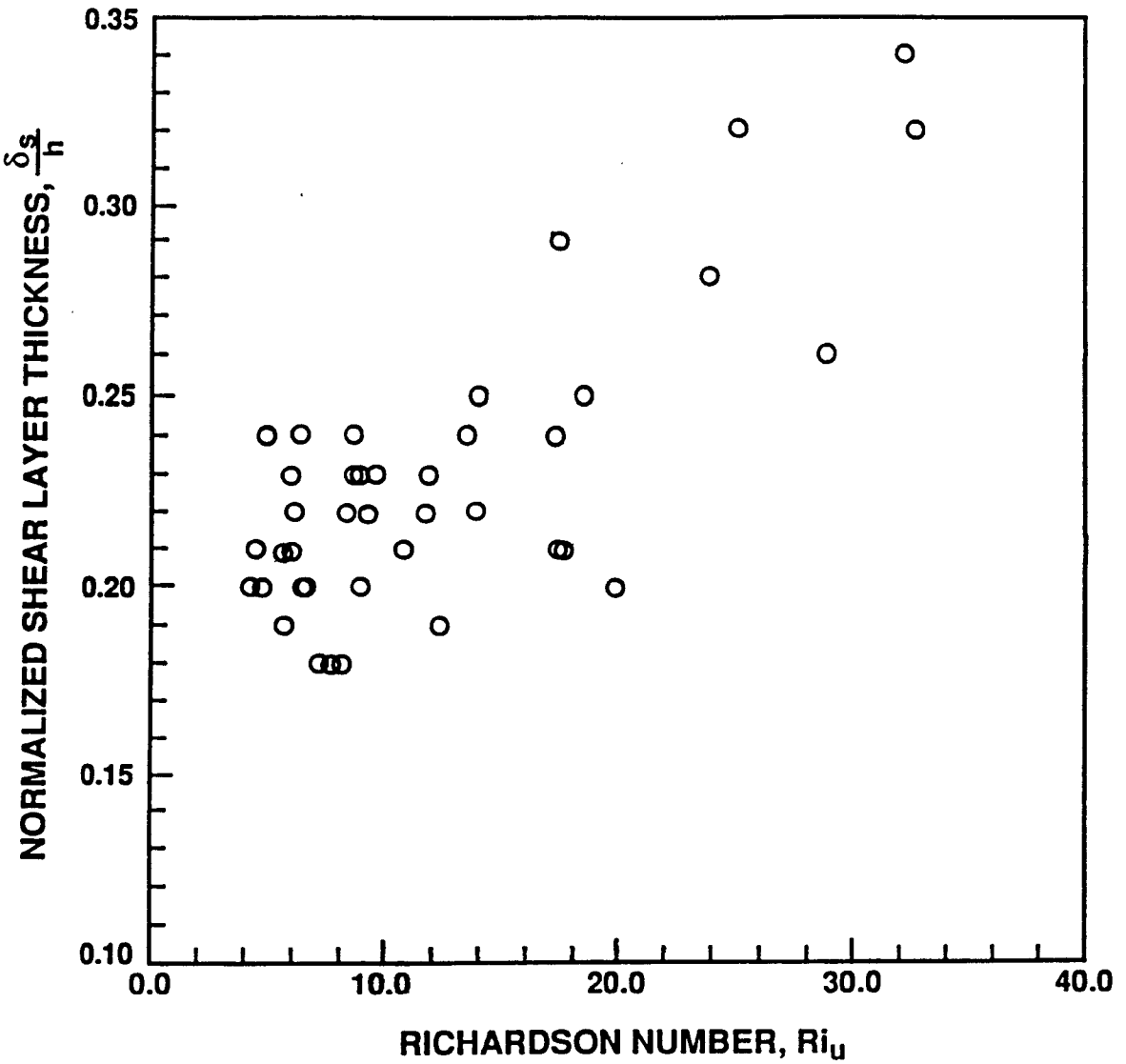

Figure 6.5: Non-dimensional shear layer thickness vs. Richardson number

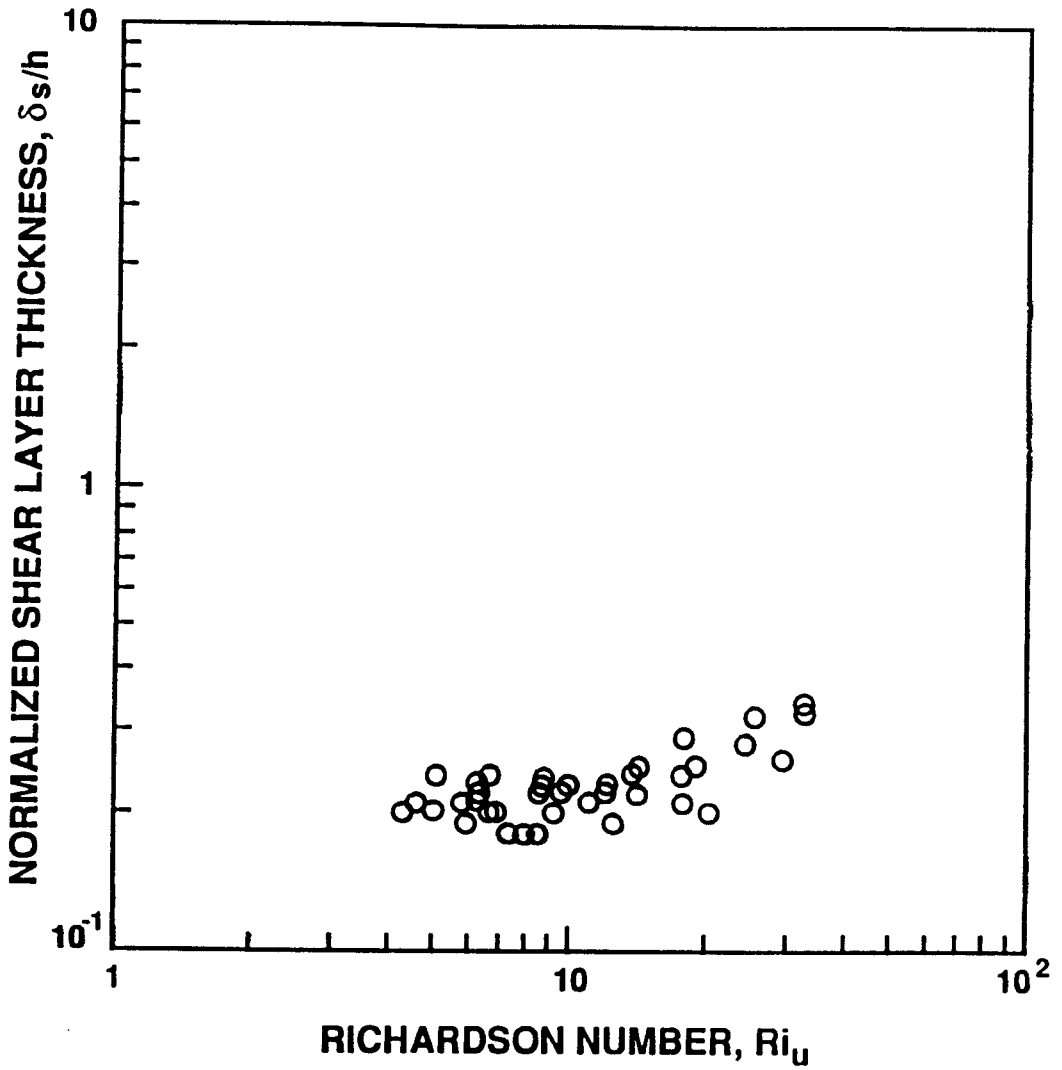

Figure 6.6: Non-dimensional shear layer thickness vs. Richardson number on a log-log scale

time. Thus, it appears that the thickness of the shear layer increased with increasing Richardson number, unlike in Moore and Long (1971). More accurate methods of measurement are required for velocity profiles before any definitive conclusions can be reached.

6.5 Observations on the Interface

When the pump section was turned on to start the experiment, the entrainment process started out with turbulent entrainment of the diffuse intermediate layer which formed when the fluid mud was introduced under the water layer while setting up the two-layer system. Figure 6.7 was taken within half a minute of starting the pump system. The grid squares are 2 *times* 2 cm. This intermediate layer eroded completely within 1-1.5 minutes. Although the contribution to the density of the mixed layer was minimal, there was a significant contribution to the turbidity of the mixed layer, thereby rendering it opaque and obstructing visibility. Small amounts of dye were injected and this dye stained the mixed-layer as it moved around the flume and gave a color contrast with respect to the fluid mud layer. Initially, the effect of the splitter plate in producing additional vorticity at the entrance to the observation section was quite pronounced and was visible as deepening of the interface there (this tilt was generally perceptible for about the first 8-10 minutes). Mixing was caused by massive internal waves (upto 8 cm wave height in the upstream portion of the observation section) breaking, as the steep velocity gradient in the thin interface caused significant scour (of the interface). Figures 6.8 and 6.9 were taken back-to-back in the same run at $Ri_u \sim 7$. Wave heights were about 4 cm. The interface was highly irregular and action of eddies causing entrainment is visible towards the left of the photographs. Entrainment due to internal wave breaking seemed to cause most of the mass flux at $Ri_u < 10$. Another mechanism of entrainment, evident for $Ri_u > 10$, was as seen in the sequence of Figures 6.10, 6.11, 6.12 and 6.13. Figure 6.10 shows the highly irregular interface with eddies scour-

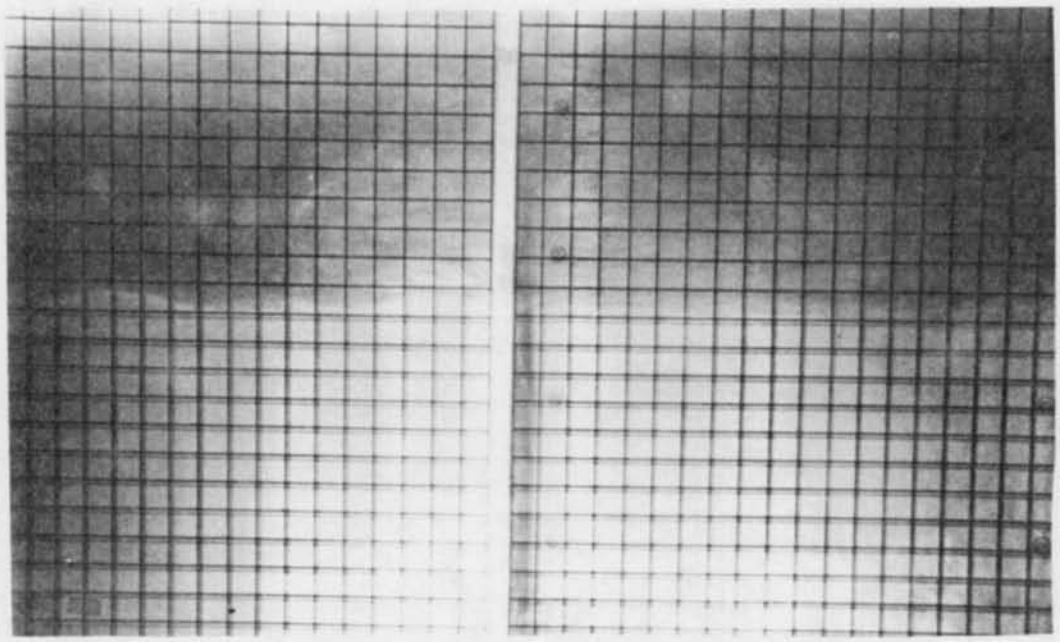

Figure 6.7: Turbulent entrainment at t $\sim$ 0.5 minute. Sediment- kaolinite.

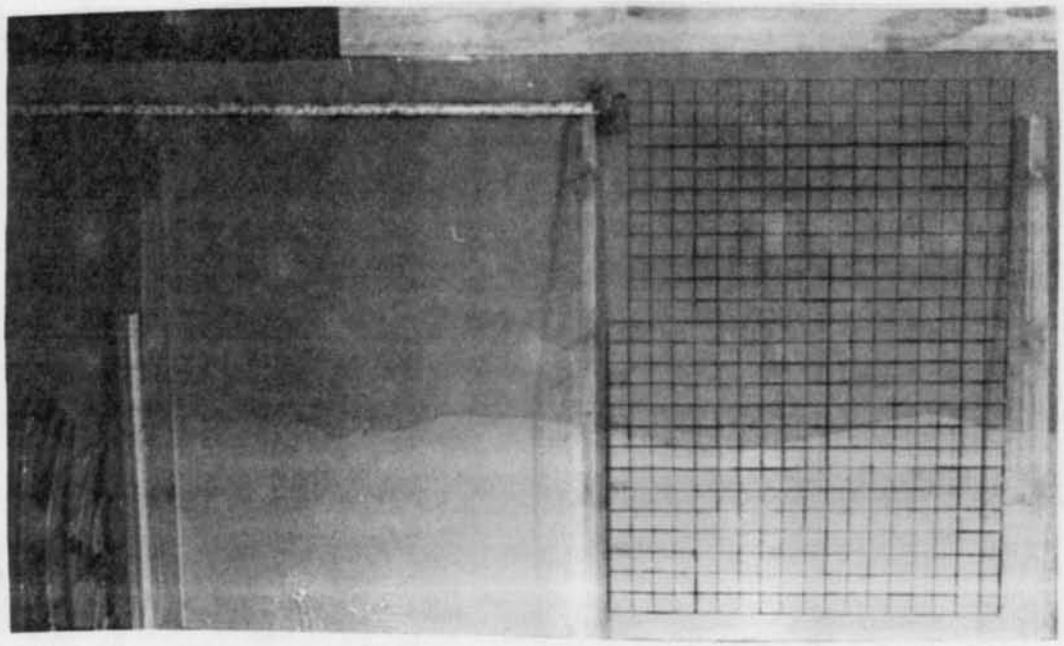

Figure 6.8: Interface at $Ri_u < 10$. Sediment-kaolinite.

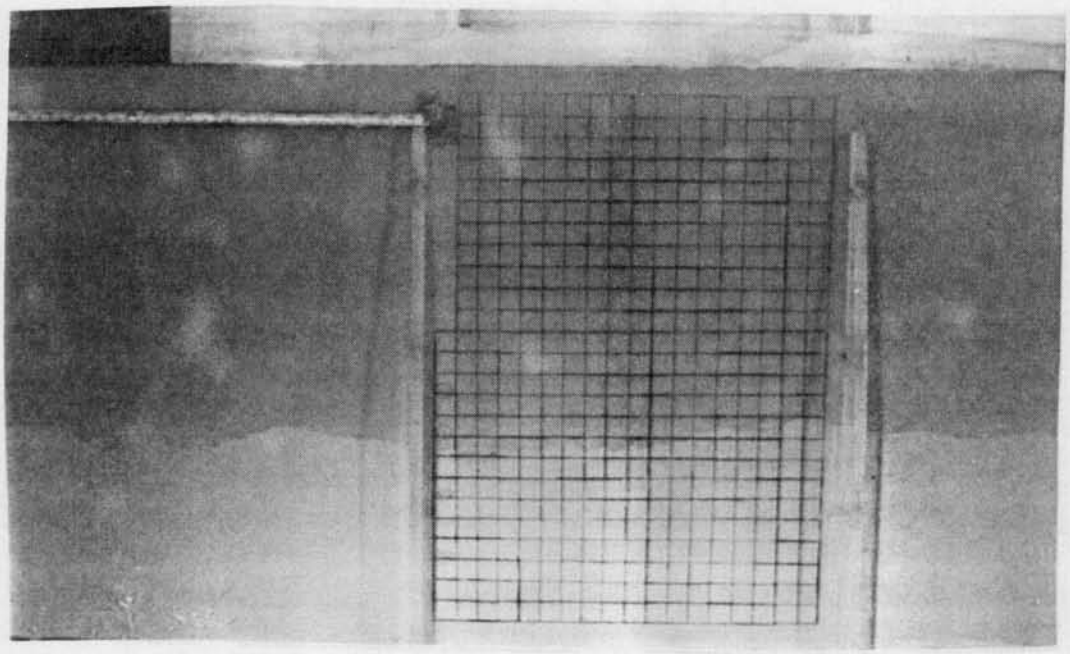

Figure 6.9: Interface at $Ri_u < 10$. Sediment-kaolinite.

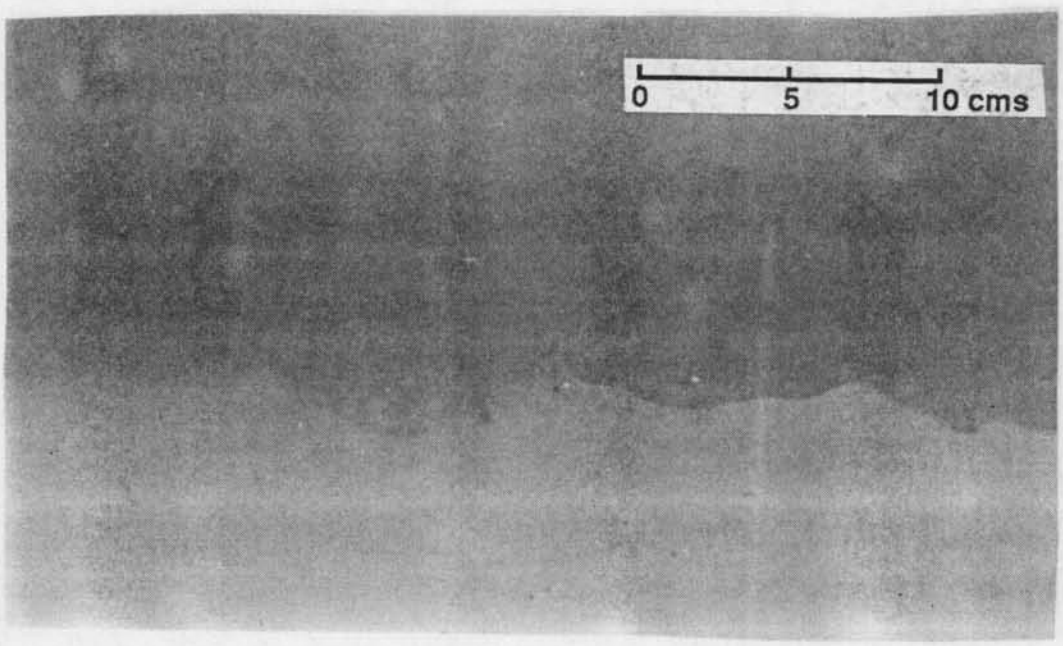

Figure 6.10: Highly irregular interface at $Ri_u > 10$. Sediment- kaolinite.

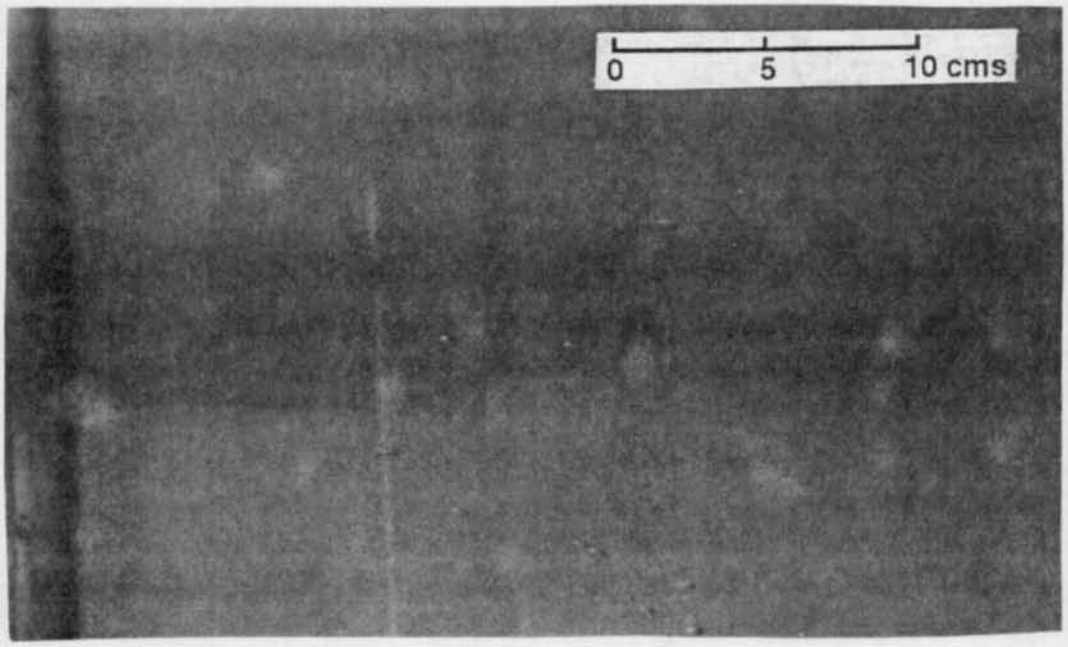

Figure 6.11: Scour of growing crest at $Ri_u > 10$. Sediment- kaolinite.

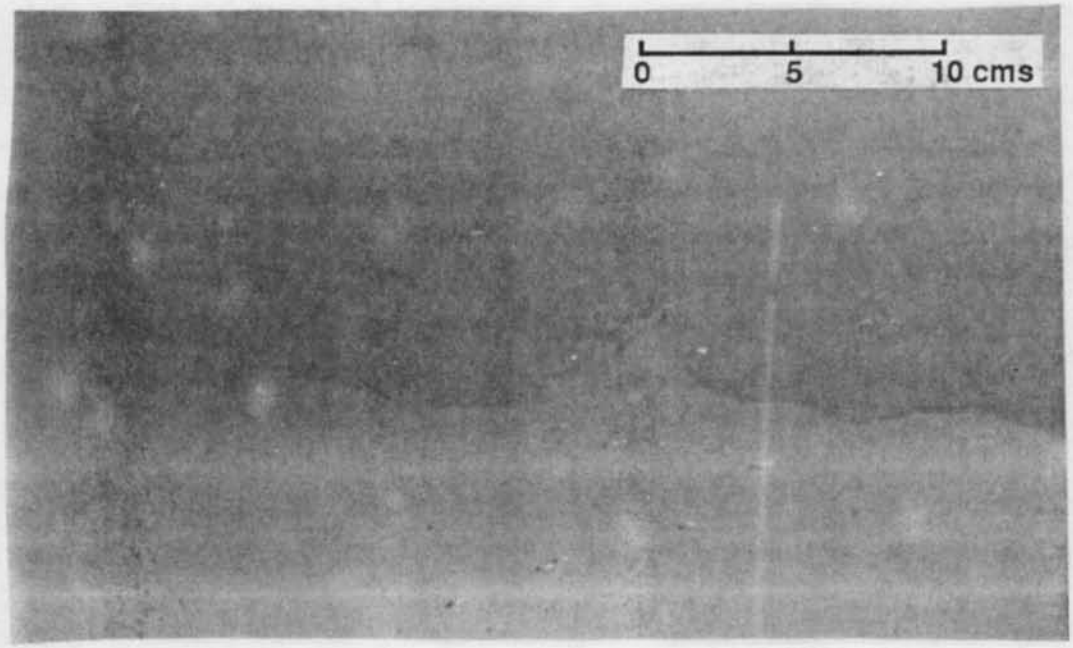

Figure 6.12: Scour of grown crest at $Ri_u > 10$. Sediment- kaolinite.

ing the interface. Some of the undulations formed pronounced crests which grew in amplitude and sharpened with entrainment due to eddies mostly scouring their backs and tips (Figures 6.11 and 6.12). The remaining portion of the crest then subsided back towards the interface (Figure 6.13). When the same mechanism was active at slightly lower Richardson numbers ($\sim$ 10-15), after the wave sharpened at the crest, instead of breaking to form an eddy, this crest suddenly disappeared with a thin of fluid being 'ejected' from the tip (see Figure 6.14). It appears possible that the original undulations were caused by eddies from the mixed layer scouring the interface, with it's 'roller action' causing crest growth and entrainment across (the crest). When the eddy was strong enough, it could shear off the crest. These phenomena of cusping into the upper (mixed) layer and appearance of 'smoke-like wisps' from these crests cusping into the faster layer seemed to indicate the existence of Holmboe (mode 2) type of instabilities which was discussed earlier in Section 3.1 and 3.2. Referring again to this review, this appears to be feasible as $\delta_s \gg \delta$ and the levels of stratification attained were always quite high (as compared to the lower, Ri < 3, similarly defined Richardson numbers obtained in experiments with salt-stratified systems). When the Richardson number still increased (beyond $\sim$ 25), the interface was convoluted with smaller (less than 1 cm) disturbances (see Figure 6.15) which appeared to be slightly more regular.

6.6 Entrainment Rate

Table 6.2 documents the parameters that were measured during the course of each run for all the runs with kaolinite as the constituent of fluid mud (i.e., Runs 1-9). Table 6.3 does the same for runs with bentonite (i.e., Runs 10 and 11). The listed parameters are the representative ones for each time interval of each run. Table 6.4 contains the calculated parameters which further lead to the non-dimensional buoyancy flux and Richardson number for each interval of each run with fluid mud of kaolinite. Reynolds number (Re) calculated according to Re =

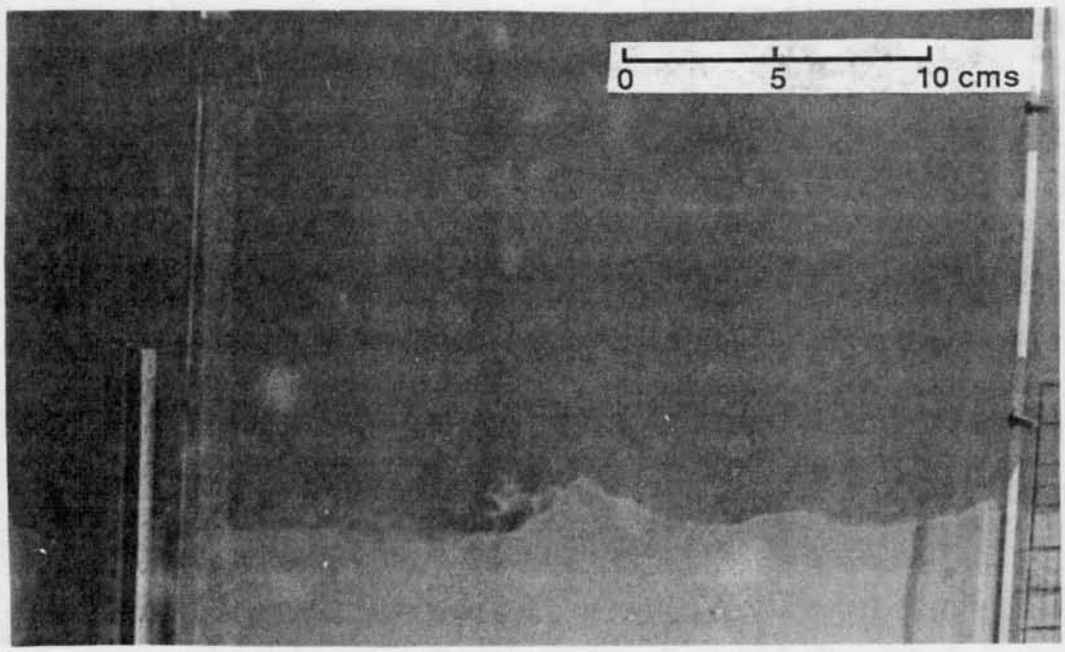

Figure 6.13: Subsiding crest at $Ri_u > 10$. Sediment-kaolinite.

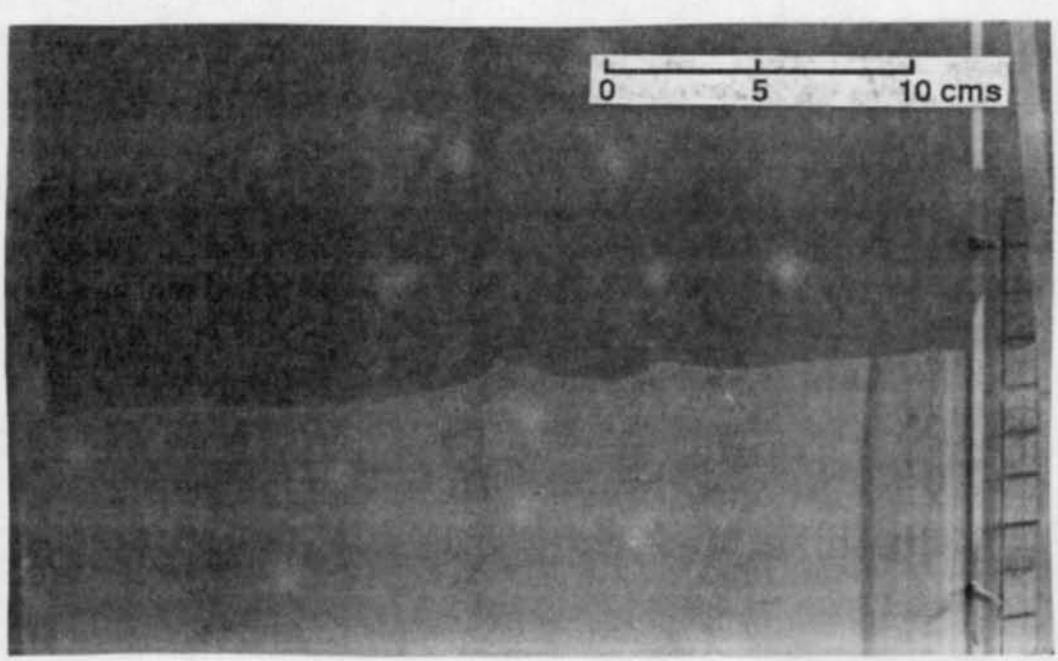

Figure 6.14: Smoke-like wisp being ejected from the tip of disturbances. Sediment-kaolinite.

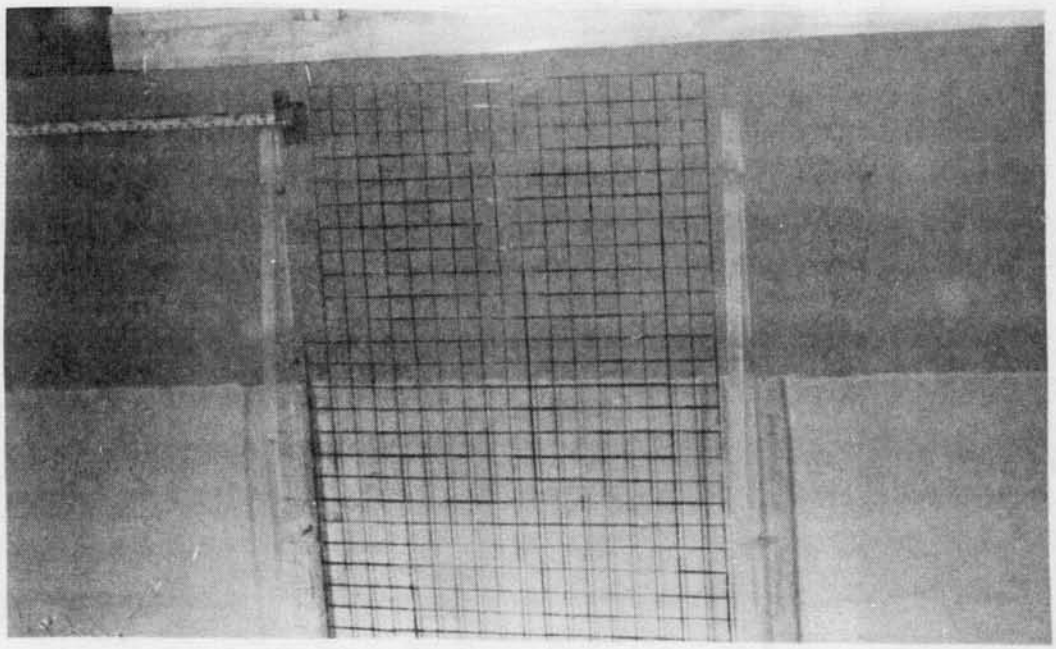

Figure 6.15: Appearance of the interface at high Richardson numbers, $Ri_u > 25$. Sediment-kaolinite.

Table 6.2: Relevant measured parameters for runs with kaolinite

RUN No.	dt min.	dm g/cm^2	h cm	H cm	C_2 g/l	$\bar{u}$ cm/s
1	9	.0546	34.4	17.6	31.2	7.4
	8	.1093	36.1	15.9	32.0	10.1
	17	.1221	40.5	11.5	46.3	13.9
	9	.1184	42.0	10.0	49.2	14.6
2	7	.0335	29.5	25.8	88.0	7.5
	16	.3125	36.3	19.0	103.0	12.1
	15	.4500	39.1	16.2	103.0	14.0
3	5	.0630	26.3	24.7	110.0	11.8
	12	.1550	27.9	23.1	112.0	10.0
	11	.0995	29.0	22.0	100.0	10.8
	13	.1500	30.5	20.5	107.0	11.0
	19	.0460	32.3	18.7	120.0	7.9
	10	.0390	33.1	17.9	125.0	8.2
4	21	.3660	34.0	22.0	81.0	13.1
	7	.1325	38.0	18.0	82.0	13.0
	15	.1975	41.5	14.5	92.0	10.2
	20	.1290	43.0	13.0	95.7	9.1
	21	.0871	44.3	11.7	104.5	8.8
5	8	.1670	28.4	24.6	80.0	11.9
	15	.1680	31.4	21.6	59.0	10.3
	10	.1025	33.3	19.7	66.0	8.7
	10	.0725	35.2	17.8	70.0	8.3
	12	.0400	37.0	16.0	77.0	7.4
6	9	.0775	27.0	23.7	42.5	9.5
	8	.0425	29.2	21.5	43.0	9.1
	10	.0175	31.0	19.7	46.5	8.2
	13	.0440	33.9	16.8	56.5	7.8
7	10	.1356	32.1	22.9	30.8	11.0
	8	.0925	33.0	22.0	33.7	11.0
	9	.0842	34.9	20.1	33.9	10.8
	9	.0910	35.8	19.2	40.1	10.3
8	13	.3668	31.2	25.0	56.4	13.0
	13	.1765	34.3	21.9	61.6	12.1
	13	.1009	36.8	19.4	65.8	10.0
9	9	.0550	28.8	23.0	65.0	9.6
	12	.1850	32.1	19.7	60.0	9.3
	10	.0720	35.0	16.8	80.0	9.3
	13	.1350	37.0	14.8	84.0	9.3
	15	.0255	38.8	13.0	89.0	9.2

Table 6.3: Relevant measured parameters for runs with bentonite

RUN No.	dt min.	dm g/cm^2	h cm	H cm	C_2 g/l	$\bar{u}$ cm/s
10	10	.3089	33.5	20.5	34.5	9.2
	8	.0520	35.0	19.0	33.0	9.1
	10	.0840	37.3	16.7	33.0	9.1
	15	.0630	39.3	14.7	33.0	9.0
	17	.0681	41.5	12.5	33.4	8.5
	22	.0662	43.7	10.3	33.8	7.5
11	9.5	.2135	32.0	19.6	40.0	9.9
	8.5	.0415	33.6	18.0	35.0	9.5
	9	.0505	34.4	17.2	42.0	9.0
	10	.0380	36.1	15.5	43.5	9.2
	14	.0447	37.4	14.2	42.8	9.7
	16	.0543	38.7	12.9	43.0	8.7

$\bar{u}h/\nu$ is also shown for each interval, taking $\nu = 1$ *times* 10^{-6} m^2/s. Table 6.5 is similar to Table 6.4 except that the calculations are for bentonite fluid mud.

The associated terminology is as follows:

dt = time of the interval
dm = mass per unit area transferred from fluid mud
h = depth of mixed layer
H = depth of fluid mud
$\bar{C}_1$ = mean concentration of the mixed layer
$\bar{\rho}_1$ = mean density of the mixed layer
C_2 = concentration of fluid mud at the level of the interface
$\bar{C}_2$ = mean concentration of fluid mud
Δb = buoyancy step across the interface
$\bar{u}$ = mean velocity of the mixed layer
Ri_u = Richardson number
= $\frac{h\Delta b}{\bar{u}^2}$
Q = non-dimensional buoyancy flux
= $\left(\frac{dm}{dt}\frac{g}{\bar{\rho}_1}\right)\frac{1}{\bar{u}\Delta b}$

As can be seen, the concentration of fluid mud at the level of the interface generally increased with time, although there were times when this concentration decreased in the second interval (with respect to the first) of some runs. As the buoyancy step across the interface is dependent on this concentration, during the course of each run it also, at times, decreased into the second interval of a run

Table 6.4: Entrainment rates and Richardson numbers for runs with kaolinite

RUN No.	$\bar{C}_2$ g/l	$\bar{C}_1$ g/l	$\bar{\rho}_1$ g/cm^3	Δb cm/s^2	Re ($\times 10^{-4}$)	$\mathbf{Ri}_u$	Q ($\times 10^4$)
1	63.3	1.6	1.001	18.1	2.5	11.4	7.4
	63.2	4.5	1.003	16.8	3.6	5.8	13.4
	76.7	7.1	1.004	23.8	5.6	5.0	3.5
	76.4	9.6	1.006	24.0	6.1	4.7	6.1
2	117.4	1.1	1.001	53.0	2.2	27.8	2.0
	142.8	9.5	1.006	56.8	4.4	14.1	4.6
	139.9	20.4	1.013	49.8	5.5	9.9	6.9
3	128.5	2.4	1.001	65.7	3.1	12.4	2.7
	130.7	7.8	1.005	63.3	2.8	17.7	3.3
	132.7	10.9	1.007	54.0	3.1	13.4	2.5
	135.1	15.3	1.010	55.5	3.4	14.0	3.1
	145.7	15.9	1.010	63.0	2.6	32.6	0.78
	150.0	16.7	1.010	65.5	2.7	32.2	1.2
4	98.9	10.76	1.0067	42.6	4.5	8.4	5.1
	113.5	13.11	1.0082	41.7	4.9	9.4	5.7
	127.6	16.77	1.0100	45.5	4.2	18.2	4.6
	132.4	19.07	1.0119	46.2	3.9	24.0	2.5
	139.7	20.48	1.0127	50.7	3.9	29.0	1.5
5	88.5	5.88	1.0037	45.1	3.4	9.1	6.3
	93.1	10.67	1.0066	29.3	3.2	8.7	6.0
	96.8	13.14	1.0082	32.0	2.9	14.1	6.0
	103.1	14.49	1.0090	33.6	2.9	17.2	4.2
	112.2	14.86	1.0093	37.6	2.7	25.4	1.9
6	64.8	2.87	1.0018	24.2	2.6	7.2	6.1
	69.4	4.11	1.0026	23.7	2.7	8.4	4.0
	74.9	4.44	1.0028	25.6	2.5	11.8	1.4
	85.2	5.35	1.0033	31.1	2.6	17.4	2.3
7	48.4	4.22	1.0028	16.2	3.5	4.3	12.4
	46.2	6.91	1.0043	16.3	3.6	4.5	10.5
	46.4	8.95	1.0056	16.3	3.8	4.9	8.6
	46.1	11.24	1.0070	17.5	3.7	5.9	9.1
8	65.0	11.76	1.0073	27.1	4.1	5.0	13.1
	66.1	15.84	1.0099	27.6	4.2	6.5	6.6
	69.5	17.51	1.0110	29.2	3.7	10.7	4.3
9	94.8	1.91	1.0012	38.5	2.8	12.0	2.7
	101.3	7.48	1.0047	31.9	3.0	11.9	8.4
	114.5	8.91	1.0056	43.2	3.3	17.5	2.9
	120.8	12.08	1.0075	43.6	3.4	18.7	4.2
	135.6	12.18	1.0076	46.6	3.6	21.3	.64

Table 6.5: Entrainment rates and Richardson number for runs with bentonite

RUN No.	$\bar{C}_2$ g/l	$\bar{C}_1$ g/l	$\bar{\rho}_1$ g/cm^3	Δb cm/s^2	Re ($\times 10^{-4}$)	$\mathbf{Ri}_u$	Q ($\times 10^4$)
10	34.5	9.22	1.0057	15.4	3.1	6.1	35.5
	34.4	10.31	1.0064	13.8	3.2	5.8	8.4
	34.1	11.94	1.0074	12.8	3.4	5.7	11.7
	34.5	12.92	1.0080	12.2	3.5	6.2	5.9
	35.2	13.88	1.0086	11.8	3.5	6.8	6.5
	36.2	14.70	1.0091	11.6	3.3	9.0	5.6
11	44.4	6.67	1.0042	20.3	3.2	6.6	18.2
	45.8	7.59	1.0047	16.7	3.2	6.2	5.0
	45.0	8.88	1.0055	20.1	3.1	8.5	5.0
	47.5	9.52	1.0059	20.6	3.3	8.8	3.3
	48.7	10.38	1.0065	19.7	3.6	7.8	2.7
	49.4	11.43	1.0071	19.2	3.4	9.8	3.3

before beginning to increase. The mean concentration (and hence the density) of the mixed-layer increased due to mass flux into it during the course of each run. The mean concentration of the fluid mud increased. By definition, $\frac{dm}{dt}$ is the mass flux into the mixed layer. Multiplying by $\frac{g}{\rho_1}$ gives the flux of buoyancy, q, which can be non-dimensionalized by dividing by $\bar{u}\Delta b$ to obtain the non-dimensional buoyancy flux, Q. The reason for the non-dimensionalizing parameters becomes clear with the following discussion.

As argued on dimensional grounds in Chapter 1 and further discussed in Chapter 4, it is well-known that the non-dimensional entrainment coefficient, E, is a function of the relevant Richardson number, i.e.,

$$E \sim Ri^{-n} \tag{6.5}$$

with n a positive number. However, the non-dimensional buoyancy flux should also be similarly related (Moore and Long 1971). Say, Δm is the mass that is raised from the bottom of the tank to the top, a distance $\hat{h}$. Thus, the time rate of increment in potential energy due to this mass transfer = $g\hat{h}(\Delta m/dt)$ = dV/dt, V denoting potential energy.

Averaging this rate of increase of potential energy over the mass of fluid in the tank,

$$\begin{aligned} dV_1/dt &= (1/\rho_0 \hat{h} A) dV/dt \\ &= \frac{g}{\rho_0 A}\frac{\Delta m}{dt} \\ &= (\text{mass flux}) \times g/\rho_0 \\ &= \text{buoyancy flux, q} \end{aligned} \tag{6.6}$$

where V_1 is the potential energy per unit mass and ρ_0 is a representative density for the fluid in the tank.

Thus, the buoyancy flux q, can be thought of as a time rate of change of potential energy per unit mass. The relation of Kato and Phillips (1969), which was discussed

in Section 4.2 is repeated here for convenience

$$\frac{2}{u_*\Delta b}\frac{dV_1}{dt} = \frac{u_e}{u_*} = E = A_1 Ri_*^{-1} \tag{6.7}$$

where A_1 is some constant. Utilizing equations (6.6) and (6.7) we have,

$$\begin{aligned} Q &= q/(\bar{u}\Delta b) \\ &= (1/\bar{u}\Delta b)dV_1/dt \\ &\sim A_2/Ri_u \end{aligned} \tag{6.8}$$

where A_2 is another constant. This is similar to equation (6.5), and thus the relationship to the relevant Richardson numbers should be similar.

With the preceding discussion in mind, Q was plotted against Ri_u in Figure 6.16. Data from all the Runs are included in the figure. There is again a substantial amount of scatter in the figure. It is conjectured that more accurate methods of measurement might yield improved results. Though bentonite had been chosen to observe the effects of degree of cohesion of the sediment, the (initial) concentration of bentonite fluid mud could not be increased above 39 g/l because of difficulty in premixing it prior to introducing it into the flume (see Section 5.2). Thus, experiments with bentonite were only at low Richardson numbers. It is surmised that at these low concentrations (when apparently, the sediment suspension behaves like a 'fluid') the effect of sediment cohesion might not manifest itself strongly enough to yield a detectable change in the entrainment rate from that of a comparitively weakly cohesive sediment like kaolinite. The increased scatter of bentonite data was because of increased inaccuracy in measuring concentration profiles (see Section 5.2) and should not be seen as indicating any seperate trend. A trend line was drawn to the data, which was according to the relationship

$$Q = \frac{A\,(Ri_u)^{-0.9}}{[(B)^2 + (Ri_u)^2]^m} \tag{6.9}$$

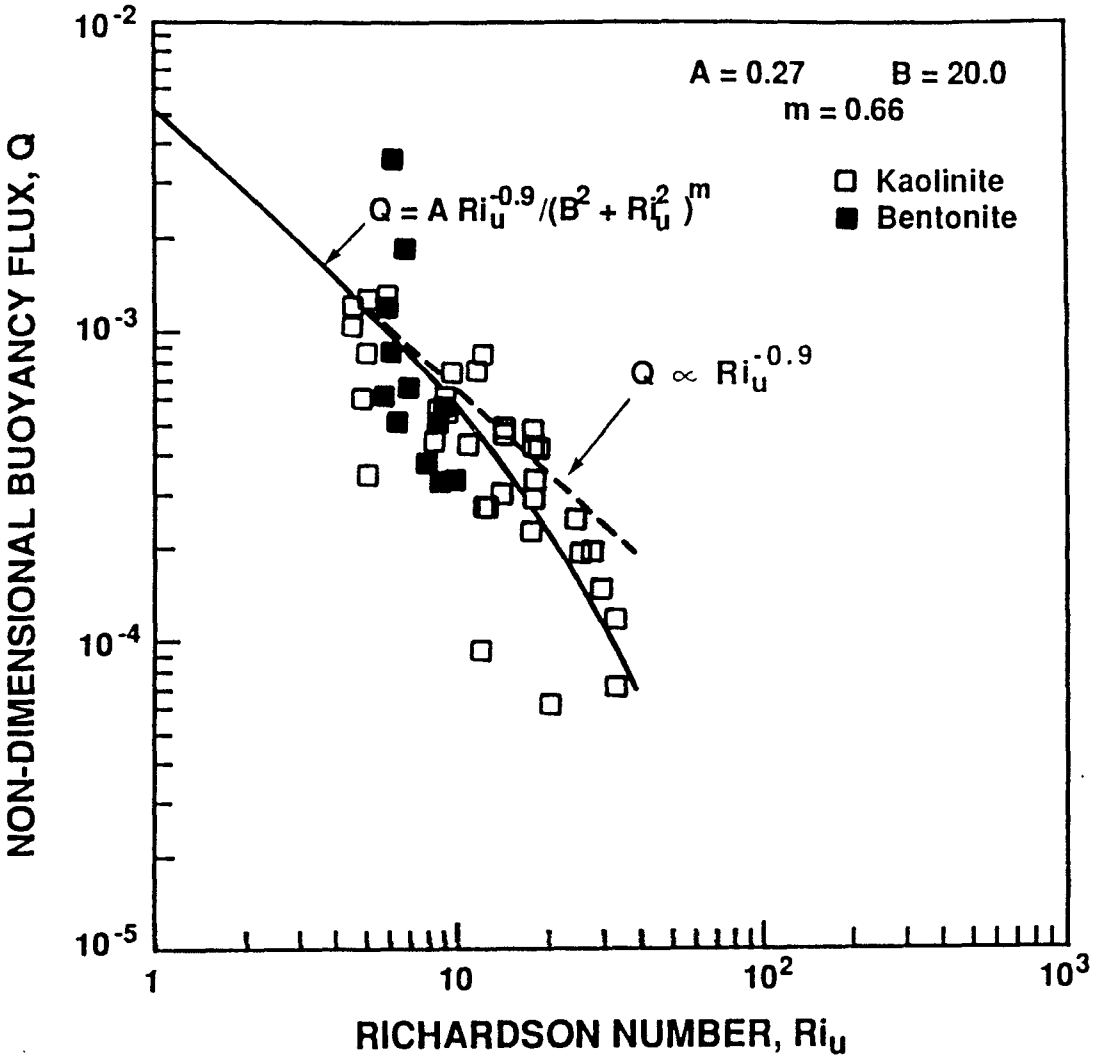

Figure 6.16: Non-dimensional buoyancy flux vs. Richardson number for all the experiments.

where A = 0.27, B = 20, m = 0.66. It is felt that the only effect of the splitter plate (which was apparent visually in the initial stages of each experimental run) on this preceding relation might have been to cause some discrepency in the value of the constants (A, B and m) of the above relation, but the basic relationship between Q and Ri_u seems to be adequately quantified by this relation. The dashed line indicates a trend

$$Q \propto (Ri_u)^{-0.9} \tag{6.10}$$

This trend is quite similar to the relationship of equation (6.5) with n = 1 which has been found by many investigators to hold true for salt-stratified experiments (as discussed earlier in Chapter 4). The n = 1 relation and possible reasons for the difference in the exponent of the present investigation is now examined. The n = 1 relationships can be considered in terms of energy changes. Kato and Phillips (1969) showed that the rate of increase of potential energy per unit mass is related to the rate of dissipation of turbulent energy per unit mass.

From equations (6.5) with n = 1 and (6.7) and assuming $u_* \sim \tilde{u}$ (where $\tilde{u}$ = rms turbulent velocity = $\overline{(u'^2)}^{1/2}$) (Townsend 1956),

$$dV_1/dt = Ku_*^3/2h \sim \tilde{u}^3/h \tag{6.11}$$

where K is some constant and u_* is the friction velocity.

Batchelor (1953) found that the rate of change of turbulent kinetic energy per unit volume in isotropic turbulence is given by,

$$\epsilon = d\tilde{u}^2/dt \simeq \tilde{u}^3/l_1 \tag{6.12}$$

where, ϵ = turbulent energy dissipation rate, l_1 = length scale of the energy containing eddies.

Assuming that the mixed layer depth h is of the order of the size of the energy containing eddies,

$$\epsilon \simeq \tilde{u}^3/h \tag{6.13}$$

Thus, from equation (6.11),

$$dV_1/dt \simeq \tilde{u}^3/h \simeq \epsilon \tag{6.14}$$

If as for the Moore and Long (1971) experiments,

$$Q \propto Ri_u^{-1} \tag{6.15}$$

then,

$$q = Q(\bar{u}\Delta b) \sim \bar{u}^3/h. \tag{6.16}$$

Equation (6.16) is not exactly of the form of equation (6.14). However, from measurements of the rms velocity, Moore and Long (1971) observed that

$$\tilde{u} \simeq K_3(\Delta u) \sim \bar{u} \tag{6.17}$$

where K_3 is a constant and Δu is the interfacial velocity jump. Thus, $dV_1/dt \sim \tilde{u}^3/h$ as in the form of equation (6.14).

This evidence seems to indicate that in geophysical situations and similar experiments, $q(\sim dV_1/dt) \propto \epsilon$, with the "constant" of proportionality probably depending on the coefficients of viscosity and diffusivity.

For the present experiments, at low mixed layer concentrations, apparently there is not much additional dissipation of kinetic energy to counteract the downward buoyancy flux due to sediment fall velocity (see equation 6.4), as indicated by the $Q \propto Ri_u^{-0.9}$ trend (as compared with the $Q \propto Ri_u^{-1}$ trend of salt-stratified systems). However, at Richardson numbers greater than ~ 25, the buoyancy flux falls off much more drastically when, it is surmised that, a greater fraction of the input energy is used up in just maintaining the sediment particles in suspension in the mixed layer.

6.7 Discussion in Terms of Equilibrium Peclet Number

The vertical transport of fine sediments (neglecting advective fluxes) in turbulent suspensions can be expressed approximately by assuming Fickian diffusion and

eddy diffusivity. Fick's law states that the transport of matter across a normal area is proportional to the concentration gradient of matter. Denoting the vertical turbulent velocity by w' and the characteristic turbulent mixing length scale by L_e, the eddy diffusion coefficient may be defined as (Teeter 1986)

$$K_z = -(\frac{1}{2} L_e w') \tag{6.18}$$

With these considerations,

$$\frac{\partial C}{\partial t} = -\frac{\partial F_z}{\partial z} \tag{6.19}$$

where F_z is the vertical flux. If $F_z = -w_s C - K_z \frac{\partial C}{\partial z}$ (with w_s the sediment particle or aggregate fall velocity) the well-known transport equation is obtained

$$\frac{\partial C}{\partial t} = \frac{\partial}{\partial z}(w_s C + K_z \frac{\partial C}{\partial z}) \tag{6.20}$$

The equation can be non-dimensionalized by introducing the variables $Z = z/H$, $T_a = w_s t/H$ and $T_d = K_z t/H^2$ where H is a length scale (e.g., a relevant depth), w_s is the settling velocity, T_a and T_d are non-dimensional advective and diffusion time scales. The ratio of these length time is the Peclet number of the suspension, i.e.,

$$Pe = \frac{T_a}{T_d} = \frac{w_s H}{K_z} \tag{6.21}$$

With these substitutions into equation (6.20), one obtains

$$\frac{\partial C}{\partial T_a} = \frac{\partial}{\partial Z}(C + \frac{1}{Pe}\frac{\partial C}{\partial Z}) \tag{6.22}$$

or,

$$\frac{\partial C}{\partial T_d} = \frac{\partial}{\partial Z}(Pe\, C + \frac{\partial C}{\partial Z}) \tag{6.23}$$

The motion of particles or aggregates in turbulent flows is the net effect of the flow conditions and the particle's or aggregate's settling velocities. In the equilibrium state, the turbulent and settling fluxes are balanced. For this state of equilibrium, both equations (6.22) and (6.23) yield

$$Pe = -\frac{1}{C}\frac{\partial C}{\partial Z} \tag{6.24}$$

$$= -\frac{H}{C}\frac{\partial C}{\partial z} \tag{6.25}$$

If the difference in concentration from top to bottom is ΔC and the average concentration of the suspension is $\bar{C}$, equation (6.25) can be written as

$$Pe = \frac{\Delta C}{\bar{C}} \tag{6.26}$$

Numerical modeling of the transport equation with realistic data by Teeter (1986) showed the relation to be slightly modified and of the form

$$\frac{\Delta C}{\bar{C}} = \frac{1.5\ Pe}{1+P} \tag{6.27}$$

where P is the probability that a particle reaching the bed will deposit and remain there, i.e., P = 0 for equilibrium suspensions whence

$$\frac{\Delta C}{\bar{C}} \sim 1.5\ Pe \tag{6.28}$$

For the present experiments even though the primary objective was to observe the effects of buoyancy, the mixed layer can be similarly considered. At high Richardson numbers, the buoyancy flux deviated rather drastically from the $Q \propto (Ri_u)^{-0.9}$ relation, and apparently the mass flux into the mixed layer is small or negligible, i.e., the mixed layer suspension can be considered to be in equilibrium with no efflux or influx. Peclet numbers were calculated for the runs which had values of Richardson number *greater* than 20 towards the *latter* part of the runs, according to the relationships

$$\Delta C = C_2 - \bar{C}_1 \tag{6.29}$$

and

$$\bar{C} = (\bar{C}_1 + C_2)/2 \tag{6.30}$$

and are presented in Table 6.6.

The results are surprisingly close to the value (Pe = 1.5) obtained by Teeter (1986), in spite of the fact that the assumption that the mixed layer is actually

Table 6.6: Peclet numbers for equilibrium conditions

RUN No.	Ri_u	Pe
3	32.6	1.53
	32.2	1.53
4	29.0	1.34
5	25.4	1.35
9	21.3	1.52

homogeneous (measurements of concentration in the mixed-layer seemed to indicate that there might be a slight gradient of concentration near the the level of the interface), and appear to indicate that when the shear is strong enough initially, the fluid mud layer starts to entrain, but at a progressively (with time) slower rate as the Richardson number increases. The mixed layer tends towards an equilibrium suspension, i.e., a suspension in which the turbulent and settling fluxes are in balance, when there is fixed energy input (through the pump system) with equilibrium Peclet numbers tending towards 1.5 .

6.8 Comparison with Soft Bed Erosion

A soil bed has a measurable effective stress while a high density suspension (e.g., fluid mud) is without an effective stress (Ross, 1988). Thus, beds erode at higher shear stresses than fluid muds which can be easily resuspended. As mentioned in Chapter 1, most of the existing fine sediment transport models neglect the state of fluid muds when considering vertical transport. It is thus worthwhile to examine this aspect in terms of the empirical relation fitted to the data (Q vs. Ri_u) of the present investigation with erosion rates predicted for soft beds.

Soft beds are freshly deposited beds which are undergoing consolidation. The erosion rate given by Parchure and Mehta (1985) is

$$\frac{\bar{E}}{\bar{E}_f} = \exp[\alpha'(\tau_b - \tau_s)^{1/2}] \tag{6.31}$$

where, $\bar{E}$ = dm/dt = erosion rate, $\bar{E}_f$ is the floc erosion rate, τ_b is the bed shear stress, τ_s the bed shear strength and α is a rate coefficient. Representative values for kaolinite obtained by Parchure and Mehta (1985) are α = 18.4 m/N$^{1/2}$ and $\bar{E}_f = 0.5 \times 10^{-5}$ g/cm^2/min. The bed shear stress is given by

$$\tau_b = \rho g n^2 u^2 / h^{1/3} \tag{6.32}$$

where n is Manning's resistance coefficient, u the current velocity, h the water depth and ρ is the fluid (assumed water) density.

Typical representative values of n = 0.02, τ_s = 0.2 N/m^2 and h = 1 m and bed surface concentration of 100 g/l were chosen for plotting equation (6.31) in conjunction with equation (6.32) in Figure 6.17. As can be seen, the bed starts to erode only after the current velocity reaches $\sim$ 25 cm/s while there is resuspension of fluid mud even at low current velocities. The rate of erosion of soft beds approaches of fluid muds when the current velocity increases beyond $\sim$ 36 cm/s, but it is surmised that the erosion of the fluid mud layer overlying a bed will be advanced by that time. The validity of equation (6.9) at high velocity values when the Richardson number drops to below $\sim$ 4 (which is equivalent to u $\sim$ 40 cm/s in the present configuration) is questionable. However, the calculations verify the initial conjecture that ignoring the state of fluids muds by only considering bed erosion in modeling sediment transport, especially at low current velocities (as occur, for example, immediately following slack water in estuaries) can lead to substantial underestimation of upward sediment mass flux rates.

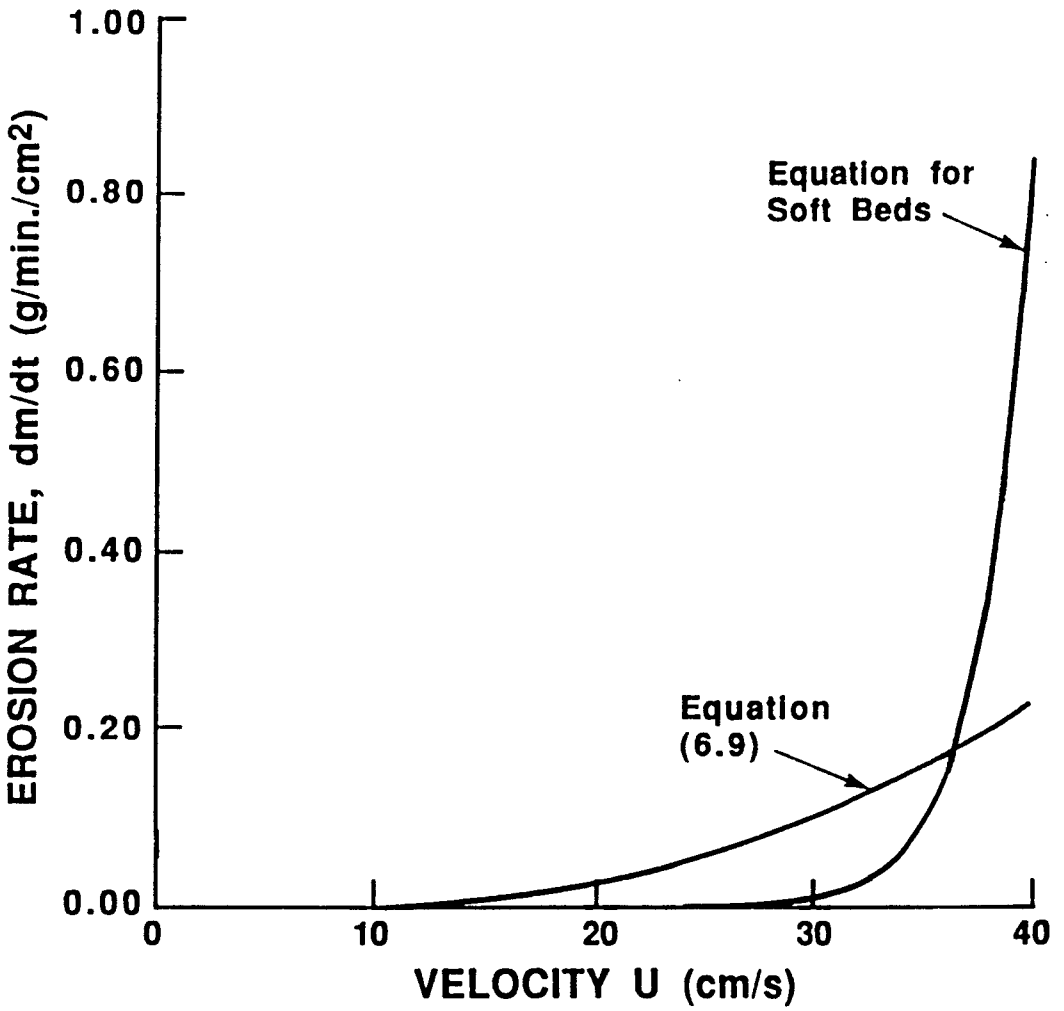

Figure 6.17: Comparison of erosion rates of soft beds with the rates predicted by equation (6.9).

CHAPTER 7
SUMMARY AND CONCLUSIONS

7.1 Summary

With the aim of simulating the effects of turbulent velocity shear at the interface of a two-layered water-fluid mud system, which is a natural occurance in estuarial environments, a laboratory experiment was designed and executed in the Coastal Engineering Laboratory of the University of Florida. A flume was constructed of plexiglass to assist visual observation, and was a 'race-track' shaped recirculating unit with annular sections of relatively large radius of curvature connecting the pump and observation sections. Horizontally homogeneous turbulent shear flow was produced by a specially designed disk pump which consisted of plexiglass plates of two different diameters alternately stacked on two counter- rotating shafts such that a large disk of one of the shafts (almost) meshed with a smaller disk of the other. Fluid was pulled along the outer gaps between the plates, and ejected in horizontal streams. Fluid velocities were augmented by using a screw propeller downstream of the pump, which did not destroy horizontal homogeneity of the flow. The disk pump and the screw propeller were always operated in tandem and together are referred to as the pump system. Gradients in the mean flow developed below the level of the disk pump and the resultant shear scoured the interface of the two- layered system of water-fluid mud in place inside the flume, thereby causing entrainment.

7.2 Conclusions

The main conclusions of the investigation are as follows:

1. The flow caused the layer above the level of the density interface to be essentially well-mixed as there was mass flux of sediment into it, and the buoyancy jump across the interface generally increased with time. The Richrdson number generally increased with the progress of each run.

2. The mean velocity of the mixed-layer decreased with time (at constant energy input via the pump system) which might be attributed to (a) increase in the volume of the mixed-layer being directly driven by the pump system, (b) wall friction effects, and (c) additional dissipation of turbulent energy on sediment particles in the mixed-layer with increasing concentration of this mixed-layer due to the entrainment of fluid mud with the progress (in time) of each run.

3. The plot of shear layer thickness, δ_s as a function of the Richardson number had considerable scatter, but indicated that $\delta_s \sim 0.23h$ for a sub-range of the Richardson number ($4 < Ri_u < 20$) with a slight increase beyond this sub-range (in contrast to Narimousa and Fernando 1987, and Moore and Long 1971). The assumption of no diffusion of momentum under the level of the interface might not always be true. Also, the conditions for two different runs were not exactly duplicated for the same Richardson number, e.g., a value of $\mathrm{Ri}_u = 10$ may have been obtained in the second time interval of a run while it may have occured in the later intervals of the other. There will be greater dissipation of kinetic energy in the second case in trying to counteract the settling tendency of more sediment particles, as the concentration of the mixed layer increases with time.

4. The interface was highly irregular and initially convoluted with massive ($\sim$ 6-8 cm) undulations. The heights of these disturbances decreased with the progress of each run. Internal wave breaking caused most of the buoyancy flux for $\mathrm{Ri}_u < 10$, whereas the action of eddies in shearing off non-linearly

growing, cusping crests of disturbances appeared to affect most of this mass flux into the mixed-layer for Richardson numbers beyond this range. Visual observations seemed to indicate that the mechanism of instability was generally the Holmboe mode.

5. The Richardson number generally increased during the course of each run. The plot of the non-dimensional buoyancy flux, Q, into the mixed-layer as a function of the Richardson number indicated that this could be expressed as

$$Q = \frac{A\,(Ri_u)^{-0.9}}{[(B)^2 + (Ri_u)^2]^m} \tag{7.1}$$

with A = 0.27, B = 20 and m = 0.66 for the range of Richardson numbers considered. This indicates that at low Richardson numbers, the relation is similar to that obtained for many salt-stratified systems (which can be shown to indicate that the rate of increase of potential energy of the system is of the same order as dissipation). However, for values of Richardson number > 25, the trend line indicates a much steeper fall off than for salt- stratified experiments thereby indicating additional dissipation of kinetic energy as the mixed-layer concentration increases. Though there was some intrusive effect of the splitter plate at the earlier times of each run, it is felt that the only way that the splitter plate would have affected the relationship between Q and Ri might have been to slightly alter the values of the constants in the above equation.

6. Calculations (in terms of equilibrium Peclet number) for the mixed-layer for runs which progressed to high Richardson numbers ($Ri_u > 20$) during the latter part of the run indicate this mixed-layer can be considered to be similar to an equilibrium suspension without mass influx or efflux, which implies cessation of entrainment.

7. Comparison with erosion of soft beds confirms that, especially at lower (< 35 cm/s) current velocities, the rate of fluid mud resuspension (or entrainment, which is proportional to the cube of the flow velocity) can dominate over that of bed erosion (which is proportional to the square of the flow velocity).

7.3 Recommendation for Further Work

1. One of the initial objectives of the present investigation was to determine the effect of varying the degree of cohesion of the constituent sediment of fluid mud on entrainment rates. This could, however, not be fully investigated owing to the difficulties associated with pre-mixing bentonite fluid mud as mentioned in Chapter 5. Thus, time constraints prevented investigation at higher Richardson numbers. It is felt this facet of the experiment warrants further study.

2. It is also recommended that more experimental runs be carried out which progress from low initial values of Richardson number with substantial rates of entrainment, to the point of (almost) cessation of discernable entrainment at high Richardson number. These should then be compared with experiments which *start* at high Richardson numbers to determine the effect of additional dissipation of turbulent kinetic energy due to higher mixed-layer concentrations on entrainment.

3. Further, it might also be instructive to improve upon the efficiency of the driving pump system to conduct experiments with higher initial mean mixed-layer velocity values (and thus Richardson numbers < 4) to determine any other changes in the entrainment relation. More accurate ways to determine velocity profiles of the mixed-layer and under the level of the interface are necessary.

APPENDIX A
TEST MATERIALS

A.1 Kaolinite

Commercially available kaolinite was used as the constituent of fluid mud in Runs # 1-9. The mean diameter of the sediment was 1.1 microns, with a range of 0.2 - 40 microns. Free moisture was 1.43%. The chemical composition as given by the suppliers, Feldspar Corporation, Edgar, Florida is presented in Table A.1.

A.2 Bentonite

Bentonite (Volclay HPM-20) was obtained from American Colloid Company, Arlington Heights, Illinois and was described as high purity air-floated sodium bentonite consisting of micron-sized particles. Dry particle sizes were rated as minimum 99% finer than 74 microns and 98% finer than 44 microns. It is a hydrous aluminum silicate composed primarily of clay mineral montmorillinite. The chemical formula is (approximately)

$$(Al, Fe_{1.67}, Mg_{0.33})Si_4O_{10}(OH_2)Na^{+} Ca^{++}_{0.33}$$

The chemical composition is given in Table A.2.

Table A.1: Chemical composition of kaolinite

Chemical	%
SiO_2	46.5
Al_2O_3	37.62
Fe_2O_3	0.51
TiO_2	0.36
P_2O_5	0.19
MgO	0.16
Na_2O & K_2O	0.42
CaO	0.25
SO_3	0.21
V_2O_5	< 0.001

Table A.2: Chemical composition of bentonite

Chemical	%
SiO_2	63.02
Al_2O_3	21.08
Fe_2O_3	3.25
FeO	0.35
MgO	2.67
Na_2O & K_2O	2.57
CaO	0.65
H_2O	5.64
Trace Elements	0.72

APPENDIX B
A NOTE ON RICHARDSON NUMBER

B.1 Introductory Note

This section traces the evolution of the definition of the critical Richardson number for stability of shear stratified flow. The criterion of stability of an inviscid, stratified flow of density $\rho(z)$ and mean horizontal velocity U(z) appeared in G.I.Taylor's Adams Prize winning essay of 1915 as $Ri > Ri_{cr}$ where

$$Ri = \frac{[(g/\rho)(-d\rho/dz)]}{(dU/dz)^2} \tag{B.1}$$

$$= \frac{N^2}{(dU/dz)^2} \tag{B.2}$$

where N is the buoyancy frequency.

B.2 Small Disturbances

Taylor (1931a) solved what is now known as the Taylor- Goldstein equation (equation 2.46) for small disturbances for a semi-infinite fluid in which N and dU/dz were constant and concluded that stable waves of all wavelengths can exist for Ri $> 1/4$, and that no waves (stable or unstable) can exist if Ri $< 1/4$. He also considered three and four-layered fluid systems with equal density jumps across each of the density interfaces and constant dU/dz in the mid-section and the results led him to the conjecture that the critical overall Richardson number might tend to 1/4 as the number of layers tend to infinity.

Miles (1961) considered a form of the Taylor-Goldstein equation without the Boussinesq approximation and with analytical velocity and density distributions to conclude that sufficient conditions for stability were $dU/dz \neq 0$ and $Ri(z) > 1/4$ throughout the flow. Howard (1961) generalized Miles' (1961) result without the

restrictions of analytical U(z) and ρ(z) (which is the form discussed in Section 2.2.2). Howard also showed that the complex disturbance wave speed c must lie within a semi-circle based on the range of U.

B.3 Energy Considerations

Richardson (1920) considered the energy transfer to turbulent eddies in a transport model developed by Reynolds (1895) and showed that, for equal coefficients for the diffusion of heat (K_h) and momentum (K_m), a sufficient condition for stability of arbitrary disturbances is Ri > 1. If the assumptions are eschewed, stability is predicted for

$$R_f = \frac{K_h}{K_m}\frac{N^2}{(dU/dz)^2} = \frac{K_h}{K_m}Ri > 1 \qquad \text{(B.3)}$$

where R_f is the flux Richardson number.

Taylor had obtained a similar relation through energy arguments at about the time of his Adams prize winning essay but delayed publishing until 1931. His argument (see 1931b) is as follows : The rate of increase of potential energy due to the displacement, η, from equilibrium is $\frac{1}{2}\rho g\beta(\frac{d\overline{\eta^2}}{dt})$, where $\beta = -(1/\rho)\frac{d\rho}{dz}$. The work done per unit area and unit time on a horizontal layer of thickness dz by the Reynolds stress τ is $\tau\alpha dz$ where α = dU/dz. Assuming $\tau = \rho K_m\alpha$, the mean rate of energy transport per unit volume is $\rho K_m\alpha^2$. Neglecting molecular diffusion and radiation implies

$$\frac{1}{2}\rho g\beta\frac{d\overline{\eta^2}}{dt} = \rho K_m\alpha^2 \qquad \text{(B.4)}$$

He further argued that the rate of transport of a quantity S across a horizontal surface A is $A\overline{w\eta}(dS/dz)$ where w is the vertical velocity and that $K_h = \overline{w\eta} = \frac{1}{2}\frac{d\overline{\eta^2}}{dt}$ whence equation (B.4) reduces to $R_f = 1$.

Chandrasekar's (1961) argument considering the interchange of two equal parcels was discussed in Section 2.2.2 which showed $Ri_{cr} = 1/4$. Miles (1961) refined this argument as he felt that the buoyancy force was not properly considered in the analysis and the derived condition was not *sufficient*. Consider two particles at at

elevations z and z + δz, of densities ρ and $\rho + \delta\rho$ and with velocities U and U + δU respectively, which move up $\gamma\delta z$ and $(1-\gamma)\delta z$ respectively with resultant mixing at elevation z + $\gamma\delta$z respectively. The work done in raising a parcel in equilibrium at z_1 to $z_1 + \eta$ against the downward force

$$F = g[\rho(z_1) - \rho(z_1 + \eta)] \tag{B.5}$$

$$\text{is}\Delta W = \beta\rho g\eta^2/2 \tag{B.6}$$

Thus, the work done in mixing the two parcels is

$$\delta W = \frac{1}{2}\rho g\beta[(\gamma\delta z)^2 + (1-\gamma)^2(\delta z)^2] \tag{B.7}$$

$$\geq \frac{1}{4}\rho g\beta(\delta z)^2 \tag{B.8}$$

The minimum work ($\gamma = 1/2$) corresponds to complete mixing as the density of the mixed parcel will be the same as that of the surrounding fluid ($\rho + \gamma d\rho$). Neglecting the effects of variations of density in calculations of momentum and energy, conservation of momentum implies that the velocity of the mixed parcel must be (U + U + δU)/2 and thus, the net change in kinetic energy due to the mixing is (see Section 2.2.2)

$$\delta T = \frac{1}{4}\rho(\delta U)^2 \tag{B.9}$$

Mixing is possible only if $\delta T > \delta W$, implying stability if $\text{Ri}_{cr} = 1$.

BIBLIOGRAPHY

Abraham, G. 1988 Turbulence and mixing in stratified tidal flows, *Physical Processes in Estuaries*, Dronkers, J. and van Leussen, W., editors, Springer-Verlag, Berlin, 149-180.

Atkinson, J.F. 1988 Interfacial mixing in stratified flows, *Journal of Hydr. Res.* 26, 1988, No. 1, 27-31.

Batchelor, G.K. 1953 *The theory of homogeneous turbulence*, Cambridge Univ. Press, Cambridge.

Browand, F.K., and Wang, Y.H. 1972 An Experiment on the Growth of Small Disturbances at the Interface between Two Streams of Different Densities and Velocities, *International Conference on Stratified Flows*, Novosibirsk, USSR 491-498.

Browand, F.K., and Winant, C.D. 1973 Laboratory observations of shear-layer instabilities in stratified fluid, *Boundary layer Meteor.* 5, 67-77.

Bryant, R., James, A.E. and, Williams, D.J.A 1980 Rheology of cohesive suspensions, *Industrial Embayments and their Environmental Problems, A Case study of Swansea Bay*, Collins, M.B et al., editors, Pergamon Press, New York, 279-287.

Chandrasekhar, S. 1961 *Hydrodynamic and Hydromagnetic Stability*, Clarendon Press, Oxford.

Christodoulou, G.C. 1986 Interfacial mixing in stratified flows, *Journal of Hydr. Res.* 24, 77-92.

Chu, V.H., and Baddour, R.E. 1984 Turbulent gravity- stratified shear flows, *J. Fluid Mech.* 138, 353-378.

Corcos, G.M., and Sherman, F.S. 1976 Vorticity concentration and the dynamics of unstable free shear layers, *J. Fluid Mech.* 73, 241-264.

Deardorff, J.W. 1983 A multi-limit mixed layer entrainment formulation, *J. Phys. Oceanog.* 13, 988-1002.

Deardorff, J.W., and Willis, G.E. 1982 Dependence of mixed-layer entrainment on shear-stress and velocity jump, *J. Fluid Mech.* 115, 123-150.

Deardorff, J.W., and Yoon, S.C. 1984 On the use of annulus to study mixed layer entrainment, *J.Fluid Mech.* 142, 97-120.

Delisi, D.P., and Corcos, G. 1973 A study of internal waves in a wind tunnel, *Boundary Layer Meteor.* 5, 121-137.

Dixit, J.G. 1982 Resuspension potential of deposited kaolinite beds *Master's thesis*, University of Florida, Gainesville.

E, X., and Hopfinger, E.J. 1987 Stratification by solid particle suspension, *Proc. 3rd Int. Symp. on Stratified Flows*, CIT, Pasadena, CA.

Ellison, T.H., and Turner, J.S. 1959 Turbulent entrainment in stratified flows, *J. Fluid Mech.* 6, 423-448.

Fernando, H.J.S. 1988 The growth of a turbulent patch in a stratified fluid, *J. Fluid Mech.* 190, 55-70.

Hazel, P. 1972 Numerical studies of the stability of inviscid parallel shear flows, *J. Fluid Mech.* 51, 39-61.

Helmholtz, H. von 1868 Uber discontinuirliche Flussigkeits-bewwgungen, *Monats. Konigl. Preuss. Akad. Wiss. Berlin* 23, 215-228.

Hinze, J.O. 1975 *Turbulence*, McGraw-Hill, New York.

Holmboe, J. 1962 On the behavior of symmetric waves in stratified shear layers, *Geophys. Publ.* 24, 67-113.

Howard, L.N. 1961 Note on a paper of John W.Miles, *J. Fluid Mech.* 10, 509-512.

James, I.S.F., and Mulhearn, P.J. 1983 The influence of external turbulence on sheared interfaces, *Geophys. Astrophys. Fluid Dyn.* 24, 49-62.

Kantha, L.H., Phillips, O.M., and Azad, R.S. 1977 On turbulent entrainment at a stable density interface, *J. Fluid Mech.* 79, 753-768.

Kato, H., and Phillips, O.M. 1969 On the penetration of a turbulent layer into a stratified fluid, *J. Fluid Mech.* 37, 643-655.

Kirby, R. 1986 Suspended fine cohesive sediment in the Severn Estuary and the Inner Bristol Channel, *Report to the United Kingdom Atomic Energy Authority* Report no. ETSU-STP-4042, Taunton, Somerset.

Kirby, R., and Parker, W.R. 1983 Distribution and Behavior of fine sediment in the Severn Estuary and Inner Bristol Channel, U.K., *Canadian Journal of Fisheries and Aquatic Sciences* 40, supplement 1, 83.

Lawrence, G.A., Lasheras, J.C., and Browand, F.K. 1987 Shear instabilites in stratified flows, *Proc. 3rd Int. Sym. on Stratified Flows*, CIT, Pasadena, CA.

Lofquist, K. 1960 Flow and stress near an interface between stratified liquids, *Phys. Fluids* 3, 158-175.

Long, R.R. 1973 Some properties of horizontally homogeneous statistically steady turbulence in a stratified fluid, *Boundary Layer Meteor.* 5, 139-157.

Long, R.R. 1974 The influence of shear on mixing across density interfaces, *Technical report no. 4*, Dept. of Mechanics and Earth and Planetary Sciences, Johns Hopkins Univesity.

Long, R.R. 1978 A theory of mixing in a stably stratified fluid, *J. Fluid Mech.* 84, 113-124.

McLean, S.R. 1985 Theoretical modeling of deep ocean sediment transport, *Marine Geology* 66, 243-265.

Miles, J.W. 1961 On the stability of heterogeneous shear flows, *J. Fluid Mech.* 10, 496-508.

Moore, M.J., and Long, R.R. 1971 An experimental investigation of turbulent stratified shearing flow, *J. Fluid Mech.* 49, 635-655.

Narimousa, S., and Fernando, H.J.S. 1987 On the sheared density interface of an entraining fluid, *J. Fluid Mech.* 174, 1-22.

Narimousa,S., Long, R.R., and Kitaigorodskii, S.A. 1986 Entrainment due to turbulent shear flow at the interface of a stably stratified fluid, *Tellus* 38A, 76-87.

Odell, G.M., and Kovasznay, L.S.G. 1971 A new type of water channel with density stratification, *J. Fluid Mech.* 50, 535-543.

Parchure, T.M., and Mehta, A.J. 1985 Erosion of soft cohesive beds, *J. Hydraul. Eng.* 111(10), 1308-1326.

Phillips, O.M. 1977 *Dynamics of the Upper Ocean*, 2^{nd} edition, Cambridge University Press, Cambridge.

Reynolds, O. 1895 On the dynamical theory of incompressible viscous fluids and the development of the criterion, *Phil. Trans. R. Soc. Lond. A186*, 123-164; *Scientific Papers* 2, 533-577.

Richardson, L.F. 1920 The supply of energy to and from turbulent eddies, *Proc. R. Soc. Lond. A97*, 354-373.

Ross, M.A., Lin, C.P., and Mehta, A.J. 1988 On the definition of fluid mud, *ASCE Speciality Conference on Hydraulic Engineering*, Williamsburg, Virginia.

Rouse, H., and Dodu, J. 1955 Turbulent diffusion across a density discontinuity *La Houille Blanche* 10, 530-532.

Scranton, D.R., and Lindberg, W.R. 1983 An experimental study of entraining, stress-driven, stratified flow in an annulus, *Phys. Fluids* 26(5), 1198-1205.

Sherman, F.S., Imberger, J., and Corcos, G.M. 1978 Turbulence and mixing in stably stratified waters, *Annual Rev. of Fluid Mech.* 10, 267-288.

Smyth, W.D., Klaassen, G.P., and Peltier, W.R. 1987 The non-linear evolution of Holmboe waves, *Proc. 3rd Int. Sym. on Stratified Flows*, CIT, Pasadena, CA.

Taylor, G.I. 1915 Eddy motion in the atmosphere, *Phil. Trans. R. Soc. Lond. A215*, 1-26; *Scientific Papers* 2, 1-23.

Taylor, G.I. 1931a Effect of variation in density on the stability of superposed streams of fluid, *Proc. R. Soc. Lond. A132*, 499-523; *Scientific Papers* 2, 219-239.

Taylor, G.I. 1931b Internal waves and turbulence in a fluid of variable density, *Rapports et Procès-Verbaux des Rèunions du Conseil Permanent International pour d'Exploration de la Mer 76*, 35-42; *Scientific Papers* 2, 240-246.

Teeter, A.M. 1986 Vertical transport in fine-grained suspensions and newly-deposited sediment, *Estuarine Cohesive Sediment Dynamics*, Mehta, A.J., editor, Springer-Verlag, Berlin.

Thorpe, S.A. 1973 Experiments on instability and turbulence in a stratified shear flow, *J. Fluid Mech.* 61, 731-751.

Townsend, A.A. 1956 *The structure of turbulent shear flow*, Cambridge Univ. Press, Cambridge.

Turner, J.S. 1968 The influence of molecular diffusivity on turbulent entrainment across a density interface, *J. Fluid Mech.* 33, 639-656

Turner, J.S. 1973 *Buoyancy effects in fluids*, Cambridge University Press, Cambridge.

Turner, J.S. 1986 Turbulent entrainment: the development of the entrainment assumption, and it's application to geophysical flows, *J. Fluid Mech.* 173, 431-471.

van Leussen, W., and van Velzen, E. In Press High concentraion suspensions: their origin and importance in Dutch estuaries and coastal waters, *J. Coastal Res.* Special issue no.5 (in press).

Wolanski, J., Asaeda, T., and Imberger, J. In Press Mixing across a lutocline, *Limnol. and Oceanogr.* 34.

Wright, L.D., Wiseman, W.J., Bornhold, B.D., Prior, D.B., Suhayda, J.N., Keller, G.H., Yang, Z.S., and Fan, Y.B. 1988 Marine dispersal and deposition of Yellow River silts by gravity driven underflows, *Nature* 332, 629-632.

Yih, C.S. 1955 Stability of two dimensional parallel flows for three dimensional disturbances, *Quart. Appl. Math.* 12, 434-435.

Zemen, O., and Tennekes, H. 1977 Parameterisation of the turbulent energy budget at the top of the daytime atmospheric boundary layer, *J. Atmos. Sci.* 34, 111-123